CRCLEME
Cooperative Research Centre for
Landscape Evolution & Mineral Exploration

OPEN FILE
REPORT
SERIES

CSIRO
EXPLORATION
AND MINING

AMIRA
Australian Mineral Industries Research Association Limited ACN 004 448 266

HYDROGEOCHEMISTRY OF THE PANGLO GOLD DEPOSIT

D.J. Gray

CRC LEME OPEN FILE REPORT 41

October 1998

(CSIRO Division of Exploration Geoscience Report 125R, 1990.
Second impression 1998)

AMIRA
Australian Mineral Industries Research Association Limited ACN 004 448 266

CRCLEME
Cooperative Research Centre for
Landscape Evolution & Mineral Exploration

CSIRO
EXPLORATION
AND MINING

HYDROGEOCHEMISTRY OF THE PANGLO GOLD DEPOSIT

D.J. Gray

CRC LEME OPEN FILE REPORT 41

October 1998

(CSIRO Division of Exploration Geoscience Report 125R, 1990.
Second impression 1998)

CRC LEME is an unincorporated joint venture between The Australian National University,
University of Canberra, Australian Geological Survey Organisation and CSIRO Exploration and Mining
Headquarters: CRC LEME c/o CSIRO Exploration and Mining, Private Bag, PO Wembley, Western Australia, 6014

RESEARCH ARISING FROM CSIRO/AMIRA REGOLITH GEOCHEMISTRY PROJECTS 1987-1993

In 1987, CSIRO commenced a series of multi-client research projects in regolith geology and geochemistry which were sponsored by companies in the Australian mining industry, through the Australian Mineral Industries Research Association Limited (AMIRA). The initial research program, "Exploration for concealed gold deposits, Yilgarn Block, Western Australia" (1987-1993) had the aim of developing improved geological, geochemical and geophysical methods for mineral exploration that would facilitate the location of blind, buried or deeply weathered gold deposits. The program included the following projects:

P240: Laterite geochemistry for detecting concealed mineral deposits (1987-1991). Leader: Dr R.E. Smith.
Its scope was development of methods for sampling and interpretation of multi-element laterite geochemistry data and application of multi-element techniques to gold and polymetallic mineral exploration in weathered terrain. The project emphasised viewing laterite geochemical dispersion patterns in their regolith-landform context at local and district scales. It was supported by 30 companies.

P241: Gold and associated elements in the regolith - dispersion processes and implications for exploration (1987-1991). Leader: Dr C.R.M. Butt.
The project investigated the distribution of ore and indicator elements in the regolith. It included studies of the mineralogical and geochemical characteristics of weathered ore deposits and wall rocks, and the chemical controls on element dispersion and concentration during regolith evolution. This was to increase the effectiveness of geochemical exploration in weathered terrain through improved understanding of weathering processes. It was supported by 26 companies.

These projects represented "an opportunity for the mineral industry to participate in a multi-disciplinary program of geoscience research aimed at developing new geological, geochemical and geophysical methods for exploration in deeply weathered Archaean terrains". This initiative recognised the unique opportunities, created by exploration and open-cut mining, to conduct detailed studies of the weathered zone, with particular emphasis on the near-surface expression of gold mineralisation. The skills of existing and specially recruited research staff from the Floreat Park and North Ryde laboratories (of the then Divisions of Minerals and Geochemistry, and Mineral Physics and Mineralogy, subsequently Exploration Geoscience and later Exploration and Mining) were integrated to form a task force with expertise in geology, mineralogy, geochemistry and geophysics. Several staff participated in more than one project. Following completion of the original projects, two continuation projects were developed.

P240A: Geochemical exploration in complex lateritic environments of the Yilgarn Craton, Western Australia (1991-1993). Leaders: Drs R.E. Smith and R.R. Anand.
The approach of viewing geochemical dispersion within a well-controlled and well-understood regolith-landform and bedrock framework at detailed and district scales continued. In this extension, focus was particularly on areas of transported cover and on more complex lateritic environments typified by the Kalgoorlie regional study. This was supported by 17 companies.

P241A: Gold and associated elements in the regolith - dispersion processes and implications for exploration. Leader: Dr. C.R.M. Butt.
The significance of gold mobilisation under present-day conditions, particularly the important relationship with pedogenic carbonate, was investigated further. In addition, attention was focussed on the recognition of primary lithologies from their weathered equivalents. This project was supported by 14 companies.

Although the confidentiality periods of the research reports have expired, the last in December 1994, they have not been made public until now. Publishing the reports through the CRC LEME Report Series is seen as an appropriate means of doing this. By making available the results of the research and the authors' interpretations, it is hoped that the reports will provide source data for future research and be useful for teaching. CRC LEME acknowledges the Australian Mineral Industries Research Association and CSIRO Division of Exploration and Mining for authorisation to publish these reports. It is intended that publication of the reports will be a substantial additional factor in transferring technology to aid the Australian Mineral Industry.

This report (CRC LEME Open File Report 41) is a Second impression (second printing) of CSIRO, Division of Exploration Geoscience Restricted Report 125R, first issued in 1990, which formed part of the CSIRO/AMIRA Project P241.

Copies of this publication can be obtained from:
The Publication Officer, c/- CRC LEME, CSIRO Exploration and Mining, PMB, Wembley, WA 6014, Australia. Information on other publications in this series may be obtained from the above or from http://leme.anu.edu.au/
Cataloguing-in-Publication:
Gray, D.J.
Hydrogeochemistry of the Panglo Gold Deposit
ISBN 0 642 28204 8
1. Geochemistry 2. Hydrogeology 3. Gold - Western Australia.
I. Title
CRC LEME Open File Report 41.
ISSN 1329-4768

PREFACE

The hydrochemical survey of the Panglo gold deposit described in this report is one of the most detailed investigations carried out in the vicinity of any style of mineralization on the Yilgarn Block. The study has particular importance because it provides data that contribute to our understanding of the conditions under which gold may be mobilized in the weathering environment and, ultimately, accumulate as supergene deposits. Specifically, the study:

(i) demonstrates the existence of environments that permit the oxidative dissolution and mobilization of gold;

(ii) describes the characteristics of the environment;

(iii) suggests that, in this location at least, it is possible that gold is mobilized by forming complexes with iodide rather than chloride;

(iv) assesses the influence of the composition of the regolith on the groundwaters on the mobility of gold and associated elements.

This hydrogeochemical survey is complementary to studies of the regolith geochemistry at the site and the nature and surface expression of gold mineralization. Together they address many of the principal objectives of the Project.

C.R.M. Butt,
Project Leader.
October, 1990

ABSTRACT

A hydrogeochemical survey of the Panglo Gold Deposit was conducted by sampling groundwaters in open drill holes, and from drainage holes in the Trial Pit. Waters were sampled from the three main geological environments of the area, namely shales in the south-east of the study area, mafic rocks, and ultramafic rocks.

The chemical characteristics of the water samples are closely correlated with the lithology in which the water was sampled. Waters derived from shales have relatively low concentrations in Au, the pathfinders, and most of the chalcophile elements analysed, whereas waters derived from mafic and ultramafic rocks have characteristic multi-element 'signatures'. Waters associated with mafic rocks are strongly enriched in Mn, Co, and Zn, and weakly enriched in Cu and Ni, whereas waters associated with ultramafic rocks are enriched in Ni, Cr, Bi, Sc and Ag. Using these data, water samples could be distinguished into geological groupings by using chemical compositions alone.

Chemical data also suggest major variations in the degree of weathering and leaching within the sample area. Waters in the northern part of the study area are highly acidic and oxidizing, and have anomalously high concentrations of Au, Br, Fe, Mn, Co, Zn, Cu and Ni.

Dissolution of Au is primarily controlled by the redox status of the solution. Elevated Eh levels are caused by Mn oxidation, permitting the oxidative dissolution of native Au and its mobilization by either the chloride or the iodide complexes. Dissolution of Au as the iodide complex occurs as a consequence of the relatively high concentrations of I at this site. Such a Au mobilization mechanism has not, in the author's experience, been previously documented for groundwaters. The concentration of dissolved Au is high, and would represent a reasonable exploration method at this site.

TABLE OF CONTENTS

LIST OF FIGURES

Page No.

LIST OF TABLES

LIST OF ABBREVIATIONS

DO	Dissolved Oxygen
Eh	Oxidation Potential
SI	Log [(Ion Activity Product)/(Activity Product for Equilibrium)] = Measure of Over- or Under-saturation
M-S	Mafic-Sediment
M-Sf	Intermediate between Mafic-Sediment and Shale
M-U	Intermediate between Mafic-Sediment and Ultramafic
Sf	Shale
TDS	Total Dissolved Solids (Salinity)
U	Ultramafic

LIST OF COMPOUNDS

Ammonia	NH_3
Bicarbonate	HCO_3^-
Gold chloride	$AuCl_2^-$
Gold iodide	AuI_2^-
Nitrate	NO_3^-
Sulphate	SO_4^{2-}
Thiosulphate	$S_2O_3^{2-}$

LIST OF MINERALS

Alunite	$KAl_3(SO_4)_2(OH)_6$
Calcite	$CaCO_3$
Celestine	$SrSO_4$
Dolomite	$CaMg(CO_3)_2$
Feldspar	$NaAlSi_3O_8$
Ferrihydrite	$Fe(OH)_3 \cdot xH_2O$
Goethite	$FeOOH$
Gypsum	$CaSO_4 \cdot 2H_2O$
Halite	$NaCl$
Hematite	Fe_2O_3
Illite	$K_{0.7}(Mg,Fe^{3+},Al)_{2-3}(Si,Al)_4O_{10}(OH)_2$
Jurbanite	$Al(OH)SO_4$
Kaolinite	$Al_2Si_2O_5(OH)_4$
Pyrite	FeS_2
Pyrolusite	MnO_2
Quartz	SiO_2
Strontianite	$SrCO_3$
Vermiculite	$(Na)_{0.7}(Mg,Fe^{3+},Al)_{2-3}(Si,Al)_4O_{10}(OH)_2 \cdot nH_2O$

1. Introduction

This report describes the results of a hydrogeochemical survey of the Panglo (South Paddington) gold deposit (Fig. 1). Specific fields of interest were:

(i) use of gold and other pathfinder elements in water as an exploration tool;

(ii) what ions cause mobility of gold, and how these ions are influenced by groundwater chemistry and water-rock interactions;

(iii) further understanding of the chemical and geological factors influencing the chemistry of waters in the Yilgarn Block;

(iv) development of techniques for analysis of groundwater data from mineralized areas;

(v) interaction with laboratory investigations and other site studies.

This work was performed in conjunction with other investigations into the geochemistry and mineralogy of the regolith (Scott 1989a, b, 1990), and on the exploration potential of soils and plants at this site (Lintern and Scott, 1990). This report relates effects on the groundwater chemistry from the underlying geology, weathering processes and hydrology.

The results of this work contribute to a compilation of data for mineralized and unmineralized regions in the Yilgarn Block. This compilation will advance our knowledge of groundwater characteristics, particularly in reference to the formation of geochemical haloes in the regolith and the use of groundwaters in exploration.

2. Methodology

2.1. Site Characteristics

The Panglo Gold Project is located some 30 km north of Kalgoorlie along the Kalgoorlie-Leonora Highway. A map of the mine area is shown in Fig. 1. The area has a arid climate with an average annual rainfall of about 250 mm, most of which falls during the cooler months of May to August. However, there is a significant component of summer rainfall from erratic thunderstorms. The average rainfall and pan-evaporation, as measured at Kalgoorlie, are shown in Fig. 2.

2.2. Water Sampling

Sampling was done on three separate occasions. Samples P1 to P41 were collected by CSIRO personnel in March 1989, on established exploration holes, using a specially designed pump sampler. Samples P42 to P47 were collected by Pancontinental personnel, from pumping of dewatering bores, in mid 1989. Finally, samples P48, P49 and P50 were collected in Dec. 1989 by CSIRO personnel, from PVC pipes penetrating into the walls of the Trial Pit, to a distance of about 100 m laterally. The location of the sampled holes are shown in Fig. 1 and listed in Table 1.

The samples are referred to by number rather than by the hole names, which can be determined from Table 1. Data for sea water, compiled from Weast *et al.* (1984), are given for comparison.

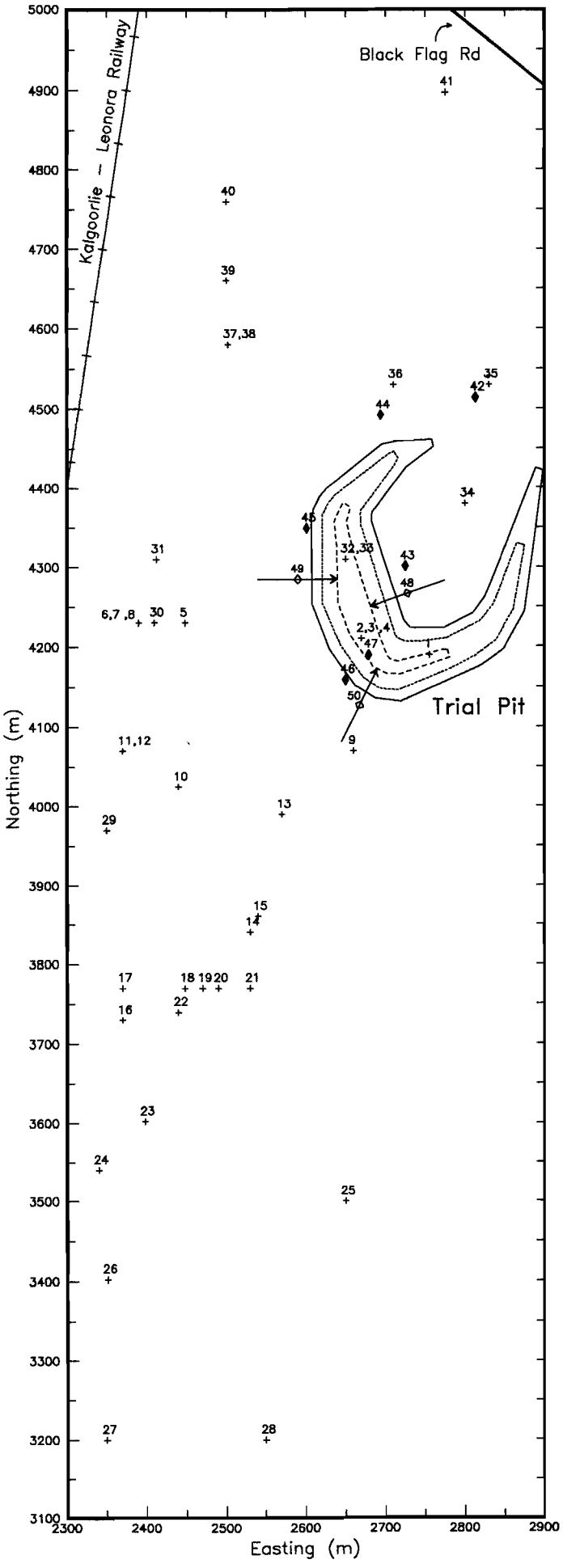

Fig. 1 Map of the Panglo Mine Area, with Sampling Holes.

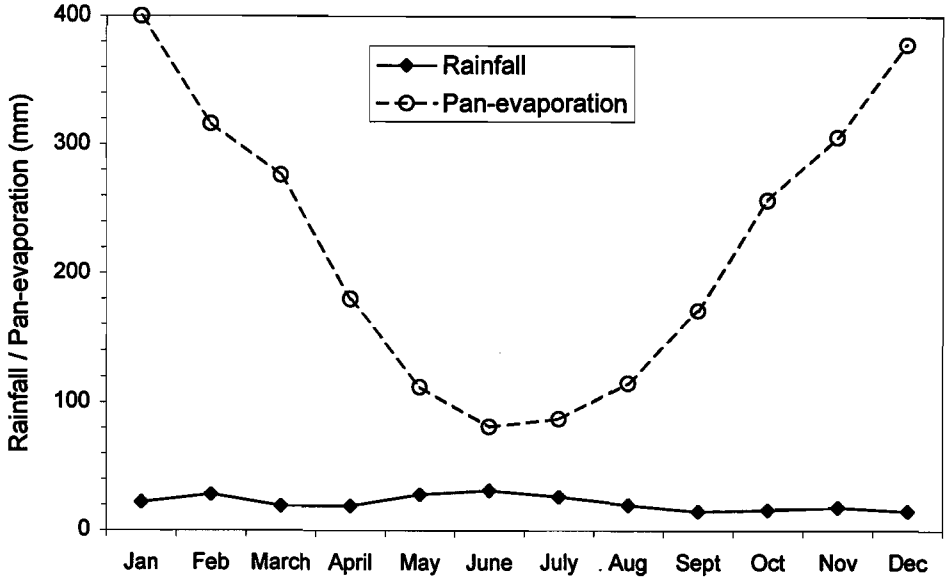

Fig. 2. Average Rainfall and Pan-evaporation, as measured at Kalgoorlie

2.3. Water Analysis

The following observations were made at the time of sampling:
Depth to watertable
Sampling depth
pH
Temperature
Conductivity
Oxidation Potential (Eh)
Dissolved Oxygen (DO)
Ferrous ion concentration (Fe^{2+})

A 40 ml water sample was collected in a polythene bottle (with overfilling to remove all air) for later HCO_3^- analysis by alkalinity titration in the laboratory. A 250 ml water sample was through a 45μm millipore filter in the field and 125 ml were acidified. The acidified portion of the filtrate was analysed for Na, K, Mg, Ca, Sr, Si, Al, Fe, Mn, Co, Cr, Cu, Ni, Zn, Ag, As, Bi, by flame AAS on a Varian AA875 and ICP-OES on a Hilger E-1000 ICP with a high solids torch. The waters were also analysed for Ba, Cd, Pb, Sb by ICP, but these were all below the detection limits. Matrix effects for the ICP analysis were minimized by diluting with acid to a constant sodium concentration and using standards matched to the same salinity.

The unacidified portion was analysed by Ion Chromatography, for Cl^-, Br^-, SO_4^{2-} and NO_3^-, using a DIONEX AS4A column under standard eluent conditions (Dionex, 1985) with a conductivity detector, and for I^- and $S_2O_3^{2-}$ (thiosulphate) using a DIONEX AS5 column under standard eluent conditions (*ibid.*) with an electrochemical detector. The $S_2O_3^{2-}$ analyses were performed on solutions that were frozen in the field and thawed in the laboratory prior to analysis, so as to avoid decomposition. All samples analysed for $S_2O_3^{2-}$ were found to have concentrations below the detection limit (Appendix 1).

Table 1: Sampling Holes at Panglo, with Location and Geological Classification.

Sample Number	Hole Name	Easting (m)	Northing (m)	Geology# Group	pH/Eh* Group
P1	ARP419-1	2755	4190	Sf	HO
P2	ARM421-2	2670	4210	M-S	HO
P3		2670	4210	M-S	HO
P4	"	2670	4210	M-S	HO
P5	ARP423-5	2448	4230	M-S	HO
P6	ARP423-2	2390	4230	U	HO
P7	"	2390	4230	U	HO
P8	"	2390	4230	U	HO
P9	ARP407-2	2660	4070	Sf	HO
P10	PSRC367	2440	4025	M-S	HO
P11	ARP407-5	2370	4070	U	HO
P12	"	2370	4070	U	HO
P13	ARP399-1	2570	3990	M-S	HO
P14	ARP384-3	2530	3840	M-Sf	HO
P15	ARP386-5	2540	3860	M-Sf	HO
P16	ARP373-1	2370	3730	M-S	Mn
P17	ARP377-10	2370	3770	M-S	Al1
P18	ARP377-6	2448	3770	M-S	HO
P19	ARP377-5	2470	3770	M-S	L
P20	ARP377-4	2490	3770	M-S	Al2
P21	ARP377-2	2530	3770	M-Sf	HO
P22	ARP374-10	2440	3740	M-S	Mn
P23	PSR491	2398	3602	M-Sf	Fe2
P24	ARP342-2	2340	3540	M-S	Al2
P25	PSR627	2650	3500	Sf	Fe2
P26	PSR495	2351	3402	M-Sf	Fe1
P27	PSR616	2350	3200	Sf	Al2
P28	PSR620	2550	3200	Sf	Al2
P29	ARP397-2	2350	3970	M-S	Al1
P30	ARP423-3	2410	4230	U	HO
P31	ARP431-3	2412	4310	U	HO
P32	ARM431-2	2650	4310	M-S	Mn
P33	"	2650	4310	M-S	Mn
P34	ARP438-12	2800	4380	M-S	Mn
P35	ARP453-1	2830	4530	M-S	Mn
P36	ARP453-7	2710	4530	M-S	Al1
P37	ARP458-1	2502	4580	M-U	Mn
P38	"	2502	4580	M-U	Mn
P39	ARP466-1	2500	4660	M-U	Al1
P40	ARP476-1	2500	4760	M-U	Al1
P41	PSR402	2775	4897	M-S	Fe2
P42	Bore 2	2813	4514	M-S	Fe1
P43	Bore 4	2725	4301	M-S	Fe1
P44	Bore 5	2694	4492	M-S	Fe1
P45	Bore 7	2601	4349	M-S	HO
P46	Bore 8	2650	4159	M-Sf	HO
P47	Trial Pit	2679	4190	M-Sf	HO
P48	Pipe A	2728	4267	M-S	Fe1
P49	Pipe B	2590	4285	M-S	HO
P50	Pipe C	2668	4127	M-Sf	HO

: See Text (Section 3.2) for explanation of geological groups
* : See Table 3 for explanation of pH/Eh classes

The accuracy of the total analyses was confirmed by measuring the cation/anion balance. Any waters with balances worse than 5% were rechecked.

Gold was determined using preconcentration on activated charcoal. A one litre water sample, acidified with one ml concentrated nitric acid, was shaken for at least three days with one gram activated charcoal enclosed in nylon mesh. The activated charcoal was then ashed, and the residue dissolved in a mixture of concentrated hydrochloric and nitric acids. Laboratory investigations have indicated that using this preconcentration system will enable successful analyses of waters for Au at low concentrations, though at a lessened accuracy than via standard analyses. Calibration of the method was obtained by shaking standards of varying concentrations, and in varying salinities, with activated carbon.

Gold was analysed by Graphite Furnace AAS on a Varian AA-875 with a GTA-95 Graphite Tube Atomizer, following extraction into DIBK. Any matrix effect was compensated for by running two standard additions for each sample.

3. Results and Discussion

3.1. Layout of Results

Water data are listed in Appendix 1. The geology, Au supergene expression, topography, watertable, and the spatial distribution of various species are shown in Fig. 3 - 27. Other relevant data will also be plotted as part of the discussion.

3.2. Regional Description

The geology of the area, the supergene Au expression and the position of the Trial Pit dug in late 1989 are shown in Fig. 3. The geological map is also duplicated as a transparency (Fig. 7a) which can be used to overlap the spatial distribution maps. The western and eastern limits of the supergene Au anomaly appear to follow the ultramafic-mafic and the mafic-shale contacts, respectively, but the north and south limits are less clearly defined.

Waters were mainly classified in terms of their geological environment (Table 1):

Sf: Waters from boreholes located in the Shale/Siltstone system in the south-east part of the study area.

M-Sf: Waters from boreholes close to the interface of the Mafic/Sediment and Shale/Siltstone systems.

M-S: Waters from boreholes located in the Mafic/Sediment system. This is the system hosting the gold mineralization.

M-U: Waters from boreholes close to the interface of mafic and ultramafic rocks. These waters are situated at 2500E / 4600-4800N.

U: Waters from boreholes located within major veins of Ultramafic rocks. These waters are situated in a grouping at about 2400E / 4050-4300N.

The location of these boreholes is given in Fig. 4.

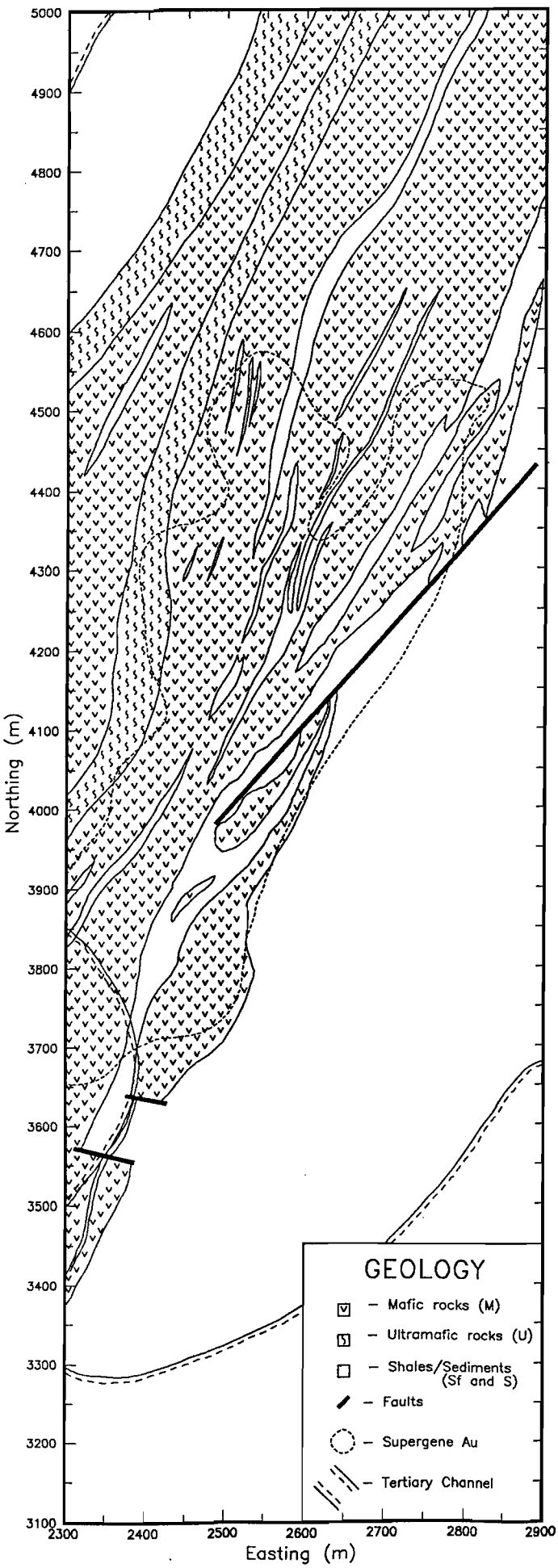

Fig. 3 Geology and Au Supergene Expression at the Panglo Mine Area.

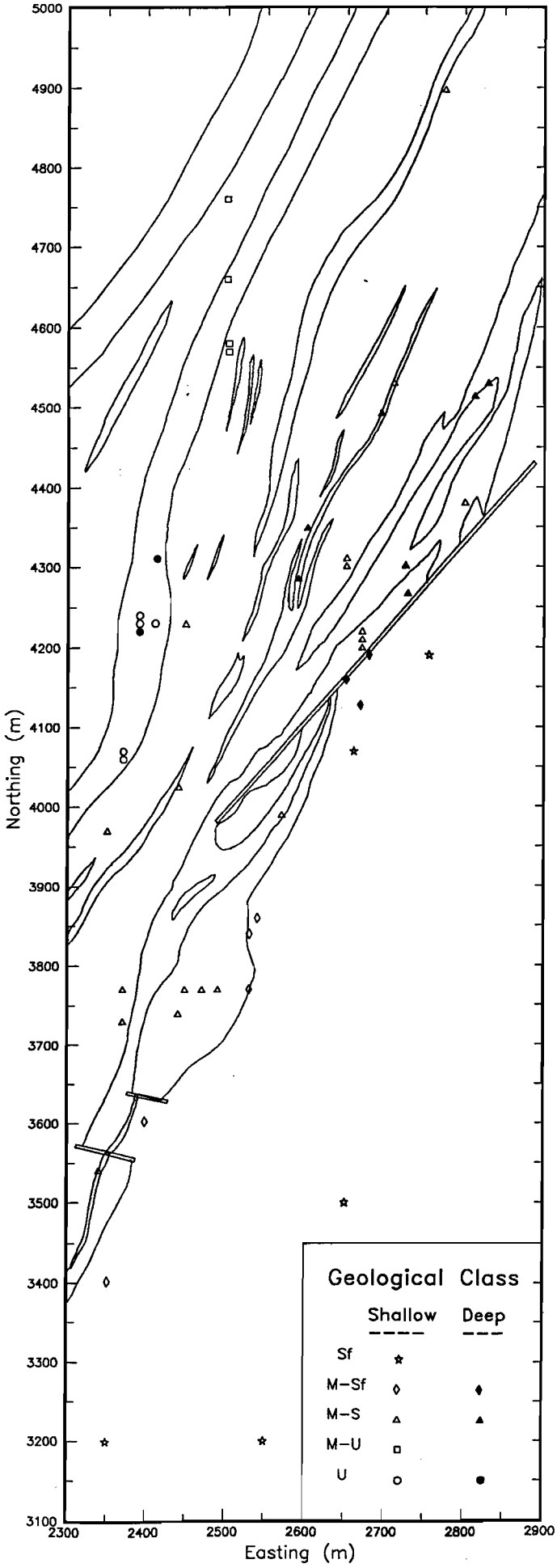

Fig. 4. Spatial Location of Geological Water Groups from Panglo

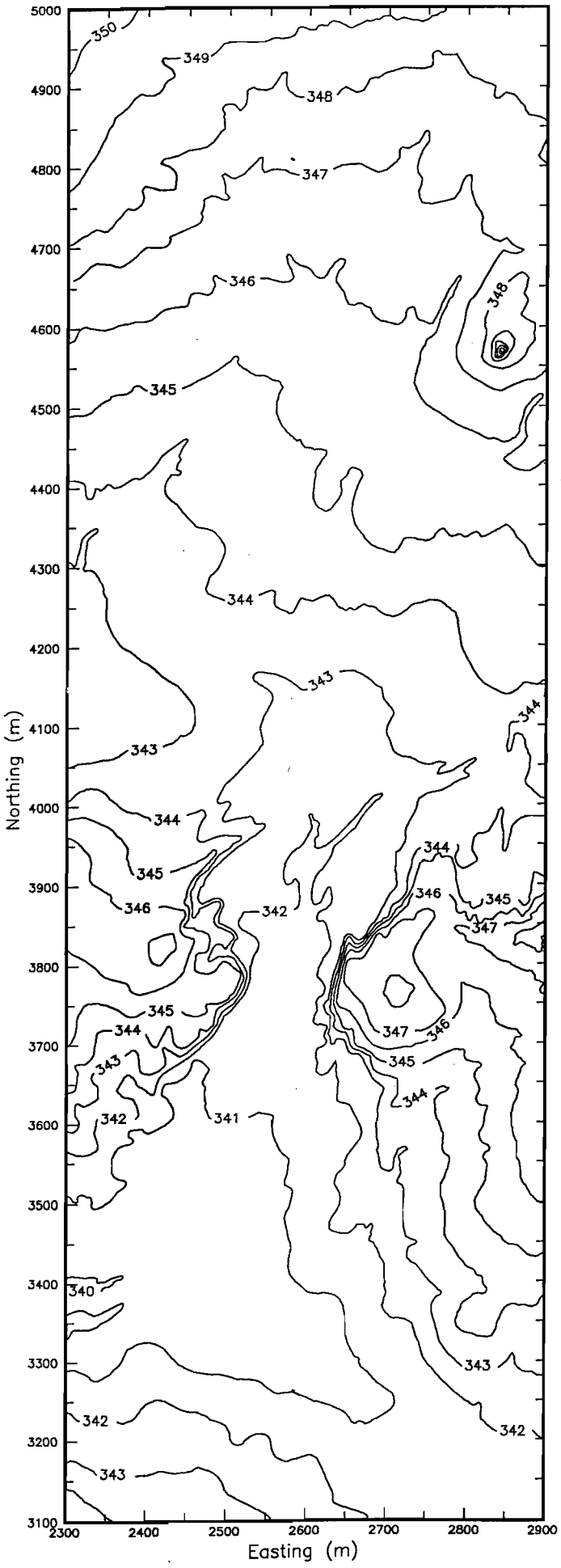

Fig. 5 Topography (in mRL) of the Panglo Mine Area.

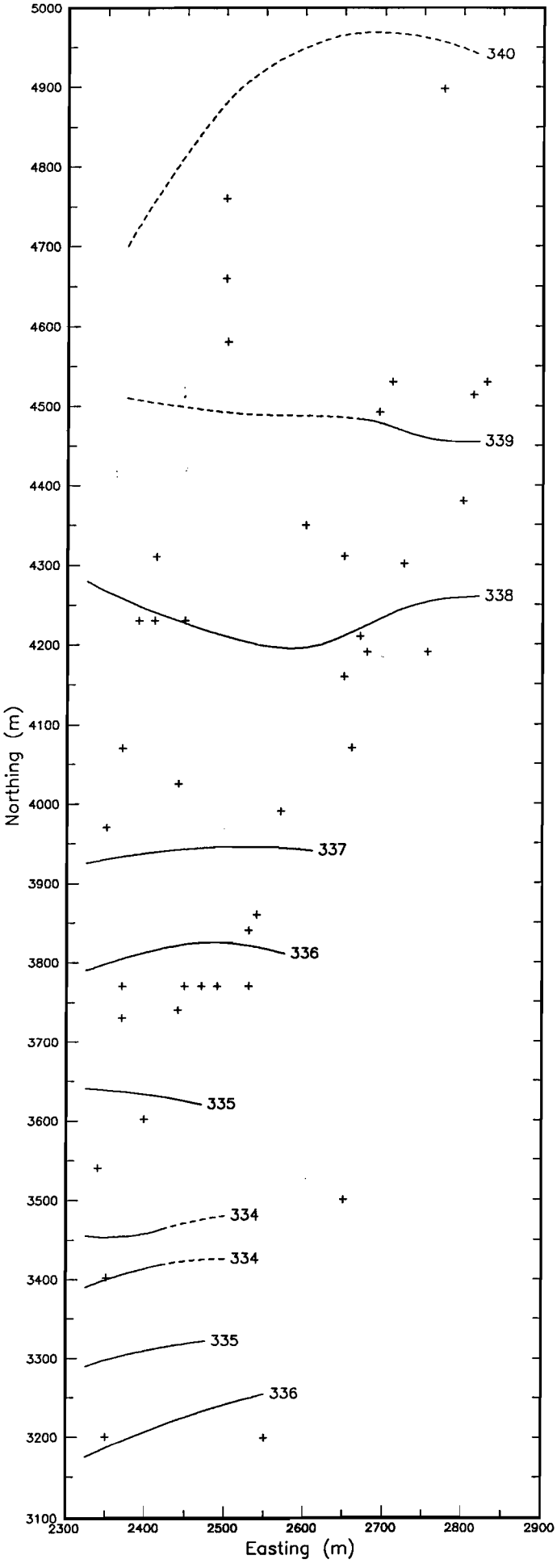

Fig. 6 Estimated Watertable Contours (in mRL) for the Panglo Mine Area.

Fig. 7 Transparencies of

(a) Geology

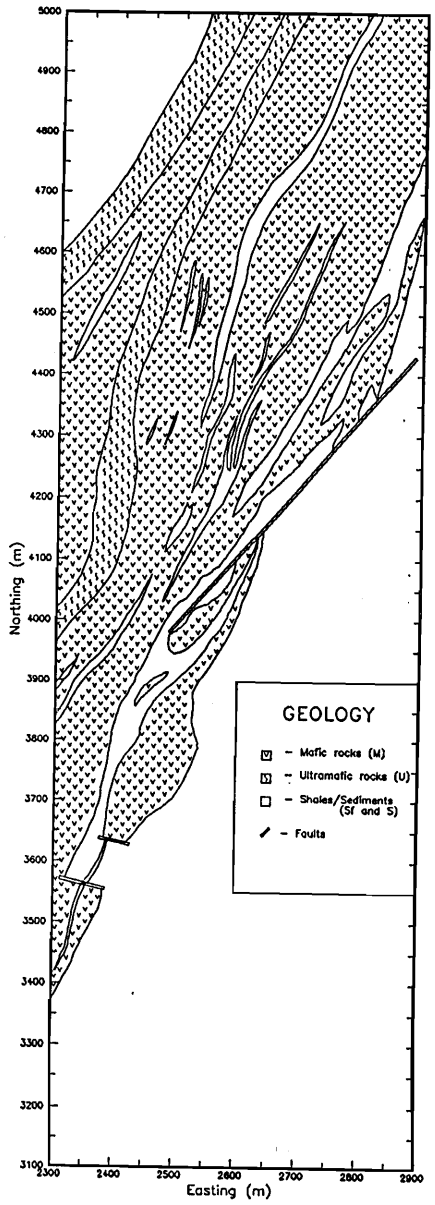

(b) pH

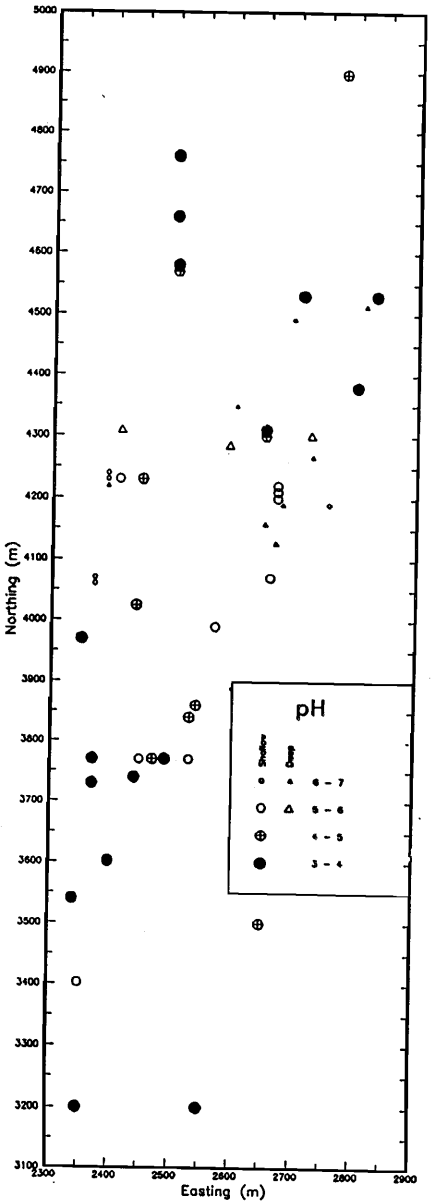

(c) Eh

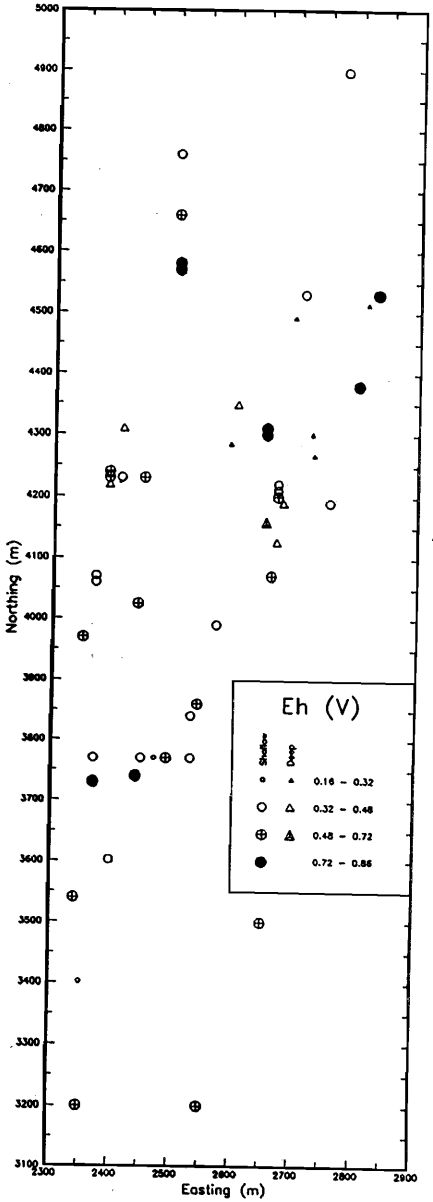

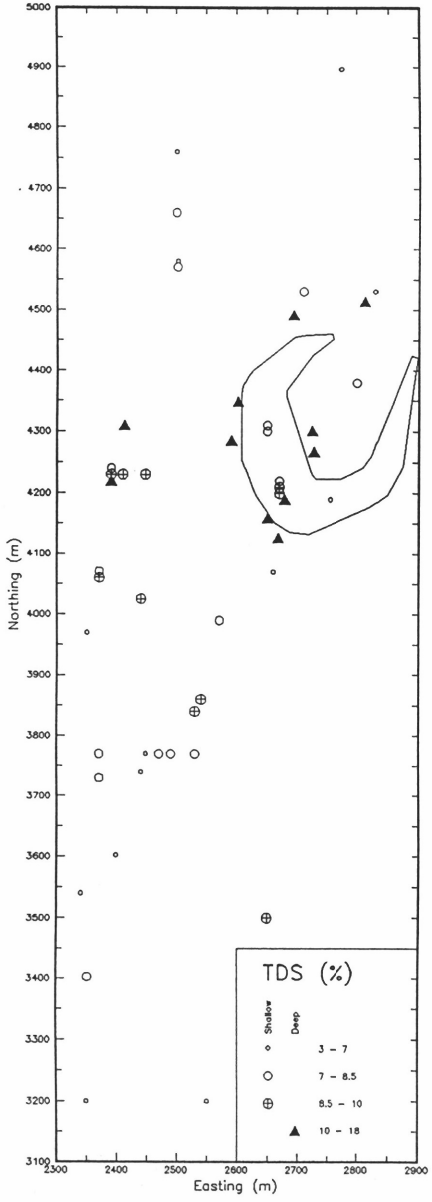

Fig. 8 TDS for water samples in the Panglo Mine Area.

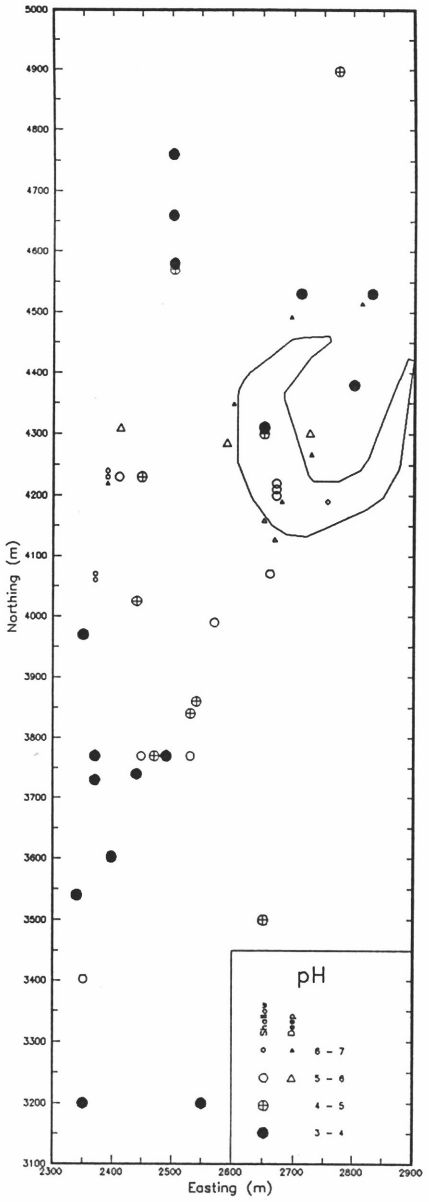

Fig. 9 pH for water samples in the Panglo Mine Area.

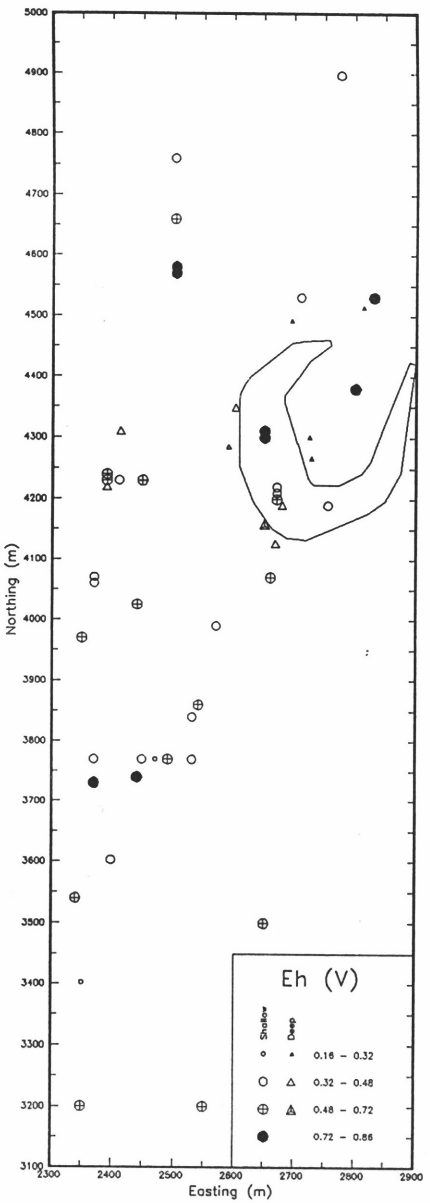

Fig. 10 Eh for water samples in the Panglo Mine Area.

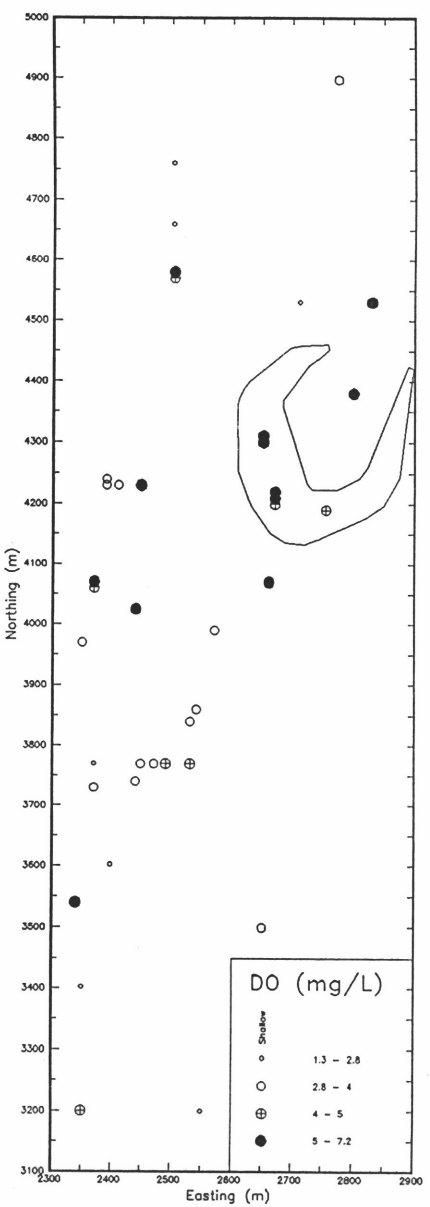

Fig. 11 Dissolved Oxygen (DO) for water samples in the Panglo Mine Area.

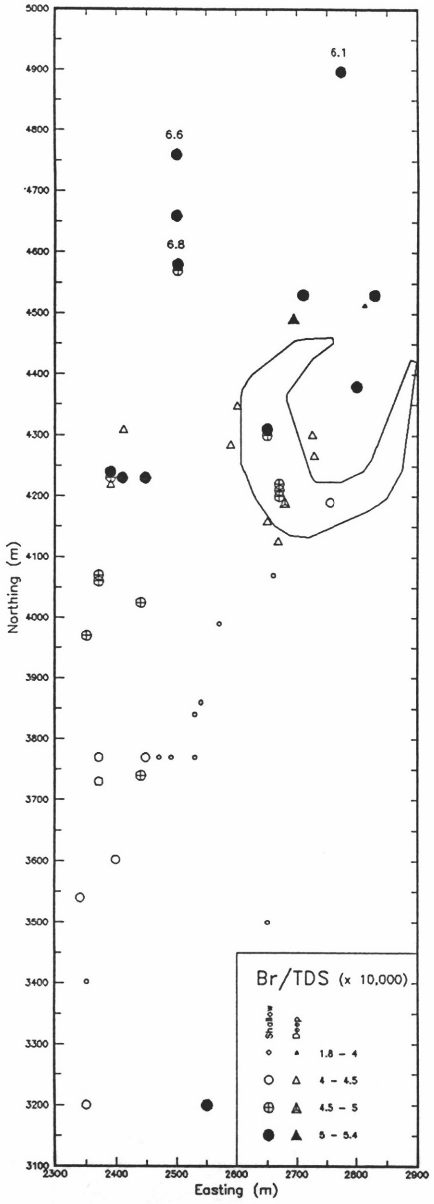

Fig. 12 Br/TDS for water samples in the Panglo Mine Area.

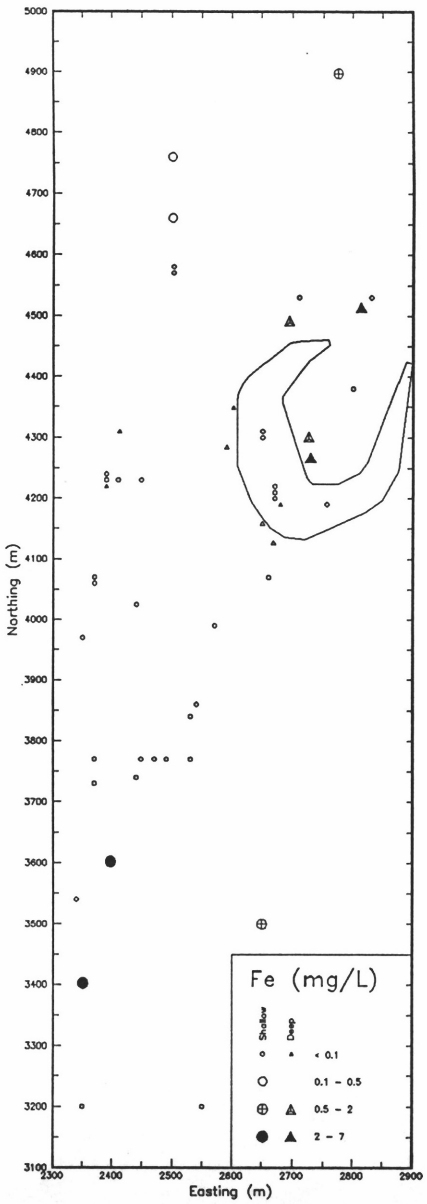

Fig. 13 Fe for water samples in the Panglo Mine Area.

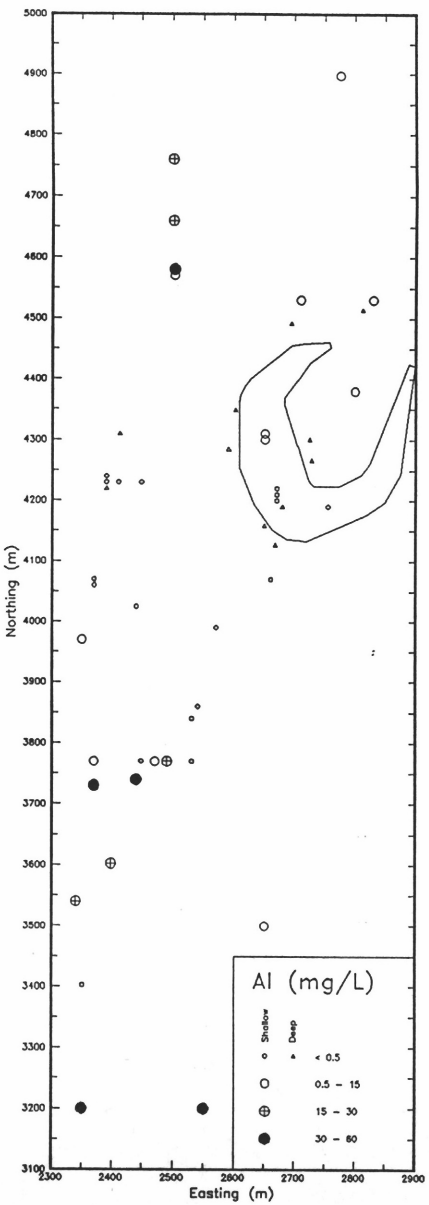

Fig. 14 Al for water samples in the Panglo Mine Area.

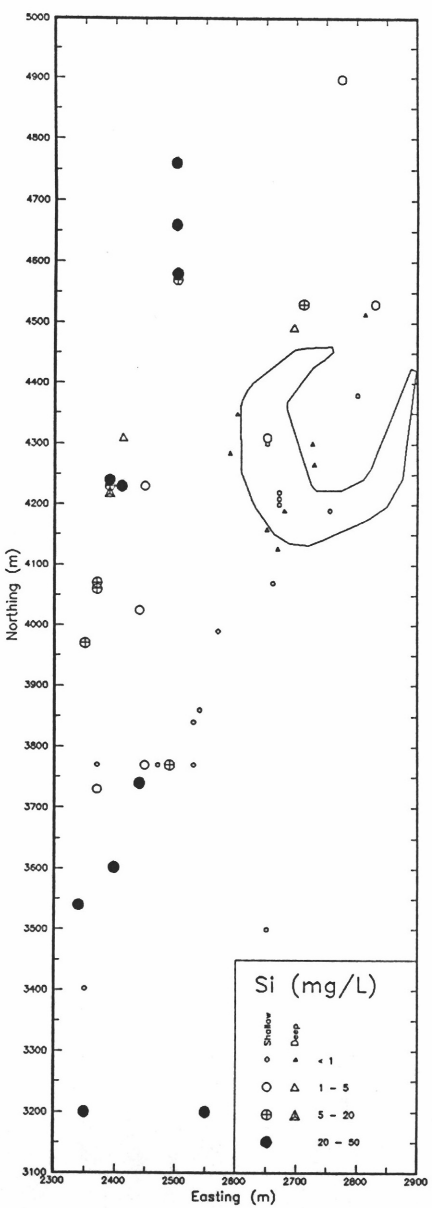

Fig. 15 Si for water samples in the Panglo Mine Area.

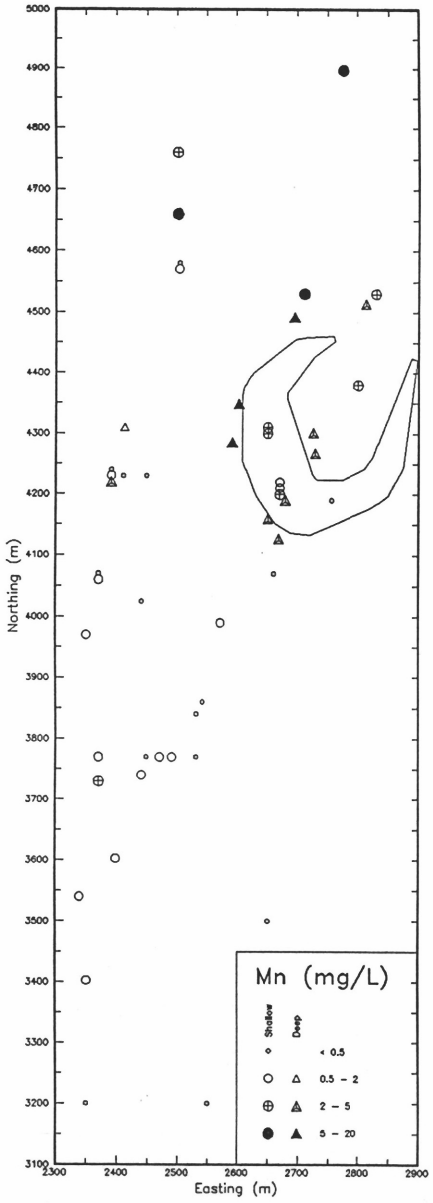

Fig. 16 Mn for water samples in the Panglo Mine Area.

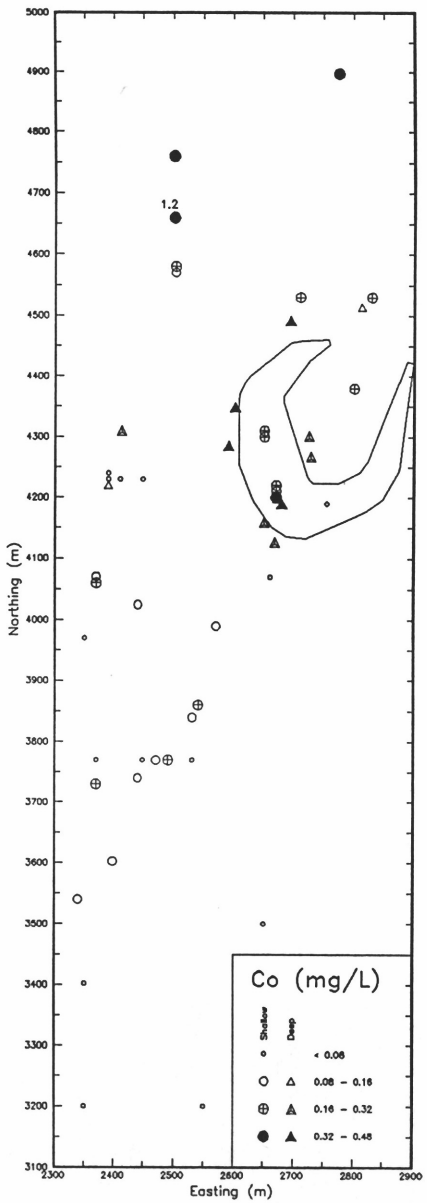

Fig. 17 Co for water samples in the Panglo Mine Area.

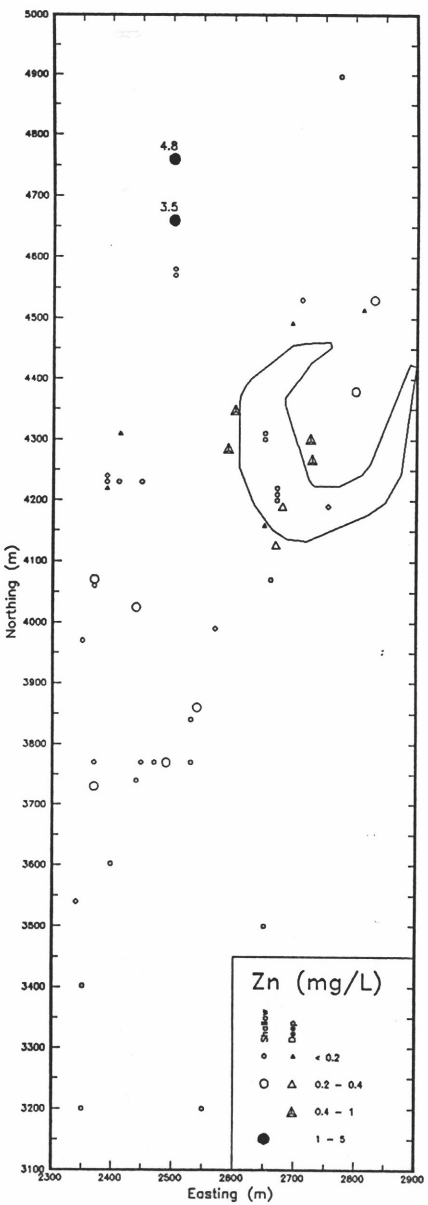

Fig. 18 Zn for water samples in the Panglo Mine Area.

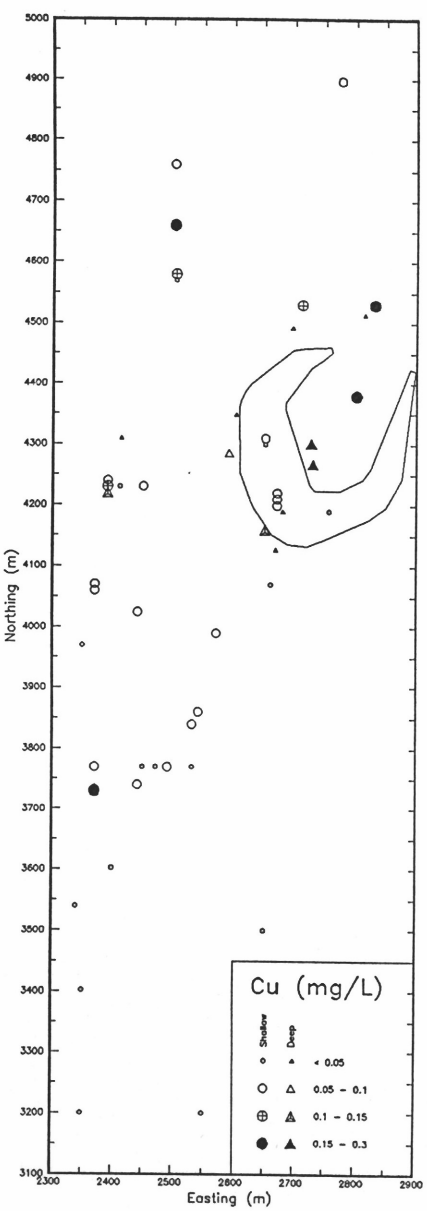

Fig. 19 Cu for water samples in the Panglo Mine Area.

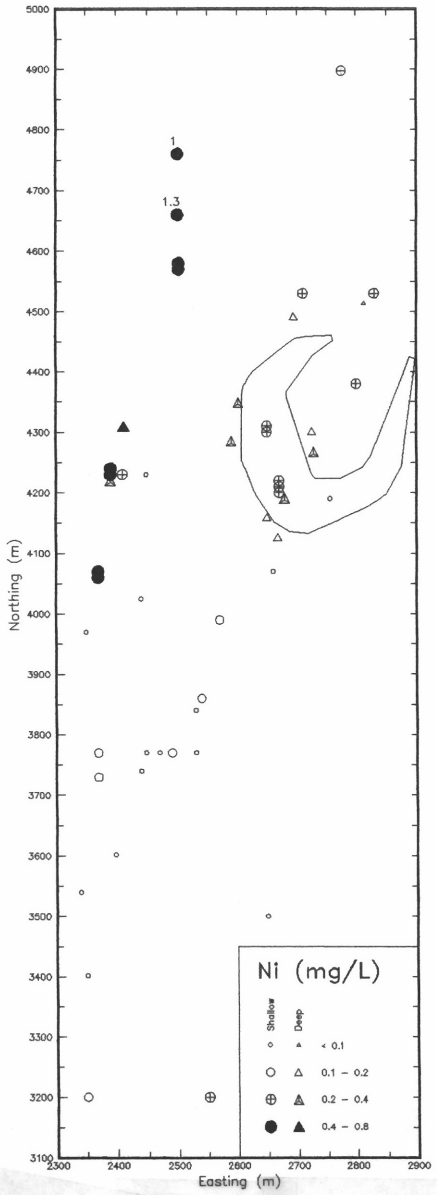

Fig. 20 Ni for water samples in the Panglo Mine Area.

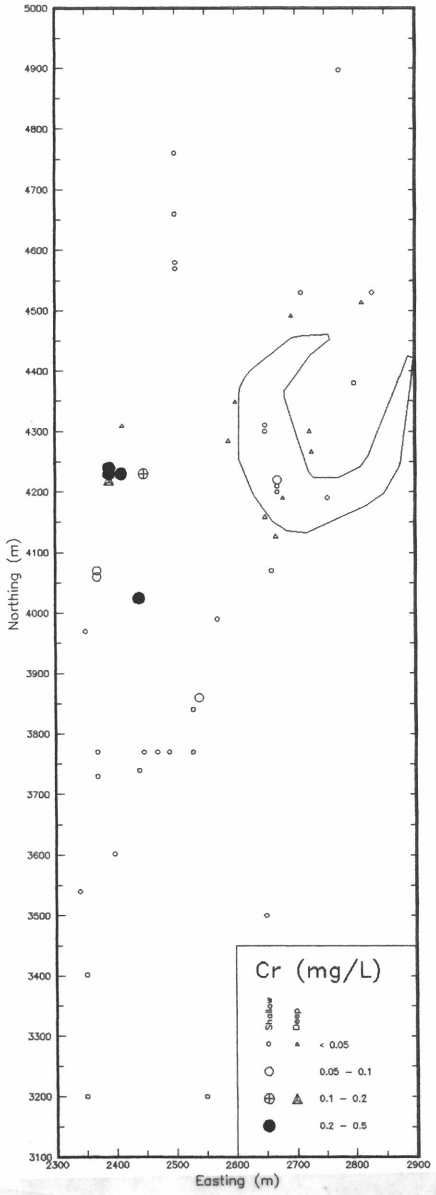

Fig. 21 Cr for water samples in the Panglo Mine Area.

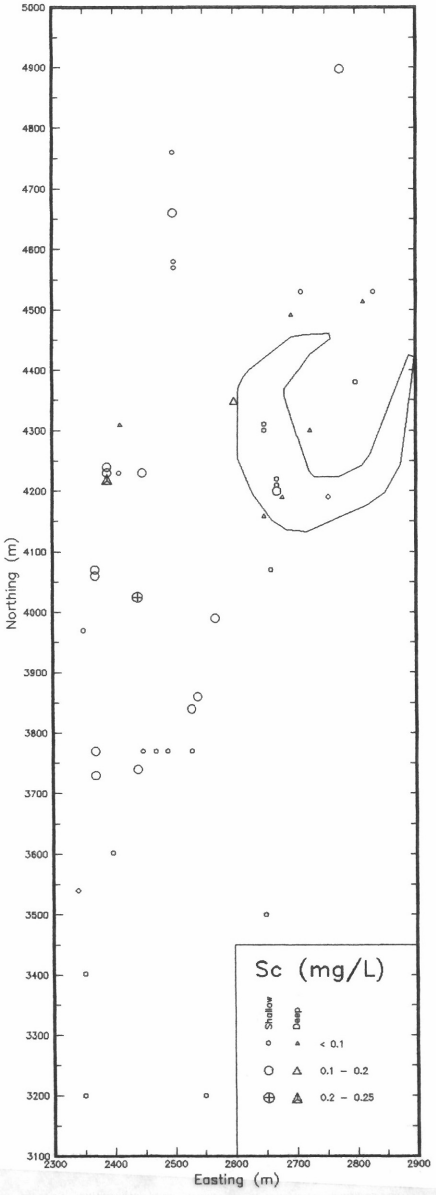

Fig. 22 Sc for water samples in the Panglo Mine Area.

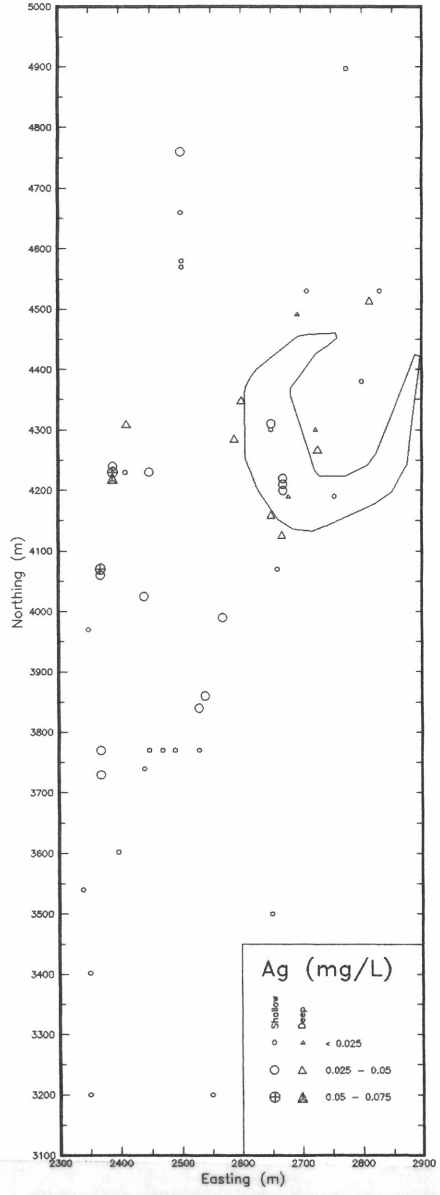

Fig. 23 Ag for water samples in the Panglo Mine Area.

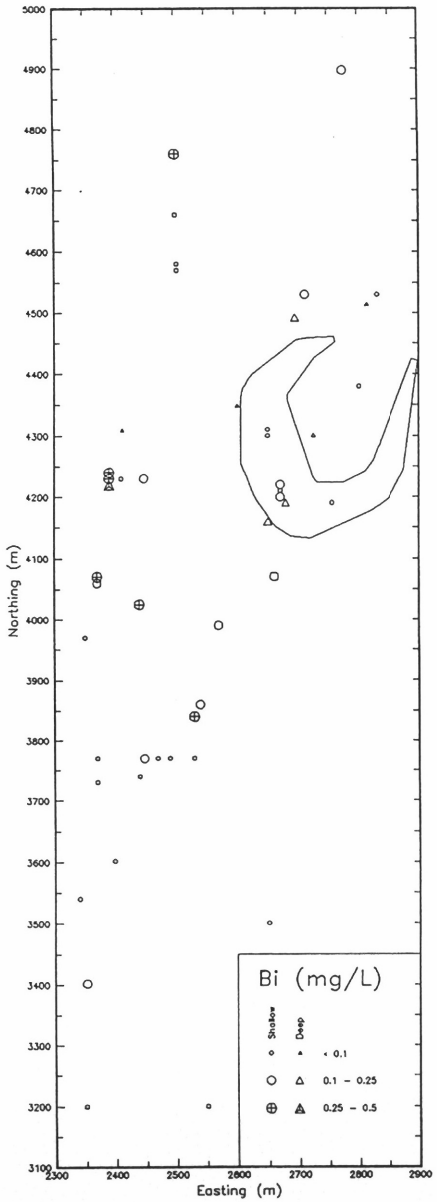

Fig. 24 Bi for water samples in the Panglo Mine Area.

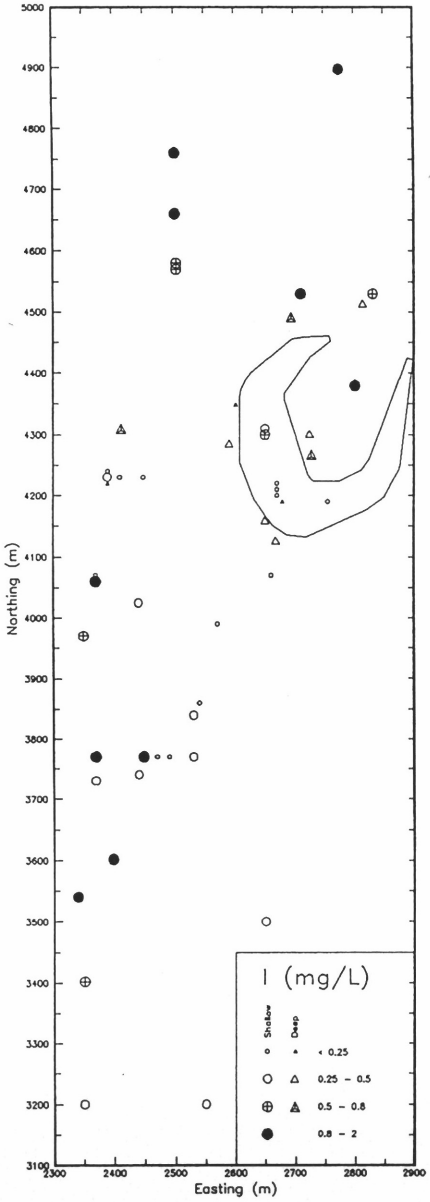

Fig. 25 I for water samples in the Panglo Mine Area.

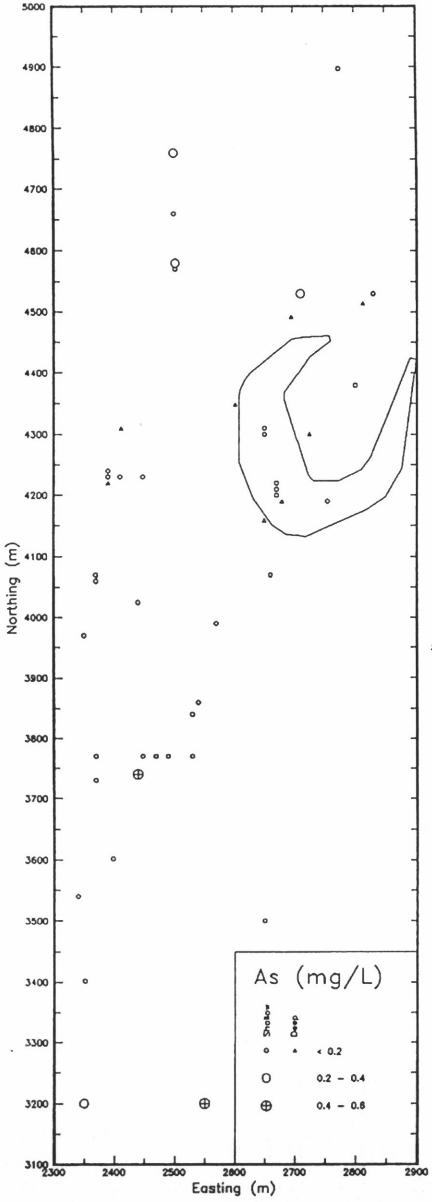

Fig. 26 As for water samples in the Panglo Mine Area.

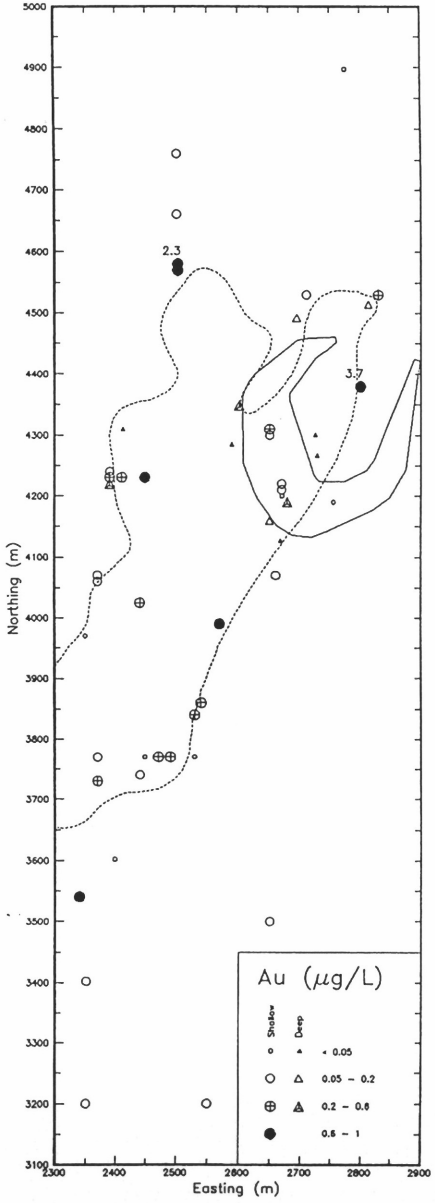

Fig. 27 Au for water samples in the Panglo Mine Area (with superimposed Au supergene expression).

Topographic and drainage details for the Panglo mine area are shown in Fig. 5. The area lies at an elevation of 340 to 350 m above mean sea level with a gentle slope across the north part of the area, with a remnant laterite hill at grid co-ordinates 2850E, 4580N. The southern part of the area has a number of features:

(i) the laterite hill centered at about 2400E, 3800N;
(ii) outcropping shale at about 2700E, 3800N;
(iii) a strongly defined southward drainage between these two features.

Presumably, groundwater flows through a number of different aquifer systems, such as fractured rocks at depth, various regolith materials closer to the surface, and the pan drainage system in the south-west of the study area.

The watertable contours for the Panglo deposit, based on the depths to water measured during sampling, are shown in Fig. 6. The watertable is strongly defined by the surface drainage contours (Fig. 5). The northern section (4000 - 5000 N) shows a gentle downward slope from 340 to 337 m. Over the area of strongly defined surface drainage (3600 - 4000 N), the watertable decreases more steeply, before draining westward at 3400 N, closely following the surface drainage. The aquifer system may be discontinuous, particularly in the north and at depth.

3.3. Major Element Hydrogeochemistry

The total dissolved solids (TDS) data for the region (Fig. 8) do not show any clear spatial trend for the surface samples, though there is an increase in salinity with depth. The major soluble elements are HCO_3^-, SO_4^-, Cl^-, NO_3^-, Br^-, Na^+, K^+, Mg^{2+}, Ca^{2+}, Sr^{2+} and H_4SiO_4 [1] . The waters are dominated by Na and Cl and most of the major ions show a very strong correlation with TDS (*e.g.* Fig. 32). The principal exceptions are HCO_3, Si and, to a lesser degree, Ca and Sr.

As will be discussed in this and later Sections, all of the deep waters have similar relative compositions, differing mainly in total salinity. Thus P8 and P31 (sampled from boreholes through ultramafic rocks) have similar compositions to waters sampled from mafic rocks (P42-P50; Appendix 1), suggesting only minor groundwater/rock interactions at depth. In comparison the major (and minor) element compositions of the shallow waters is highly variable, being strongly controlled by factors such as the geology, weathering processes and hydrology. Thus the shallow waters have been in contact with the regolith for sufficiently long to permit major interactions between the groundwater and the weathered or weathering phases.

A plot of HCO_3 content indicates that the concentration of HCO_3 is, as expected, dominated by pH effects (Fig. 28) [2] . Samples are clearly divided into a high pH (>5.5), high HCO_3 group, and a low pH (<5.5), low HCO_3 group. This difference may represent interaction of acid waters (<5.5) with solid carbonate. Thus, if an acid water contacts any carbonate minerals it will be neutralized, *e.g.*:

---

[1] Note that in general elements will be denoted purely by symbol, without valence information: *i.e.* Cl rather than Cl^-

[2] Note that the dashed line in this and later Figures shows the concentration of the designated species if it had the same ratio to TDS as in sea water. This is commonly known as the seawater dilution/evaporation line (hereafter called the seawater line). This line is horizontal for element vs. pH plots (*e.g.* Fig. 28), indicating the sea water concentration of this species, and will be an inclined line for element vs. TDS plots (*e.g.* Fig. 28), indicating the sea water dilution/evaporation line. Where the seawater line is referred to in the figure description but cannot be seen in the plot, this will be because the seawater concentration of the element is to low to be distinguished at the scale used.

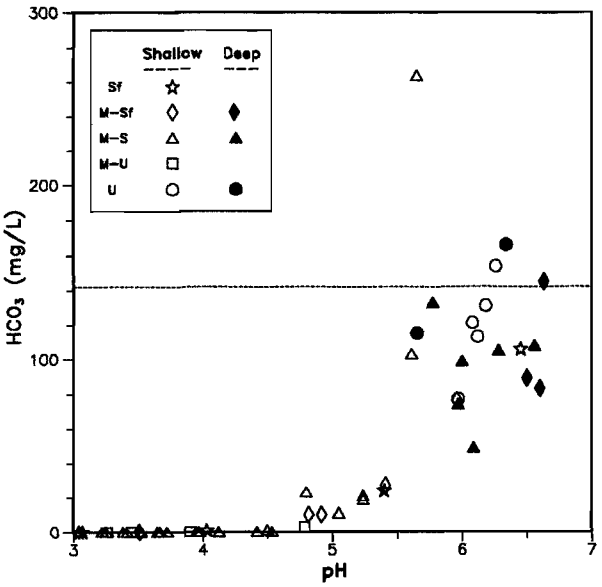

Fig. 28 HCO_3 vs. pH, with the seawater concentration shown as the dashed line.

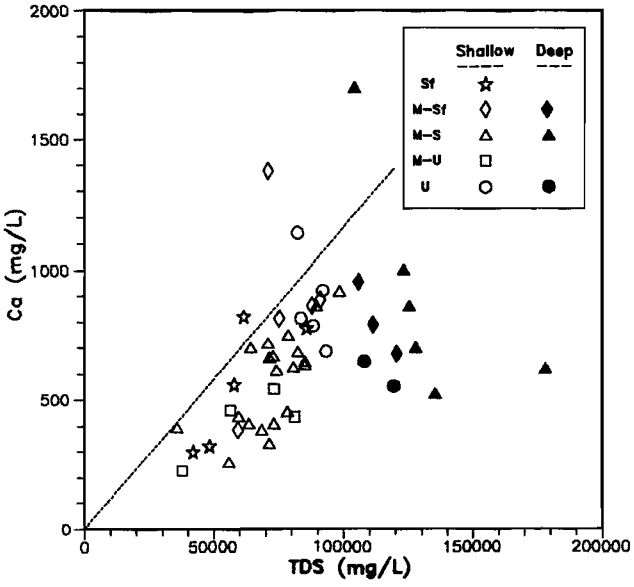

Fig. 29 Ca vs. TDS, with the seawater line shown as the dashed line.

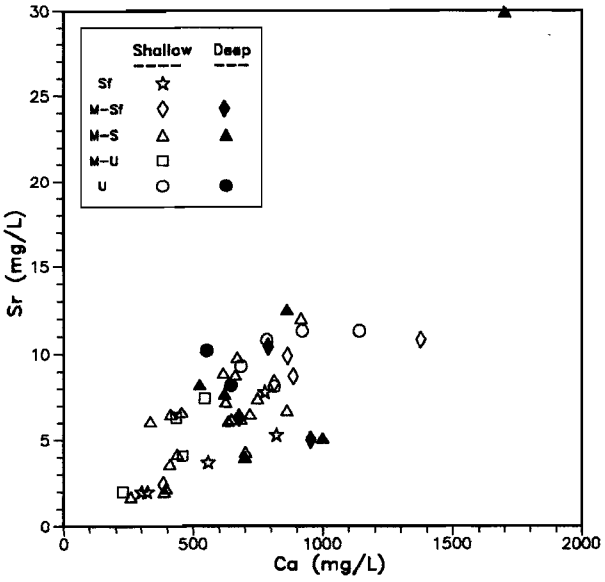

Fig. 30 Sr vs. Ca.

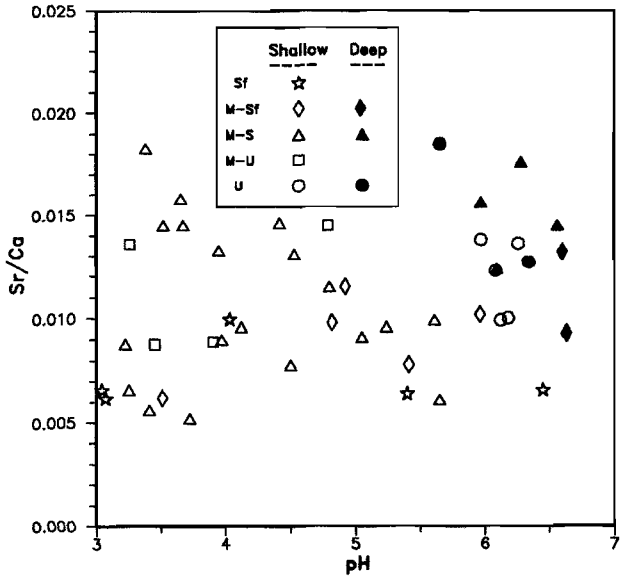

Fig. 31 Sr/Ca vs. pH.

$$CaCO_{3(S)} + H^+ \Rightarrow Ca^{2+} + HCO_3^- \quad \text{...(1)}$$
(Calcite)

and will have a high HCO_3 concentration. This proposal is compatible with speciation analysis (Section 3.8) which indicates that the waters approach saturation with respect to the carbonate minerals calcite and dolomite [$CaMg(CO_3)_2$] at neutral pH. The reaction also predicts high Ca concentrations in the high pH solutions, but this effect is not observed. Soluble Ca may be lost by gypsum ($CaSO_4 \cdot 2H_2O$) precipitation, and speciation analysis (Section 3.8) suggests that the waters are in active equilibrium with gypsum.

Such an hypothesis explains not only the clear distinction between acid and near neutral waters, but also the major variation in pH across short distances (Fig. 9). The regolith at this site contains carbonates close to the surface, as indicated by the high concentrations of Ca and/or Mg in the top metre of drill core, particularly over mafic and ultramafic rocks (Scott, 1989a,b). Any interaction with even minor amounts of carbonate will act to neutralize acid groundwaters. Thus a weathered profile having only low abundances of carbonate minerals could neutralize acid waters over extended time periods before the carbonate is totally consumed.

The alkaline earth metals Ca (Fig. 29) and Sr show a weak correlation with TDS up to about 100,000 mg/L. The saline deep waters show a plateau in concentrations of these elements above 100,000 mg/L TDS. Such an effect can be caused by precipitation of these metals, either as the carbonates calcite and strontianite ($SrCO_3$), or as the sulphates gypsum and celestine ($SrSO_4$). There is a very strong correlation between Ca and Sr, which suggests that the distributions of these elements are controlled by similar factors.

Further information may be obtained by plotting the Sr/Ca ratio against another solution variable such as pH (Fig. 31). Although there is some variation in this ratio, groundwaters in contact with shales have a particularly low Sr/Ca ratio, relative to the other waters, indicating them to be relatively lower in Sr [3].

The other major elements [Cl, SO_4, Na, Mg and, to a lesser degree, K and Br (see below)], correlate closely with each other. Thus a plot of Cl vs. TDS (Fig. 32) yields a straight line, with good agreement with the seawater line. In order to observe any systematic deviations from the seawater line for any of these elements, ion concentrations were converted to meq/L and divided by the total anions (for Cl, SO_4, Br and I) or cations (for Na, Mg, K, Ca and Sr). The average results for Panglo waters and for sea water are listed in Table 2.

The Panglo waters have higher proportions of Na and Cl and lower proportions of Mg, Ca, Sr and SO_4. Data for Br and K show more extreme differences and are discussed below. Data for I (Section 3.9) indicates that it is independent of TDS.

Bromine is dramatically lower in the Panglo waters (by about 80%), relative to sea water. It is highly soluble, even in hypersaline brines, and this data strongly suggest that most of the present salinity has been caused by dissolution of halite, rather than by evaporation. In addition, the Br data, unlike that those for ions such as SO_4, Cl, Na and Mg, deviate markedly from linearity (Fig. 33).

[3] See also Table 5

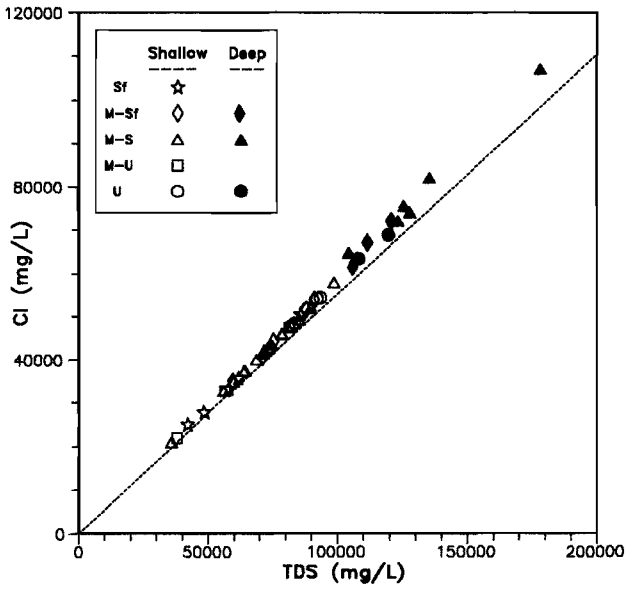

Fig. 32 Cl vs. TDS, with the seawater line shown as the dashed line.

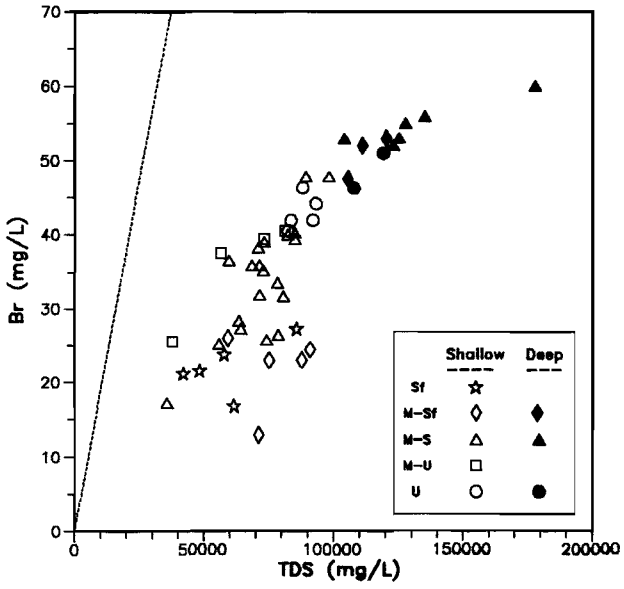

Fig. 33 Br vs. TDS, with the seawater line shown as the dashed line.

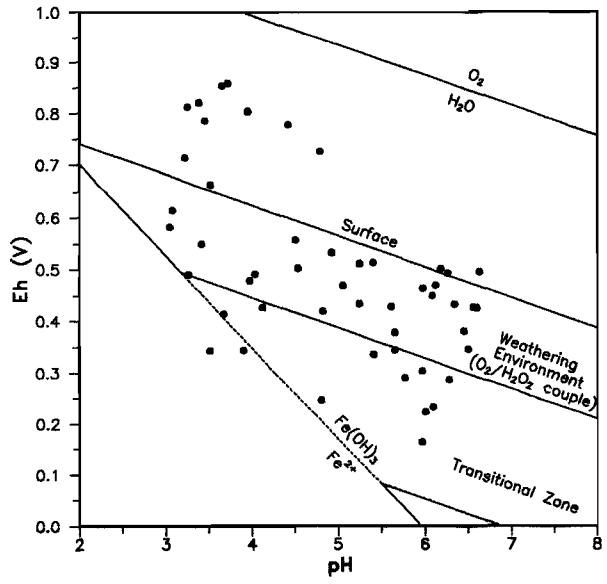

Fig. 34 Sato's (1960) summary of groundwater pH/Eh controls, with superimposed pH/Eh values for the Panglo samples.

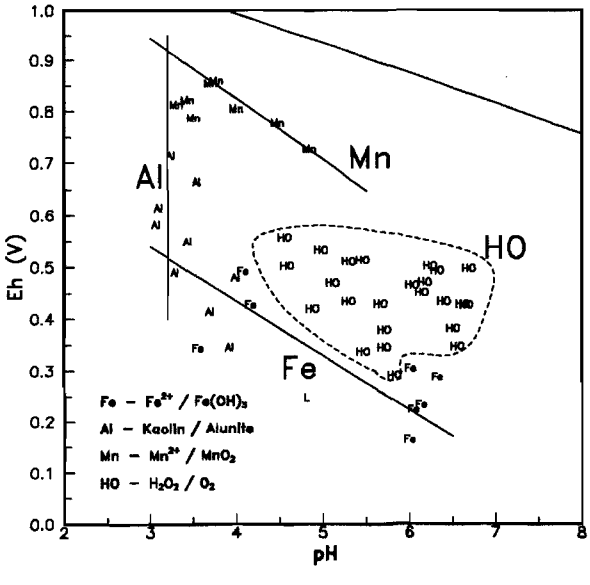

Fig. 35 Hypothesized pH/Eh controls model for Panglo, with superimposed pH/Eh values for the Panglo samples. See text (Section 3.4.1) for details.

Table 2: Percentage Ion Concentrations for Average Panglo Water, and Sea Water.

Element	Percentage meq/L	
	Averaged Panglo	Sea Water
Cl	93.7	90.2
SO_4	6.2	9.3
Br	0.03	0.14
I	0.00030	0.00008
Na	81.9	76.4
Mg	15.4	18.6
Ca	2.4	3.3
K	0.12	1.6
Sr	0.012	0.030

This deviation was investigated further. The spatial variation in the Br/TDS ratio (Fig. 12) shows that:

(i) water in the shales in the south east of the study area have (with the exception of one, very low TDS, sample) low Br/TDS ratios;

(ii) water samples in the mafic-ultramafic rock/units showed a general decrease in Br/TDS from north to south;

(iii) Br/TDS decreases markedly with depth.

This effect can also be partially seen in Fig. 33; the shallow Sf and M-Sf waters have lower Br contents than the mafic and ultramafic waters, while the deep waters tend to plateau in Br concentration while TDS contents continue to increase.

Observation (i) suggests that the shale and mafic-ultramafic systems represent two separate groundwater systems, with a major permeability barrier between them, possibly associated with a major fault system in this area (Figs. 3 or 7). Observations (ii) and (iii) imply that water travelling southward or downwards is dissolving halite, increasing salinity without increasing Br concentration, resulting in lowered Br/TDS ratios at depth or along the south tending groundwater flow-path (Fig. 12).

The K content appears to be strongly affected by the chemistry of Al and is discussed in detail in Section 3.4.4. Of particular note for this discussion is that K concentration is lowered to a similar degree to Br (about 90% lower, relative to sea water; Table 2) within the Panglo study area.

These ratio differences, and the presence of halite within the weathered profile (Scott, 1989a,b), suggest that a significant proportion of the salinity is caused by dissolution of halite, resulting in waters proportionally higher in Na and Cl and lower in other major ions than normal sea water (Table 2). Presumably, halite was deposited during a previous arid period when the waters in the area were more saline than present. Present-day groundwaters are now dissolving halite. Such a change could have resulted from changes in the backflow of saline waters from the playa to the south; changes in climate; or raising of the watertable after partial clearing, in a manner similar to that causing salinity problems in agricultural areas in the south-west of Western Australia.

3.4. pH/Eh Data

3.4.1. General Description

The pH and Eh of groundwaters describe important chemical attributes. The pH is the measure of the hydrogen ion (H^+) activity, which in aqueous solutions is present as hydronium ion (H_3O^+); pH values below 7 indicate acid solutions, whereas those above 7 are alkaline. The Eh is an analogous measure of the electron (e^-) activity. High values of Eh denote oxidizing conditions, and low values denote reducing conditions. However, Eh differs from pH in that though water can adsorb or release H^+ to form H_3O^+ or OH^-, enabling easy and reproducible measurement of pH, the H_2O molecule does not react with electrons, so that measurement and interpretation of Eh is more complicated than for pH.

Eh is controlled by reduction-oxidation couples such as Fe^{2+}/Fe^{3+} or O_2/H_2O_2, depending on the chemical environment. The Eh of solutions at depth, where pyrite is oxidizing, will be controlled by couples such as SH^-/S or SO_3^{2-}/SO_4^{2-}, which give a low Eh. Closer to the surface, Fe^{2+} begins to oxidize to Fe^{3+}. This ion quickly hydrolyses and precipitates, and Eh is controlled by the $Fe^{2+}/Fe(OH)_{3(S)}$ couple. In oxidized solutions, the O_2/H_2O_2 couple may dominate Eh, though more weakly than the $Fe^{2+}/Fe(OH)_{3(S)}$ couple, due to the slow kinetics of the reaction [4] .

Consideration of such reactions led to Sato's (1960) summary of groundwater pH/Eh controls, which is shown graphically in Fig. 34. He divided groundwaters into three environments: the depth environment which is dominated by the chemistry of magnetite/hematite and SH^-/SO_4^{2-}; a transitional zone; and the upper weathering environment, where groundwater Eh is dominated by the O_2/H_2O_2 couple. Additionally, pH is maintained below 10, under control of carbonate precipitation, and in acid conditions pH and Eh are controlled jointly by the $Fe^{2+}/Fe(OH)_{3(S)}$ couple. A compilation of groundwater Eh and pH determinations by Baas Becking *et al.* (1960) agrees with this model.

The pH/Eh values for the Panglo samples are superimposed on Fig. 34. Although some of the waters do fit into the "weathering environment" category, the very oxidizing waters show characteristics that differ from the Sato model. A more appropriate model for Panglo, based on both Eh and pH data, and on the chemical concentrations of elements such as Fe, Al and Mn, is indicated in Fig. 35. Waters are divided into four major categories:

group Fe -waters with Fe contents > 0.5 mg/L;

group HO -waters fitting the "weathering environment" category, as given by Sato (1960), *i.e.* controlled by the O_2/H_2O_2 couple;

group Al -acid, aluminous waters, pH < 4.0;

group Mn -waters with pH/Eh controlled by the redox chemistry of Mn.

The chemical characteristics of these waters are given in Table 3. The locations of the waters in each group (Fig. 36) appears to be controlled by a number of factors such as geology, hydrology and degree of oxidation of the water. This will be discussed in the following Sections.

[4] A more fundamental description of Eh theory and the problems involved in measurement and interpretation is given in Hostettler (1984).

Table 3: Chemical Characteristics of the pH/Eh Classes.

Group	Description	Chemistry	Sample Nos.
HO	"Moderately Oxidised"	$4.5 \leq$ pH Fe < 0.5 mg/L	1-15,18,21,30,31,45-47,49,50
Fe	"Fe rich"	Fe > 0.5 mg/L	23,25,26,41,42,43,44,48
Al	"Acid Al-rich"	pH < 4 / Eh < 0.72 V Fe < 0.5 mg/L	17,20,24,27-29,36,39,40
Mn	"Mn rich Oxidised"	Eh > 0.72 V Mn $\geq$ 0.5 mg/l	16,22,32-35,37,38
L	"Low Eh" (anomalous)	Eh < 0.3 V Fe < 0.5 mg/L	19

3.4.2. Group Fe Waters

Measured oxidation potentials for these waters are dominated by Fe^{2+} oxidation reactions. This group includes all waters with Fe concentration greater than > 0.5 mg/L, above the lowest concentration at which a dissolved redox active species can influence the potential of an inert electrode (considered to be about 10^{-6} M or 0.05 mg/L for soluble Fe; Doyle, 1968). This effect is demonstrated by the inverse relationship between soluble Fe and Eh (Fig. 37). The soluble Fe is probably derived from the oxidation of pyrite and other sulphide minerals:

$$2FeS_2 + 7O_2 + 2H_2O \Rightarrow 2Fe^{2+} + 4SO_4^{2-} + 4H^+ \quad \ldots(2)$$

(Pyrite)

A number of these waters are near neutrality, particularly those sampled from depth (*e.g.* P42-P44 and P48). This suggests that acid production during this oxidative weathering of sulphide minerals is neutralized by acid consuming reactions, such as dissolution of carbonates (eqn. 1) or of weathering of other minerals such as feldspars to kaolinite:

$$2NaAlSi_3O_8 + 9H_2O + 2H^+ \Rightarrow Al_2Si_2O_5(OH)_4 + 2Na^+ + 4Si(OH)_4^0 \quad \ldots(3)$$

(Feldspar) (Kaolinite)

Though expected to be slow, feldspar weathering could be able to neutralize sulphide weathering, due to the slow rate of present-day oxidation of sulphides.

Deep samples were only taken in the area around the Trial Pit. The available evidence, though limited, suggests that the deep waters containing Fe (*e.g.* P42-P44 and P48) are confined to an area north of the Trial Pit, whereas deep samples south of this point (*e.g.* P45-P47, P49 and P50) have Fe contents $\leq$ 0.1 mg/L (Fig. 13). This may be related to a relative abundance of pyrite and other sulphides to the north.

Shallow acid waters containing Fe (P23, P25 and P26; Fig. 13) were also observed in the drainage zone in the south (Fig. 5). These southern waters were malodorous, suggesting that the Fe in these waters is the result of surface biological activity.

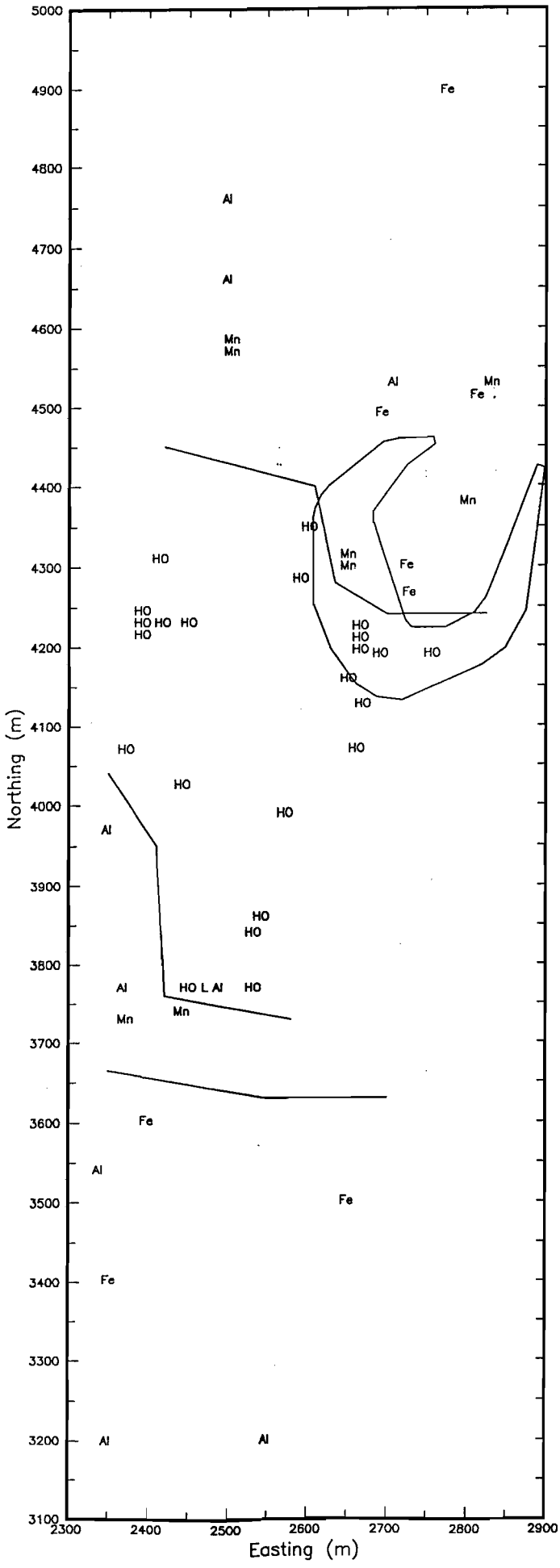

Fig. 36 Spatial location of pH/Eh groups. See text (Section 3.4.1) for details.

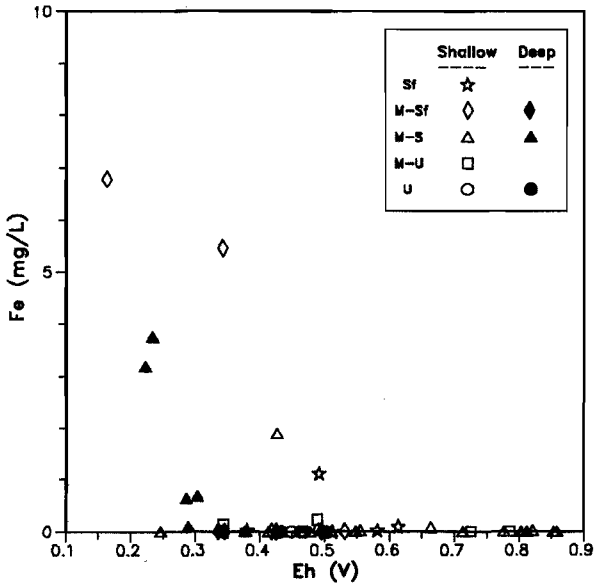

Fig. 37 Fe vs. Eh

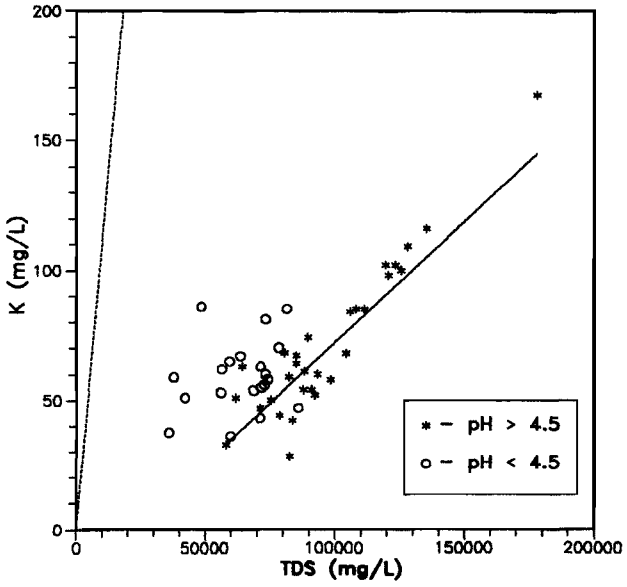

Fig. 38 K vs. TDS, with the seawater line shown as the dashed line. See text (Section 3.4.4) for details.

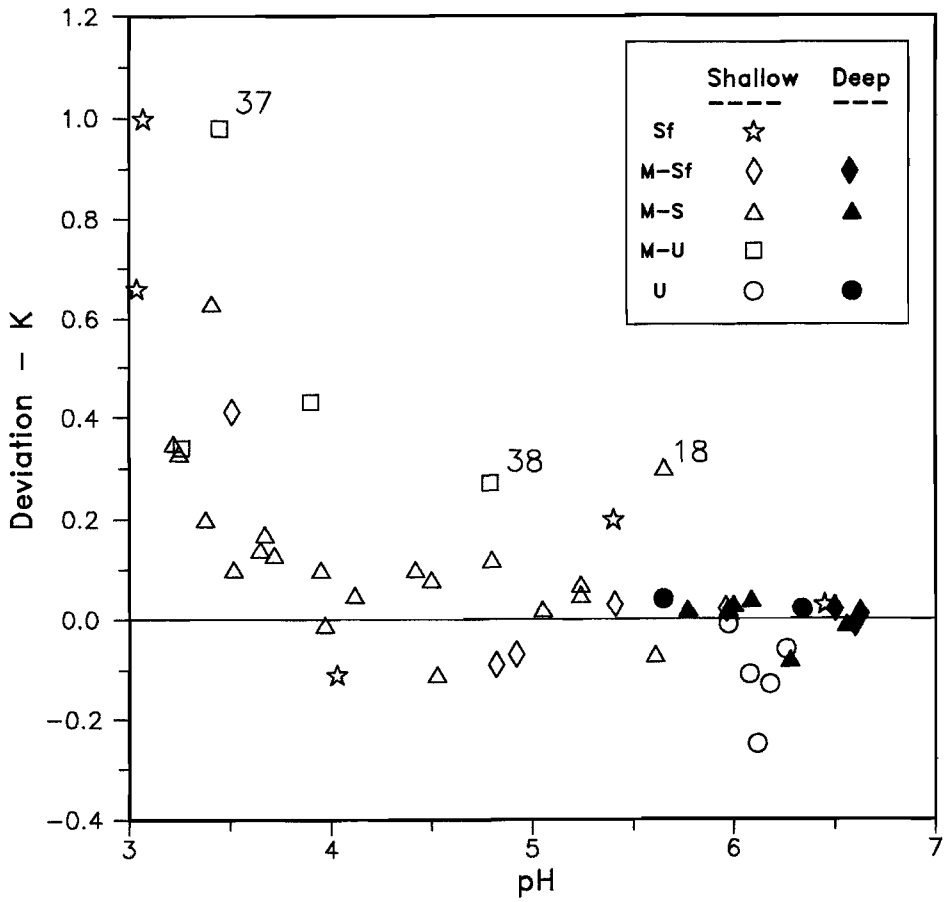

Fig. 39 Deviation of the points from the line of best fit in Fig. 38 vs. pH. Important points are noted using the sample number. See text (Section 3.4.4) for details.

3.4.3. Group HO Waters

These waters have specific pH/Eh properties. They are only weakly acidic (pH $\geq$ 4.5) and do not appear to be strongly controlled by any redox couple, such as Fe^{2+}/Fe^{3+} in the group Fe waters. This is inferred from the equilibration times for Eh measurements in the field:. the measured Eh values for HO waters (and Al waters; Section 3.4.4) generally took 5 to 15 minutes to stabilize, and in some cases were still drifting after one hour. Although there are redox couples within the range measured for these waters, the most probable being H_2O_2/O_2 (Sato, 1960), they have slow kinetics and the solution Eh will be poorly poised, consistent with their poor redox stability.

The group HO waters can be divided into 3 sub-groups:

(i) shallow waters in contact with mafic rock and/or shales (P1 - P5, P9, P10, P13 - P15, P18 and P21; Fig. 36), which range from pH 4.5 to 6.45.

(ii) deep waters (P45-P47, P49 and P50) in the Trial Pit and to the south (Fig. 36), which vary between pH 5.8 and 6.6;

(iii) shallow and deep waters in contact with ultramafic rocks (P6 - P8, P11, P12, P30 and P31; Fig. 36), which vary between pH 5.65 and 6.35;

The group HO waters (both shallow and deep) all occur in a band from about 4400N to 3800N (Fig. 36). It is possible that they represent rocks that are poorer in sulphide minerals than in the Trial Pit area. As such they would release less Fe during weathering, and hence produce less acid. This sub-group is the least chemically active of the waters, being neither strongly reducing (group Fe), strongly acid (group Al) or strongly oxidizing (group Mn).

3.4.4. Group Al Waters

These waters are characterized by high acidity (pH < 4) and the spatial location of Al (Fig. 14) is strongly controlled by pH (overlay Fig. 7b). The group Al waters occur on all the rock types except for the broad ultramafic band at 2400E / 4200N (Figs. 3 and 36). With the exception of those in contact with ultramafic rocks, and their weathering products, most of the oxidized waters sampled were acid (pH < 6) to very acid (pH 3).

None of the deep waters were acid. This is possibly due to the separation of the two acid producing processes. The first process is oxidation of pyrite and other sulphide minerals (eqn. 2) which occurs at depth. This reaction is limited by diffusion of oxidizing species such as O_2, and may be neutralized by other reactions such as carbonate or feldspar weathering (eqn. 3; Section 3.4.2). The second process, which occurs closer to the surface, is the oxidation and hydrolysis of Fe ('ferrolysis'; Brinkman, 1977):

$$2Fe^{2+} + {}^1/_2O_2 + 5H_2O \Rightarrow 2Fe(OH)_{3(s)} + 4H^+ \qquad ...(4)$$

This decoupling of the two components of pyrite oxidation (eqns. 2 and 4) is commonly observed (Blowes and Jambor, 1990). As the weathered profile in which ferrolysis occurs probably does not contain potential buffering minerals such as carbonates (eqn. 1) or feldspars (eqn. 3) groundwaters may become highly acidic. Any buffering is due to the dissolution of clay minerals such as kaolinite:

$$3Al_2Si_2O_5(OH)_4 + 18H^+ \Rightarrow 6Al^{3+} + 6Si(OH)_4^0 + 3H_2O \qquad ...(5)$$
(Kaolinite)

This acid consuming reaction is offset by acid production during precipitation of the dissolved Al as sulphates such as alunite:

$$2K^+ + 6Al^{3+} + 4SO_4^{2-} + 12H_2O \Rightarrow \underset{\text{(Alunite)}}{2KAl_3(SO_4)_2(OH)_6} + 12H^+ \quad ...(6)$$

or jurbanite:

$$6Al^{3+} + 6SO_4^{2-} + 6H_2O \Rightarrow \underset{\text{(Jurbanite)}}{6Al(OH)SO_4} + 6H^+ \quad ...(7)$$

Solution species affected by these reactions are K^+, Al^{3+} and $Si(OH)_4^0$. The plot of K vs. TDS is shown in Fig. 38. The line of numerical best fit applies to samples above pH 4.5 only. The acid samples appear to be enriched in K. The deviation of the points from the line of best fit vs. pH (Fig. 39) indicates little deviation between pH 7 and pH 4, although there appear to be some minor differences with geology. The waters in contact with ultramafic rocks have slightly lower K concentrations, relative to TDS (Fig. 39) than other waters. This is particularly marked for the shallowest waters (open circles in Fig. 39). Ultramafic rocks are usually low in K and this may be causing the reduced K concentrations. In addition, products of weathering of the ultramafic minerals may tending to preferentially absorb K. Minerals such as vermiculite (observed in weathered ultramafic profiles by Scott, 1989b, 1990) may selectively exchange Na^+ for K^+ to form illite:

$$\underset{\text{(Vermiculite)}}{(Na)_{0.7}(Mg,Fe^{3+},Al)_{2\text{-}3}(Si,Al)_4O_{10}(OH)_2\cdot nH_2O} + 0.7K^+ \Rightarrow \underset{\text{(Illite)}}{K_{0.7}(Mg,Fe^{3+},Al)_{2\text{-}3}(Si,Al)_4O_{10}(OH)_2} + 0.7Na^+ + nH_2O \quad ...(8)$$

Above pH 4 any deviation of the waters from the line of best fit is minor (Fig. 39), and K is strongly correlated with TDS. Below pH 4 there is strong increase in this deviation from the line of best fit for K, which is approximately inversely proportional to pH (Fig. 39). [The contrast between pH > 4.0 and pH < 4.0 may be actually be better than that at first inspection, as the two samples above pH 4 with significantly raised K may be anomalous. Sample 38 (see Fig. 39) was collected from deeper in the same hole as sample 37 and may represent a mixing of the acid K-enriched water (sample 37) and a deeper neutral water. Sample 18 lies close (within 50m) to highly acid waters (P19, P20 and P22) and has anomalously high HCO_3 (1.6 times greater than that of the sample with the next highest HCO_3 concentration; Fig. 28). Thus, this water may represent an acid water which has been neutralized by contact with carbonate (possibly pedogenic) but which still maintains the K/TDS 'signature' from its previous acid condition.]

These data indicate that either the more acid waters are dissolving K and/or the more neutral waters are precipitating K. This phenomenon is related to the chemistry of Al minerals such as alunite (eqn. 6), jurbanite (eqn. 7) and kaolinite (eqn. 5). A plot of $\log[Al^{3+}]+3\log[OH^-]$ [5] vs. $2\log[H^+]+\log[SO_4^{2-}]$ for all of the Panglo water samples containing measurable Al is shown in Fig. 40. This diagram is in the standard format used for investigations of acid Al rich waters (van Breeman, 1973; Nordstrom, 1982; Gundersen and Beier, 1988). The x-axis is $2\log[H^+] + \log[SO_4^{2-}]$: because $\log[SO_4^{2-}]$ is relatively constant ($= -2.62 \pm 0.06$) this axis closely

[5] Note that the [ ] denote the activity of the relevant phase, rather than the concentration. This difference may be of importance in saline solutions such as those studied here. Activities were determined using the computer program PHREEQP, which uses Pitzer coefficient calculations.

proportionates to pH, so that an approximate pH scale has also been placed on the plot for clarity. The y-axis is $\log[Al^{3+}] + 3\log[OH^-]$; $[Al^{3+}]$ denotes the total activity of Al^{3+}, which may be significantly less than total Al, particularly at pH > 5.0, at which Al is dominantly present as $Al(OH)_4^-$.

The lines of equilibrium for potentially important solid phases [6] are also shown on Fig. 40. At any particular $2\log[H^+] + \log[SO_4^{2-}]$ value (*i.e.* pH), a solution in equilibrium with one of the solid phases shown in the diagram would have a $\log[Al^{3+}]+3\log[OH^-]$ value as given by the particular line. In simple terms, at any pH the lowest line is the theoretically least soluble phase. In addition, if the solutions are equilibrating with a particular mineral then the points will lie on that particular line. The two parallel lines given for jurbanite represent the range of thermodynamic constants determined for this phase: the upper line is based on the solubility constant determined by van Breeman (1973) and the lower line is based on calculations by Nordstrom (1982). Differences between these two calculated lines are relatively minor.

It can be seen from Fig. 40 that the solid phase giving the lowest theoretical $\log[Al^{3+}]+3\log[OH^-]$ (*i.e.* the least soluble phase) is jurbanite below pH 3.5, alunite between pH 3.5 and pH 5.8 and gibbsite above 5.8. Below pH 3.5, the points are close to the jurbanite lines, which is the theoretically least soluble phase under these conditions. Above pH 3.5 there is a large amount of variation: some samples are in equilibrium with alunite (the least soluble phase), whereas others are up to two orders of magnitude over-saturated with respect to alunite and appear to be in equilibrium with jurbanite. This plot may be compared with similar diagrams for groundwaters and soil solutions from acid mine drainages in Thailand, Sarawak, Pennsylvania and Kentucky (van Breeman, 1973; Karathanasis *et al.*, 1988), which show waters to be in equilibrium with jurbanite, and commonly over-saturated with respect to alunite, and with work on acid forest soils in Denmark (Gundersen and Beier, 1988), which indicated the soil solutions to be equilibrated with alunite at the surface (A horizon) and equilibrated with jurbanite (*i.e.* over-saturated with respect to alunite) at depth (B horizon).

The data suggest that waters must equilibrate only slowly with alunite and more quickly with jurbanite, allowing them to have higher Al concentrations than would be otherwise expected and become oversaturated with respect to alunite. Nordstrom (1982) states "that jurbanite provides an approximate upper solubility limit and that alunite provides a lower solubility limit. The lower limit is rarely reached because of slow nucleation and precipitation kinetics."

No jurbanite minerals have yet been found at Panglo. It should be noted that minerals occurring in very low concentrations (*i.e.* below detection) may have major effects on water chemistry. This is discussed in more detail in Section 3.8. Thus jurbanite could be occurring in low concentrations or as semi-amorphous rims on alunite, and be undetectable by standard methods, but still be actively interacting with the groundwater.

These observations on Al solubility are consistent with those for K solubility given above. Below pH 3.5, alunite is more soluble than jurbanite. Therefore, alunite will tend to dissolve and the dissolved Al reprecipitate as jurbanite:

---

[6] Note that the alunite and kaolinite lines were drawn by assuming linear relationships between non plotted variables, namely:

$$\log[Si(OH)_4^0] = 0.75 \times \{\log[SO_4^{2-}] + 2\log[H^+]\} + 3.9 \quad \text{for kaolinite}$$

and $$2\log[K^+] + \log[SO_4^{2-}] = -8.92 \quad \text{for alunite.}$$

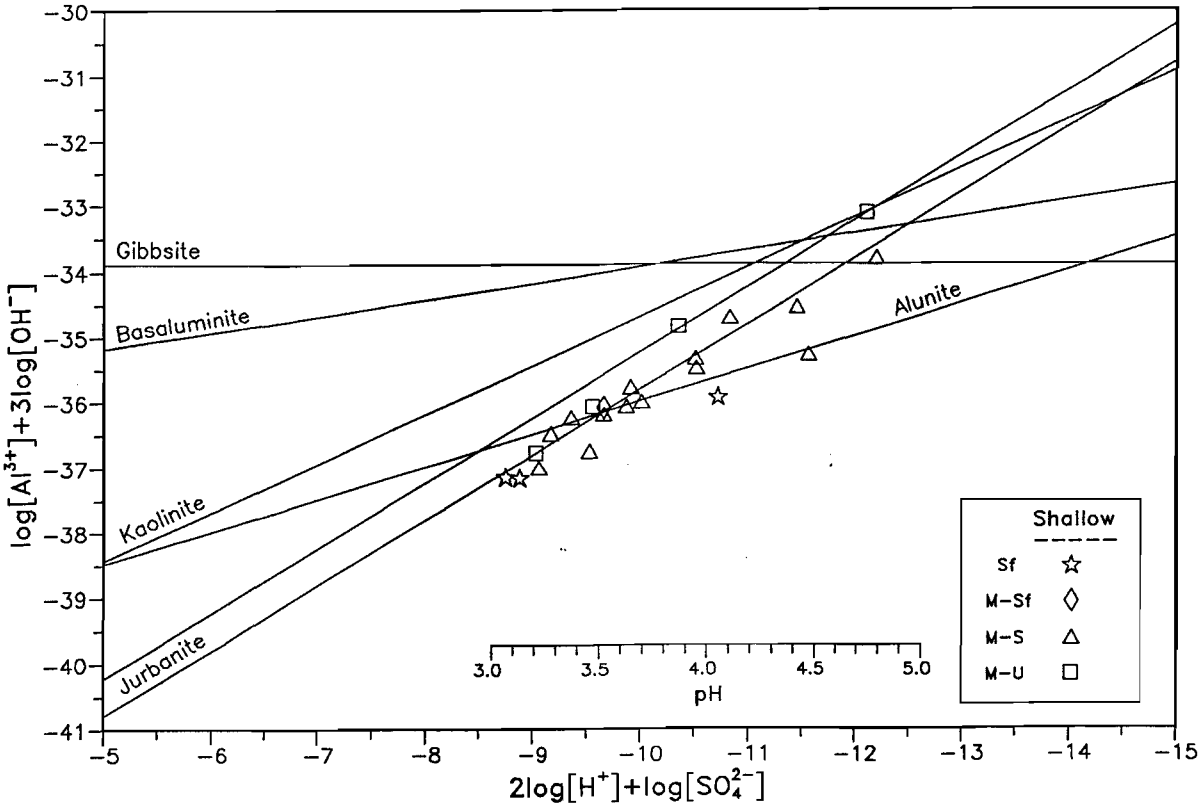

Fig. 40 Log[Al^{3+}]+3log[OH^-] vs. 2log[H^+]+log[SO_4^{2-}] for all of the Panglo water samples containing measurable Al. See text (Section 3.4.4) for details.

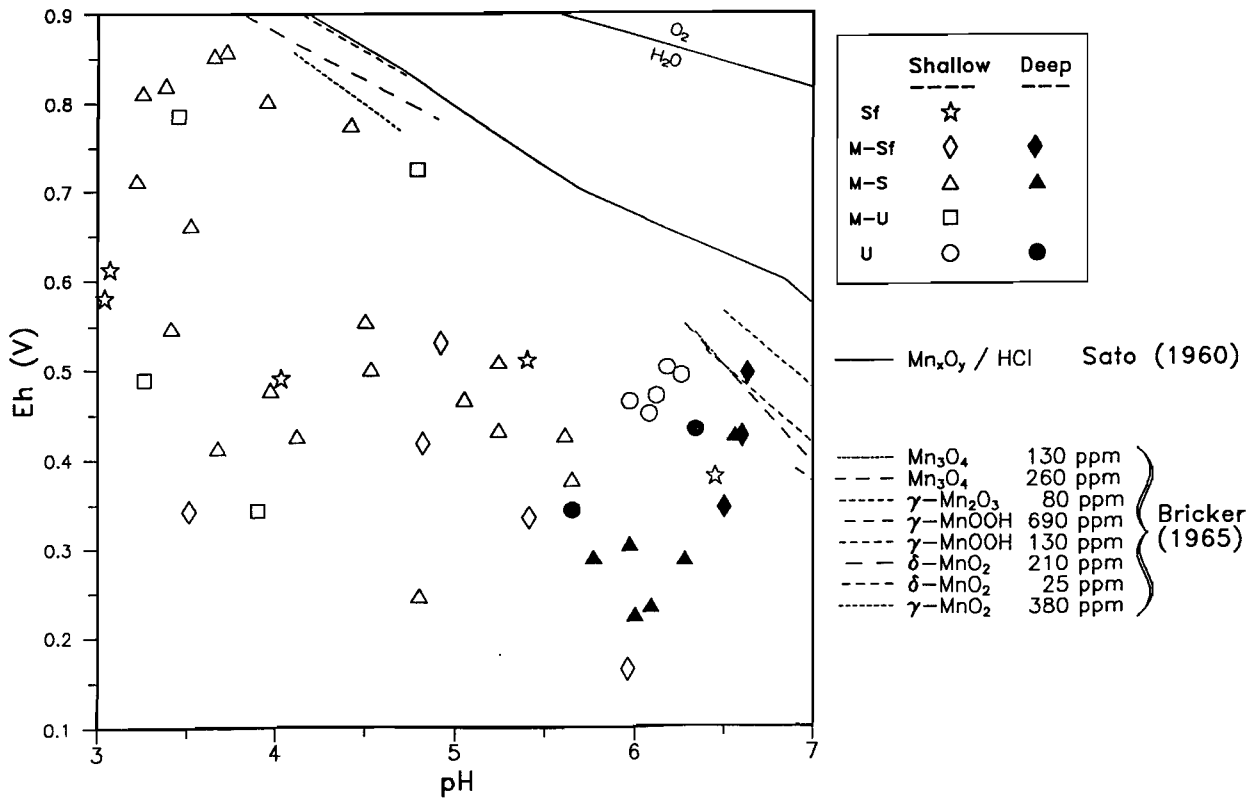

Fig. 41 Eh vs. pH for Panglo water samples. Superimposed are Eh-pH data on equilibration of Mn solutions, derived from data from Sato (1960) and Bricker (1965). See text (Section 3.4.5) for details.

$$\underset{\text{(Alunite)}}{KAl_3(SO_4)_2(OH)_6} + SO_4^{2-} + 3H^+ \Rightarrow 3Al(OH)SO_4 + K^+ + 3H_2O \quad \underset{\text{(Jurbanite)}}{} \quad ...(9)$$

This reaction results in the release of K ions, thus explaining the excess K at pH < 4 (Fig. 39).

The thermodynamic tendency of this reaction (eqn. 9) is reversed above pH 3.5, with alunite being more thermodynamically stable than jurbanite. Despite this, waters tend to remain in equilibrium with jurbanite rather than alunite, due to the slow kinetics of alunite formation.

The concentrations of dissolved Si are also increased in the acidic waters, possibly due to dissolution of kaolinite (eqn. 5) or other minerals. As indicated in Fig. 40 the Al containing waters were at equilibrium with kaolinite at higher pH, whereas at lower pH, waters were undersaturated with respect to kaolinite. Silicon concentration in the very acid waters (pH < 4) will ultimately be constrained by the solubility of amorphous Si or quartz (Section 3.8).

Thus Al hydrogeochemistry at Panglo can be summarized as follows:

(i) above pH 4.8, Al has a very low solubility and its concentration is below the detection limit;

(ii) between pH 3.5 and 4.8, kaolinite is soluble. Released Al will reprecipitate either as jurbanite or the more stable alunite. Waters more closely approach jurbanite equilibration due the slow kinetics of alunite precipitation;

(iii) below pH 3.5, both kaolinite and alunite are soluble and waters are in equilibrium with the precipitating phase - jurbanite. Conversion of alunite to jurbanite (eqn. 9) releases K into solution.

3.4.5. Group Mn Waters

As discussed previously (Section 3.4.4), groundwaters become highly acidic as a consequence of ferrolysis (mainly buffered to pH 3) . These groundwaters are depleted in Fe, and as they become further oxidized, Mn^{2+} may also oxidize and hydrolyse to solid Mn oxides and oxyhydroxides:

$$Mn^{2+} + O_2 + H_2O \Rightarrow Mn_xO_y \cdot H_2O + H^+ \quad ...(10)$$

This reaction is the Mn equivalent of ferrolysis and may control the Eh and pH of a solution in a very similar manner. Both Sato (1960) and Bricker (1965) have measured Eh and pH during oxidation of Mn-rich solutions. Results from this work are superimposed on the pH/Eh data for Panglo (Fig 41). Though there is a small amount of variation in the slope and position of the lines, depending on the stoichiometry of the particular reaction, solubility of the mineral, and Mn concentration, they all lie closely together and appear to demarcate the upper edge of the observed pH/Eh results for the Panglo waters. Thus, the zone of Mn oxidation appears to be the upper limit for the Eh of Panglo solutions. The oxidized acidic solutions, in particular, closely follow the line of Mn oxidation. As will be discussed further in Sections 3.5 and 3.8, this reaction is critical to Au mobility as it enables solutions to reach sufficiently high oxidation potentials for the oxidation of native Au.

3.4.6. Distribution of the pH/Eh Groups

The distributions of pH, Eh, DO, Fe, Mn, and the various postulated Eh/pH water groups in the mine area are shown in Figs. 9, 10, 11, 13, 16 and 36. Note that Eh is only weakly influenced by DO (Fig. 42), but rather is primarily controlled by redox couples such as $Fe^{2+}/Fe(OH)_3$, O_2/H_2O_2 or Mn^{2+}/Mn_xO_y, as discussed above (Sections 3.4.2, 3.4.3 and 3.4.5). A number of zones are suggested, as indicated in Fig. 36:

(i) a zone north of 4600N containing acidic groundwaters (Fig. 36). These waters are also highly enriched in Mn (up to 17 mg/L; Fig. 16);

(ii) a wedge shaped zone between 4600N and 4300N, encompassing about half of the Trial Pit area, which has group Fe waters at depth, and group Mn waters closer to the surface. The high Fe contents of the deeper waters indicates significant pyrite weathering (eqn. 2; Section 3.4.2). Further oxidation of the Fe^{2+} closer to the surface has produced highly acid conditions (eqn. 4; Section 3.4.4). As these acid groundwaters oxidize further, Mn^{2+} (present at high concentrations; Fig. 16) oxidizes and surface solution Eh levels are controlled by the Mn couple (eqn. 10; Section 3.4.5);

(iii) a zone comprising the southern part of the Trial Pit area (about 4300N), south to about 3750N. This has <u>all</u> of the group OH waters (and <u>only</u> group OH waters), both at depth and at the surface. The most plausible explanation for this observation is that this zone comprises an area poor in sulphide mineralization (or an area where there is little active weathering of sulphide minerals), resulting in low release of Fe, and little production of acid;

(iv) a complex zone at about 3750N, comprising waters of groups OH, Fe, Al and Mn. The presence of Fe in some samples and acid conditions in others possibly represents an area with some sulphide mineralization;

(v) a zone south of 3750N with characteristics suggesting more stagnant conditions - high Fe in the surface waters (Fig. 13), low dissolved oxygen (Fig. 11) and commonly malodorous. This area correlates with the saline drainage system in the south-west of the study area.

These pH/Eh zones occur as a result of variations in the bedrock geology, weathering reactions and the flow characteristics of the groundwater drainage system. This is discussed further in Section 3.7. In addition, the chemistry of various elements are strongly controlled by pH (*e.g.* As; Fig. 26) or Eh (*e.g.* Au; Fig. 27), and their distribution in the groundwater, will to some degree reflect the distribution of the various pH/Eh environments (Fig. 36).

3.5. Minor Element Hydrogeochemistry

Tabulated results for Al, Si, NO_3, I, Fe, Mn, Co, Zn, Cu, Ni, Cr, Sc, Ag, Bi, As and Au are given in Appendix 1. Averaged data are given in Table 4. The distribution of each element within the mine area are plotted in Figs. 13 - 27, and are discussed below. The geology, pH and Eh overlays (Fig. 7a-c) will be used extensively in this discussion.

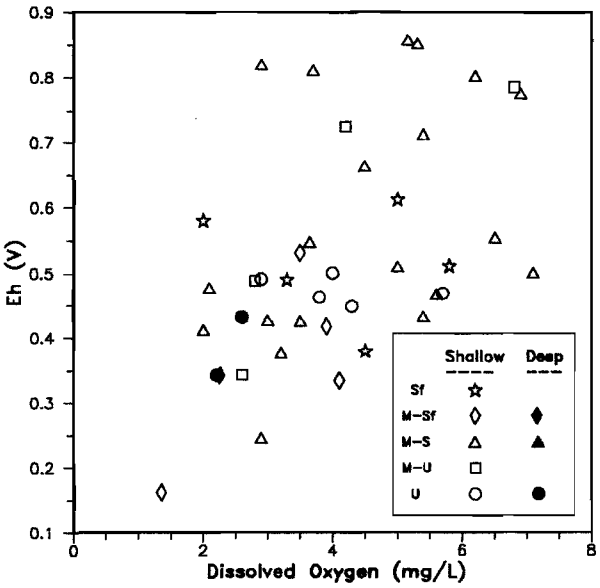

Fig. 42 Eh vs. Dissolved Oxygen.

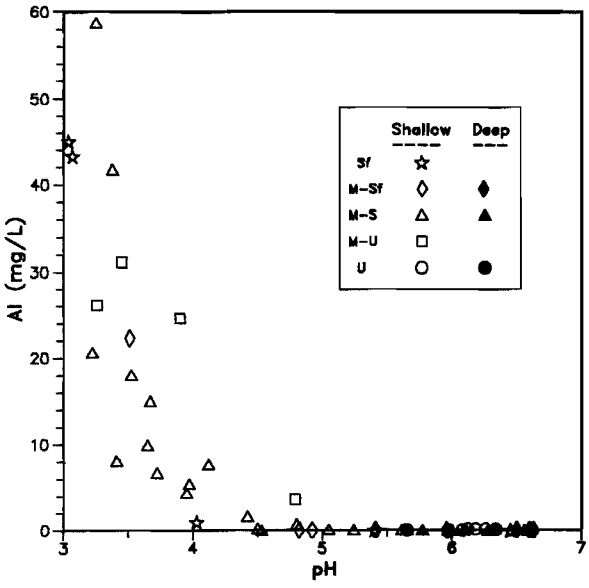

Fig. 43 Al vs. pH, with the seawater concentration shown as the dashed line.

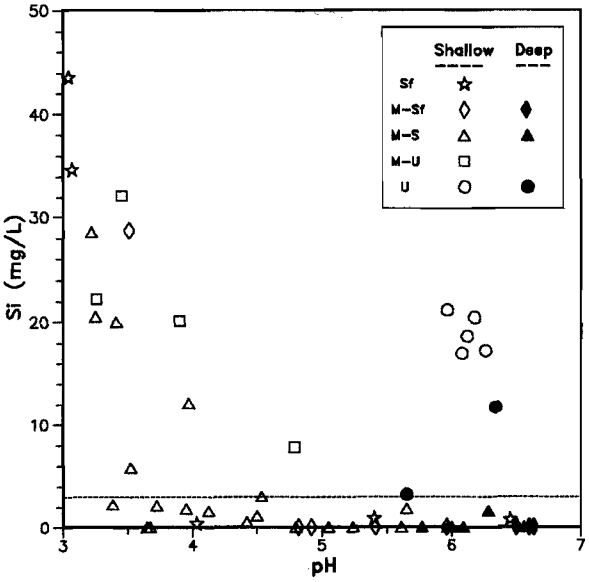

Fig. 44 Si vs. pH, with the seawater concentration shown as the dashed line.

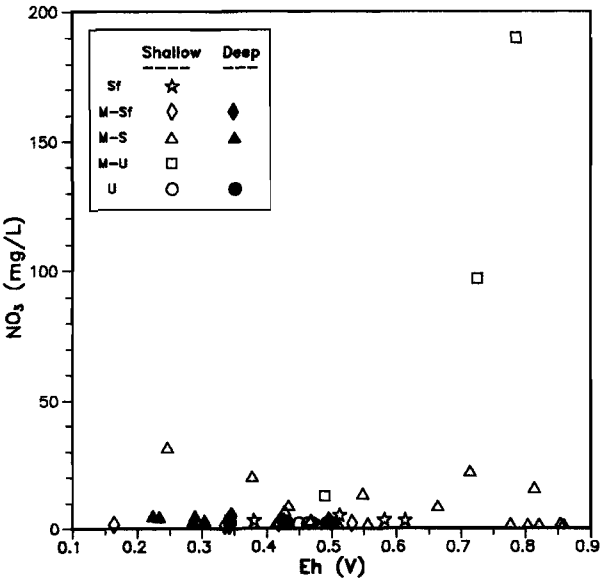

Fig. 45 NO_3 vs. Eh.

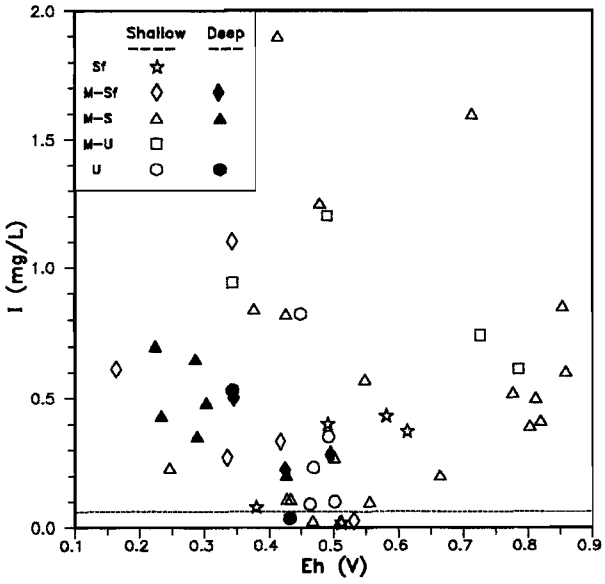

Fig. 46 I vs. Eh, with the seawater concentration shown as the dashed line.

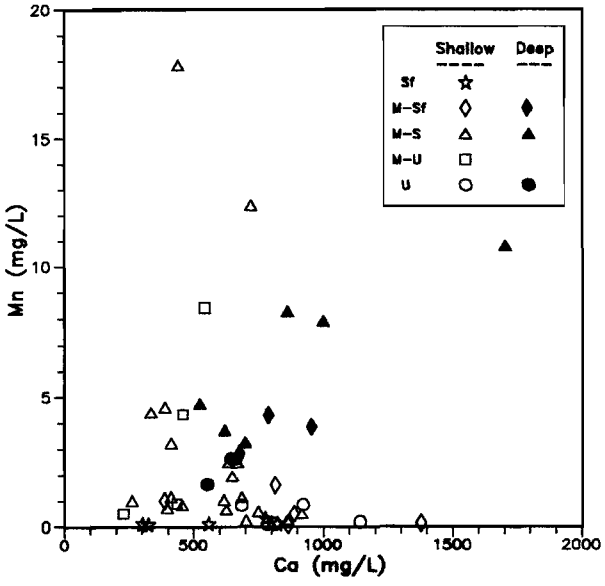

Fig. 47 Mn vs. Ca.

Table 4: Average Data for Minor Elements.

	Average mg/L	St Dev mg/L	Average meq/L	St Dev meq/L
Al	8	14	0.3	0.5
Si	8	11	0.3	0.4
NO_3	11	30	0.2	0.5
I	0.5	0.4	0.004	0.003
Fe	0.5	1.4	0.009	0.025
Mn	2.7	3.6	0.05	0.07
Co	0.20	0.18	0.003	0.003
Zn	0.3	0.8	0.004	0.013
Cu	0.07	0.06	0.0012	0.0009
Ni	0.27	0.26	0.005	0.004
Cr	0.05	0.09	0.0010	0.0017
Sc	0.09	0.05	0.0020	0.0012
Ag	0.026	0.019	0.00024	0.00017
Bi	0.12	0.10	0.0006	0.0005
As	0.10	0.14	0.0014	0.0019
Au	0.0003	0.0006	0.000002	0.000003

Aluminium

As discussed in detail in Section 3.4.4, the Al concentration is controlled by the pH (Fig. 43), and Al distribution (Fig. 14) closely corresponds to that of pH (Fig. 9). Concentrations of Al in solution are related to the dissolution or precipitation of minerals such as kaolinite (eqn. 5), alunite (eqn. 6) or jurbanite (eqn. 7). In waters with pH > 5.0, Al concentration is below the detection limit.

Silicon

A plot of Si concentration vs. pH shows several important features. The majority of the samples had Si concentrations at or below the concentration in sea water (dashed line in Fig. 44). Under acid conditions (pH < 4.0) the Si concentration increased dramatically, presumably due to dissolution of (alumino-)silicate minerals such as kaolinite (eqn. 5). In addition to the observed high Si concentrations in acid waters, another six samples had high Si concentrations (> 10 mg/L) under neutral conditions. These samples to lie in a band at 2400E from 4050N to 4250N (Fig. 15) which also has high pH (Fig. 9), highly anomalous Ni and Cr contents (Figs. 20 and 21), and possible Sc, Ag and Bi anomalies (Figs. 22 - 24). This band closely corresponds to the occurrence of ultramafic rock.

Nitrate

Distribution of NO_3 is very erratic. Nitrogen compounds are strongly concentrated by biological processes, and the data could be explained in this way. Nitrate appears to be increased in the highly oxidized M-U waters (Fig. 45), possibly due to oxidation of ammonia.

Iodide

Iodide abundances are highly variable, with no clear correlation with geology (Fig. 25), TDS, pH or Eh (Fig. 46). The most important feature is the very high concentrations of I (up to 2 mg/L; average 0.5 mg/L), in comparison with seawater (0.06 mg/L). This is observed even under highly oxidizing conditions (Fig. 46), despite the theoretical high volatility of I as I_2 gas under these conditions (Fuge, 1990). This effect may indicate enrichment of I within the mineralized area. Use

of the halides F, Cl and Br for detection of mineralization is well documented (Frick *et al.*, 1989 and references given therein). Work has suggested that I is a chalcophile element (Fuge and Johnson, 1984, 1986), extensively enriched in sulphide environments (Chitayeva *et al.*, 1971; Fuge *et al.*, 1988) and that it may be a useful pathfinder for mineralization (Xuejing *et al.*, 1981; Andrews *et al.*, 1984; Fuge *et al.*, 1986). The Panglo deposit may represent a general halide anomaly, with only the I enrichment being clearly observed, due to the overriding effect of salinity.

Given these observations, it is also possible that the high Br/TDS ratio in the northern part of the study area (Fig. 12) may be partially due to the release of Br during weathering of mineralized rock. This is discussed further in Section 3.7.

Iron

The distribution of Fe (Fig. 3) has been discussed previously (Section 3.4.2). In general, high concentrations of Fe are present in two zones: north of 4300N (particularly at depth), possibly representing Fe released during sulphide weathering (eqn. 2), and the south-west part of the study area (about 3400N to 3600N), possibly representing stagnant surface conditions.

Manganese

The concentrations of dissolved Mn are high (up to 18 mg/L), particularly north from the Trial Pit (Fig. 16). This possibly corresponds to a major zone of weathering sulphides, and may have a major role in initiating high Eh conditions (Section 3.4.5). There is a further weak anomaly at about 3700N, which correlates with the other high Eh (group Mn) waters. Manganese and Ca are correlated at depth (Fig. 47), whereas in shallow waters Mn contents are partially controlled by pH (Fig. 48), possibly due to adsorption on iron oxides.

Cobalt

Cobalt (Figs. 17 and 49) is depleted in the shallow neutral waters, relative to those at depth, and is particularly high in acid waters in contact with ultramafic profiles (squares in Fig. 49; 2500E 4700N in Fig. 17). Groundwaters in contact with shales (stars in Fig. 49) are particularly low ($\leq$ 0.05 mg/L) in Co. Cobalt is also correlated with Mn (Fig. 50), indicating that they are controlled by similar geological and chemical effects.

Zinc

The distribution of Zn (Fig. 18) appears to be under clear geological control. Zinc concentrations in the deeper Trial Pit waters are moderate (up to 1 mg/L), suggesting release during weathering of sulphides. Closer to the surface, Zn concentrations are lower ($<$ 0.4 mg/L), consistent with immobilization by adsorption on iron oxides. However the most anomalous samples are samples P39 and P40, which are acid waters in contact with ultramafic profiles, and have Zn concentrations greater than 3 mg/L. A plot of Zn vs. pH (Fig. 51) indicates that, with the exception of these two samples, Zn concentrations are strongly reduced in the shallow waters, relative to the deeper waters. As with other elements, this could again be due to iron oxide adsorption within the oxidized horizons. In addition Zn is below the detection limit in waters associated with the shales.

Copper

Copper was also clearly lower in groundwaters associated with the shales (Figs. 19 and 52). As with other first row transition metals, Cu appears to be enriched in the more acid waters (Fig. 52).

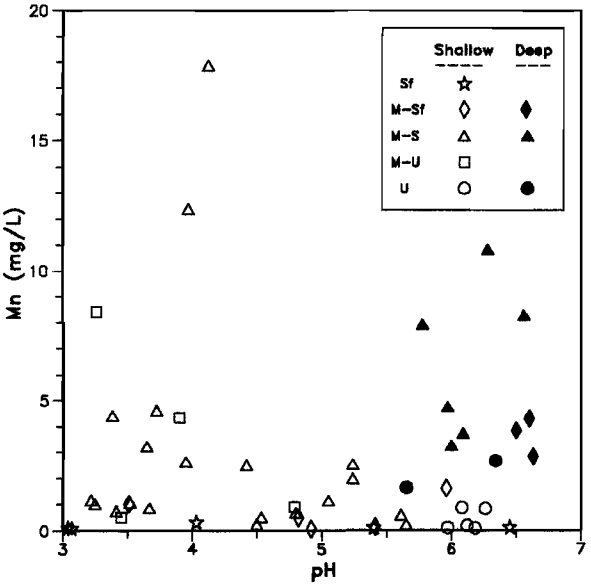

Fig. 48 Mn vs. pH, with the seawater concentration shown as the dashed line.

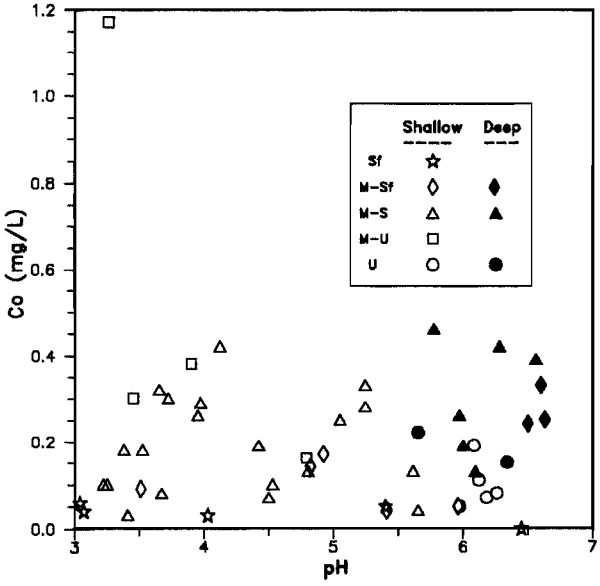

Fig. 49 Co vs. pH, with the seawater concentration shown as the dashed line.

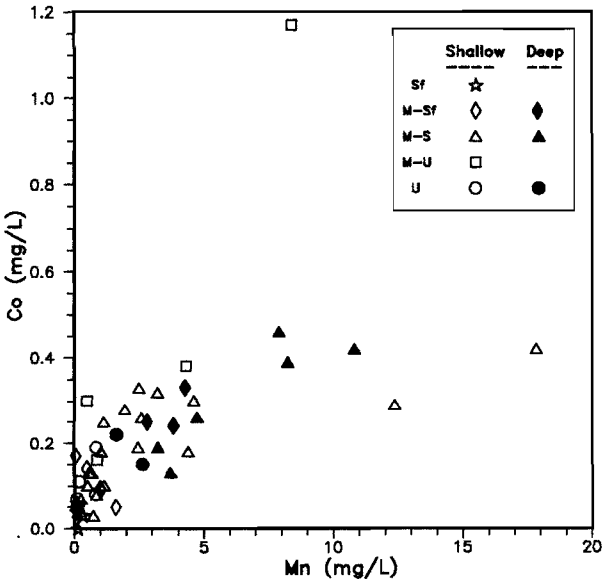

Fig. 50 Co vs. Mn.

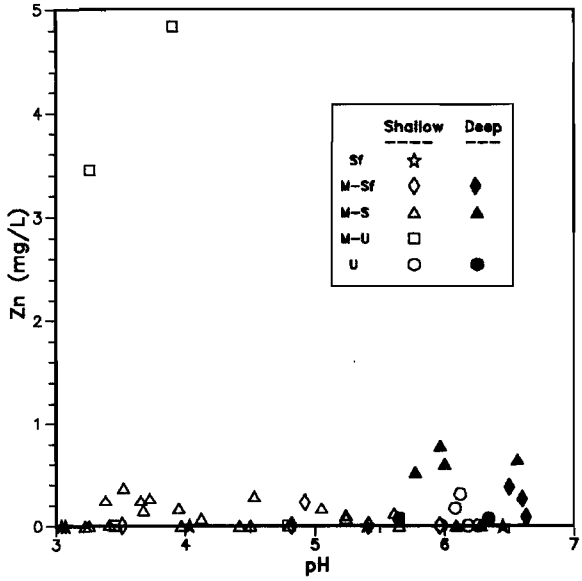

Fig. 51 Zn vs. pH, with the seawater concentration shown as the dashed line.

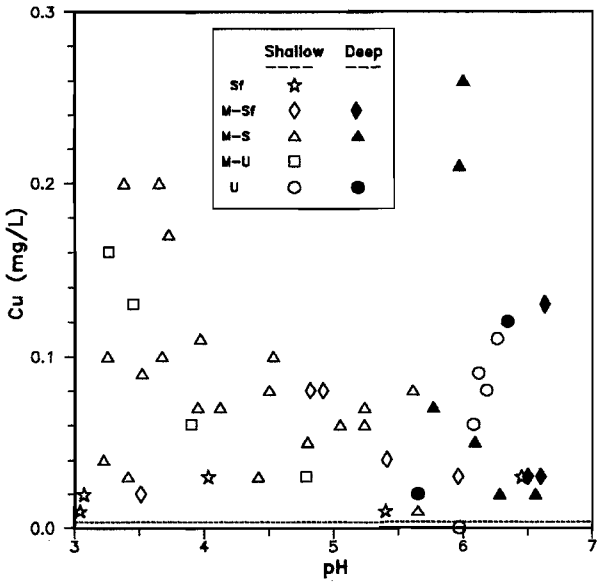

Fig. 52 Cu vs. pH, with the seawater concentration shown as the dashed line.

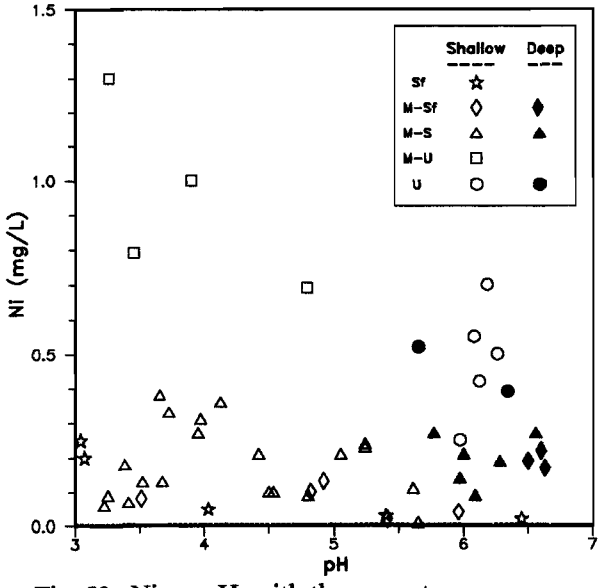

Fig. 53 Ni vs. pH, with the seawater concentration shown as the dashed line.

Nickel

The distribution of Ni (Fig. 20) indicates there to be strong geological control of groundwater concentrations. High concentrations of dissolved Ni (>0.4 mg/L), running approximately north-south from 4800N to 4050N, correspond to the known ultramafic rocks. The highest Ni values were found in the most acid samples P39 and P40. The higher levels of Ni in groundwaters contacting ultramafic profiles is also clearly observed in a plot of Ni vs. pH (Fig. 53), in which one can distinguish a number of groups: ultramafic waters (circles and squares) which are high in Ni, with increases in Ni concentration with acidity; deep waters with moderate Ni concentrations; shallow Mafic waters (triangles) which have moderate Ni concentrations and also show increases in Ni with acidity; and shale waters (stars) with low Ni concentrations, again increased at low pH levels. The increase in Ni concentrations with increased acidity, as with other transition metals, may be due to iron oxide adsorption effects.

In addition to the higher level of Ni in groundwaters contacting ultramafic profiles, there appears to be an additional control, Waters contacting mafic profiles in and north of the Trial Pit have moderate concentrations (0.2 - 0.4 mg/L) of Ni. This zone corresponds to the hypothesized area of actively weathering sulphides (Section 3.4.6; Fig. 36). South of 4000N, Ni contents in mafic waters are lower (<0.2 mg/L). Thus four zones are observed: acid waters contacting ultramafics (Ni $\geq$ 1 mg/L); neutral waters contacting ultramafics (0.4 < Ni < 0.8 mg/L); mine waters (0.2 < Ni < 0.4 mg/L); and waters south of the Trial Pit (Ni < 0.2 mg/L).

Chromium

Chromium differed from the other transition metals in that its distribution is primarily controlled by lithology rather than pH or depth. This is confirmed by the plot of Cr vs. pH (Fig. 54). The ultramafic waters (circles) and two of the mafic waters are particularly enriched. These samples correspond to the principal ultramafic unit (2400E, 4000 - 4250N; Fig. 21). Interestingly the M-U waters (*i.e.* acid groundwaters in contact with ultramafics) showed no Cr enrichment, despite their being enriched in Ni (see Section 3.7).

Scandium

Scandium concentrations are close to the detection limit and have a more scattered distribution than the transition metals (Figs. 22 and 55). However, there appears to be a weak Sc anomaly in the ultramafic waters , whereas shale waters were clearly lower in Sc than the other waters.

Silver

The Ag distribution similarly shows few clear lithological patterns (Fig. 23). The Ag vs. pH plot (Fig. 56) suggests that the shale waters are lower in Ag and the ultramafic waters are weakly enriched.

Bismuth

Bismuth concentrations were close to detection and few trends were observed, apart from a possible weak enrichment in the ultramafic waters (Figs. 24 and 57).

Arsenic

Arsenic (Fig. 26) showed little systematic variation with lithology but appear to be more abundant in the acid waters (Fig. 58). This may again be due to desorption from iron oxides at lower pH levels.

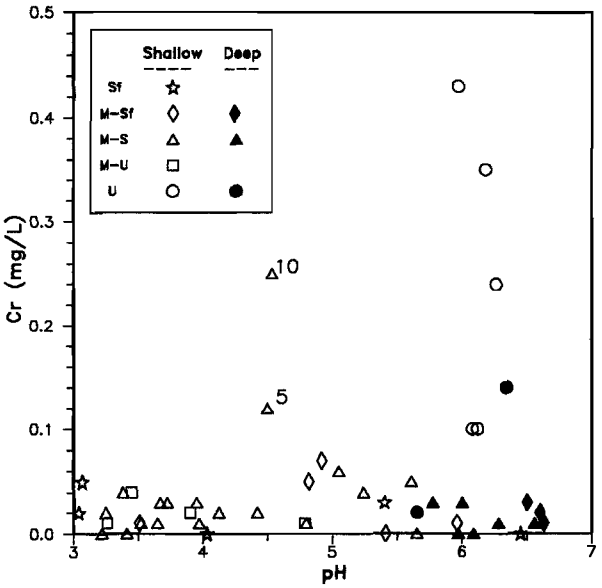

Fig. 54 Cr vs. pH, with the seawater concentration shown as the dashed line.

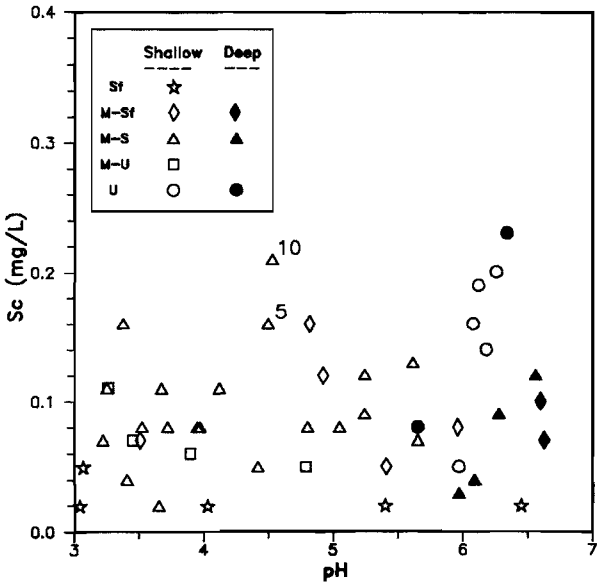

Fig. 55 Sc vs. pH.

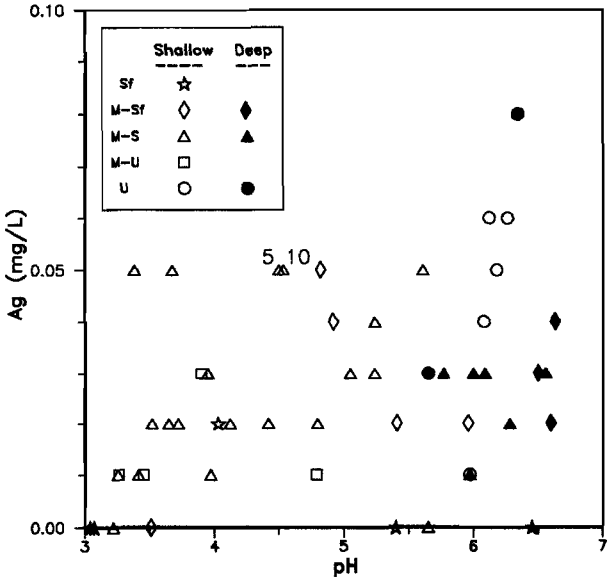

Fig. 56 Ag vs. pH, with the seawater concentration shown as the dashed line.

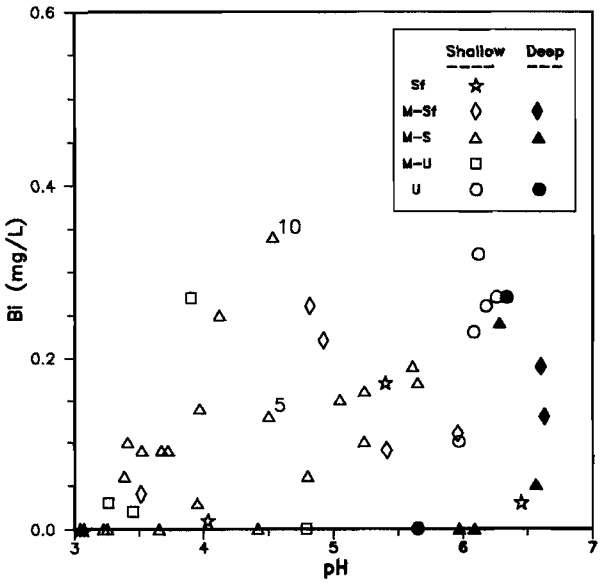

Fig. 57 Bi vs. pH, with the seawater concentration shown as the dashed line.

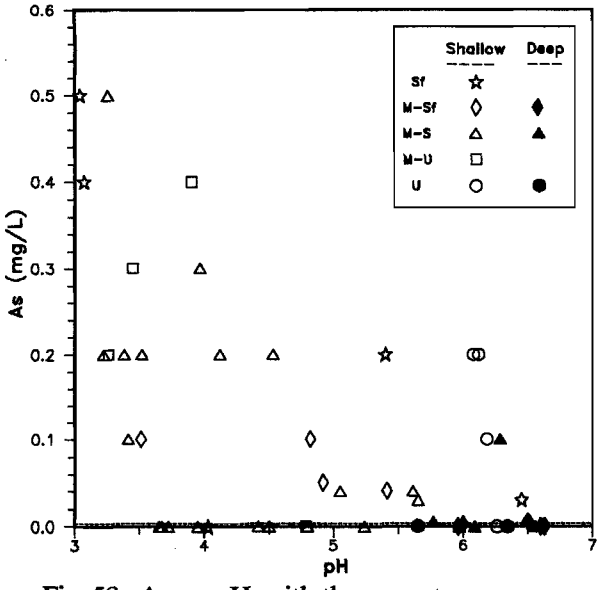

Fig. 58 As vs. pH, with the seawater concentration shown as the dashed line.

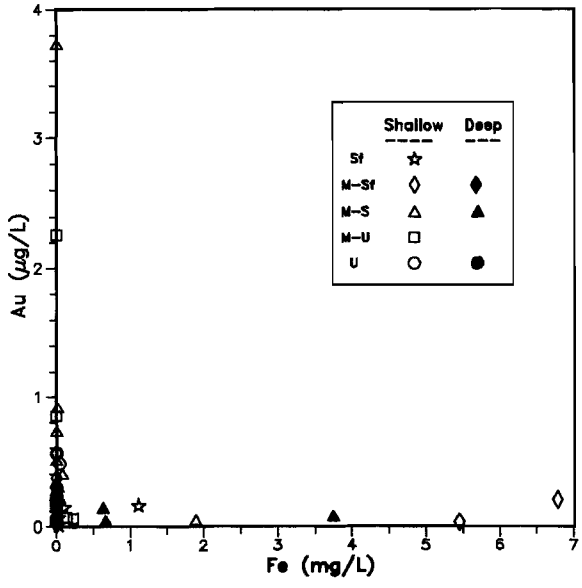

Fig. 59 Au vs. Fe.

3.6. Gold Hydrogeochemistry

As discussed in Section 3.5, most metals have distributions that can be explained in terms of pH and geological controls. The distribution pattern of Au, however, (Fig. 27) does not show any clear correlation with geology or pH (Fig. 7a and 7b). Gold would be expected to be mobilized as the $AuCl_2^-$ or AuI_2^- complexes in these waters (Section 3.8) and as such to have a higher solubility with increased Eh. The control of Au solubility via oxidation/reduction chemistry is illustrated in the plot of Au vs. Fe (Fig. 59). The relationship between the aqueous concentration of these two ions is totally antipathetic *i.e.* Au is only observed above the detection limit where Fe is less than 0.1 mg/L. This is due to the strong reducing capacity of the ferrous ion:

$$Fe^{2+} + AuCl_2^- + 3H_2O \Rightarrow Fe(OH)_{3(s)} + Au_{(s)} + 3H^+ + 2Cl^- \quad ...(11)$$

A similar, but less dramatic relationship is observed for Au vs. Eh (Fig. 60). The Eh values for the theoretical solubilization of 2 μg/L and 0.02 μg/L of Au are also shown. Samples plotting right of the 2 μg/L line should theoretically contain greater than 2 μg/L Au, whereas samples plotting left of the 0.02 μg/L line should theoretically contain less than 0.02 μg/L Au. Actual values more or less follow this trend. The most oxidized waters (Eh > 0.7 V) have Au concentrations that, though very high (up to 4 μg/L), were well below the theoretical concentration for equilibration with Au metal at the Eh values recorded for those waters. However, other factors, such as sorption of Au onto Fe or Mn oxides, may reduce concentrations of soluble Au, even in highly oxidizing waters. This plot (Fig. 60) also indicates that the shale waters are low in Au. However all other water groups (including the neutral ultramafic waters) are highly anomalous in Au (> 0.05 μg/L).

Comparison of the Au and Eh distributions (Figs. 27 and 7c) also indicates that waters rich in Au occur in the region of high Eh. This control of Au distribution by Eh suggests that the dissolved Au distribution will be strongly spatially controlled by the different pH/Eh zones (Fig. 36).

The antipathetic relationship between Fe and Au (Fig. 59), and the weak correlation between soluble Au and Eh (Fig. 60), strongly suggest that Au is being dissolved under highly oxidizing conditions, as species such as $AuCl_2^-$ or AuI_2^-. These conditions appear to have been generated by the Mn redox couple (Section 3.4.5). These results support theoretical studies that indicate the importance of the Mn couple for oxidative $AuCl_2^-$ dissolution (Miller and Fisher, 1973). The hypothesized dissolution of Au at Panglo is directly analogous to laboratory experiments in which Au was readily dissolved by a mix of Au metal, pyrolusite (MnO_2), H_2SO_4 and NaCl (Cloke and Kelly, 1964).

3.7. Geological Patterns for Groundwater

The concentrations of several elements in groundwaters may be dependant on the lithology from which the water sample was taken. This is illustrated in Table 5, which gives the average element concentration for the waters in each lithological group.

Waters from the shale unit occur in the south-west region of the study area. These samples differ markedly as follows:

(i) lowered Br/TDS (Fig. 33) and Sr/Ca (Fig. 31) ratios, relative to the other geological groups;

(ii) very low concentrations of Mn, Co, Zn, Cu, Ni, Cr, Sc and Au (Figs. 48, 49, 51 - 55 and 60), relative to the other groups of waters;

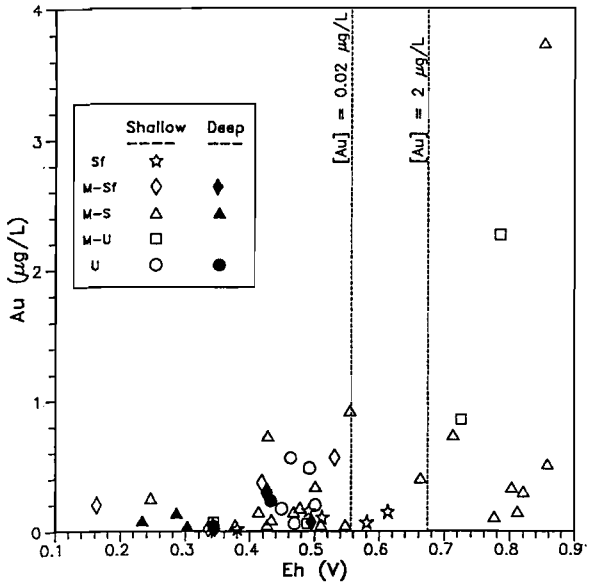

Fig. 60 Au vs. Eh. Also depicted are the Eh values for the theoretical solubilization of 0.02 μg/L and 2 μg/L of Au.

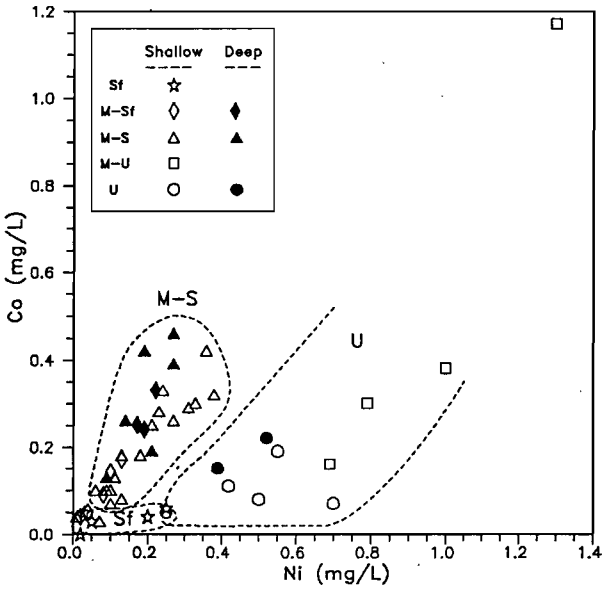

Fig. 61 Co vs. Ni.

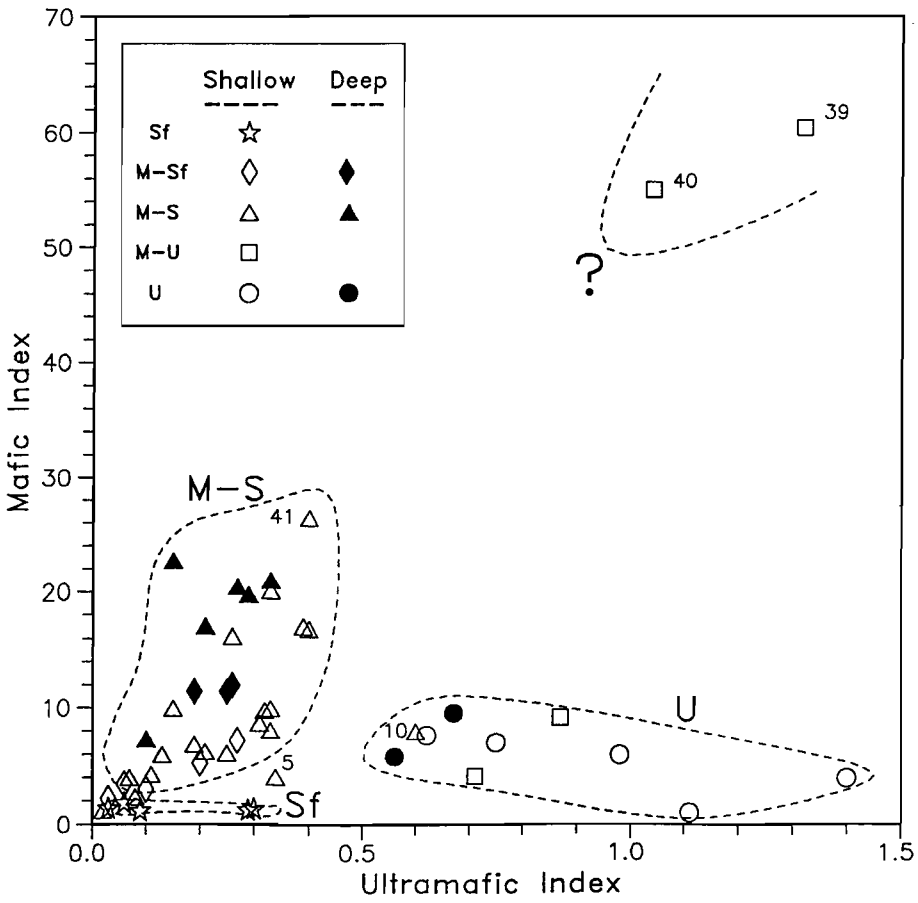

Fig. 62 Mafic vs. Ultramafic Indices for Panglo waters. See text (Section 3.7) for details.

Table 5: Average Element Concentrations in each Lithological Group
(See Table 1 for samples in each class; all concentrations in mg/L unless otherwise noted).

	Geological Designation$							
	Sf {S*} [5]	M-Sf {S} [5]	M-Sf {D} [3]	M-S {S} [20]	M-S {D#} [6]	M-U {S} [4]	U {S} [6]	U {D} [2]
Eh	0.52 (0.09)	0.36 (0.13)	0.42 (0.08	0.58 (0.19)	0.29 (0.07)	0.59 (0.21)	0.45 (0.06)	0.39 (0.06)
pH	4.4 (1.5)	4.9 (0.9)	6.6 (0.1)	4.2 (0.8)	6.1 (0.3)	3.9 (0.7)	6.0 (0.2)	6.0 (0.5)
DO@	4.1 (1.5)	3 (1.2)	nd	4.5 (1.6)	nd	4.1 (1.9)	3.8 (1.2)	2.4 (0.3)
TDS (%)	5.9 (1.7)	7.7 (1.3)	11.3 (0.7)	7.3 (1.4)	13.2 (2.5)	6.3 (1.9)	9.3 (1.4)	11.4 (0.8)
HCO_3	25 (45)	25 (30)	105 (35)	20 (60)	95 (30)	1 (2)	120 (25)	140 (35)
Sr/Ca	0.007 (0.002)	0.009 (0.002)	0.009 (0.004)	0.011 (0.004)	0.012 (0.006)	0.011 (0.003)	0.014 (0.003)	0.01 (0.004)
Br/TDS (x 10000)	3.9 (1)	2.9 (0.9)	4.5 (0.1)	5.4 (0.5)	4.4 (0.4)	5.9 (0.9)	4.7 (0.4)	4.3 (0)
K/TDS (x 10000)	10 (5	7.3 (2.1	7.9 (0.3	7.2 (1	8 (0.8	12 (2.4	6.2 (1.9	8.2 (0.4
Al	18 (24)	4 (10)	0 (0)	10 (15)	0 (0)	21 (12)	0 (0)	0 (0)
Si	16 (21)	6 (13)	0 (0)	5 (8)	0 (1)	21 (10)	16 (7)	7 (6)
NO_3	4 (1)	2 (0)	4 (1)	7 (9)	4 (1)	80 (90)	2 (0)	2 (0)
Mn	0.2 (0.1)	0.7 (0.6)	3.6 (0.8)	3.0 (4.4)	6.4 (3.0)	3.5 (3.7)	0.6 (0.6)	2.1 (0.7)
Fe	0.4 (0.8)	4 (6)	0 (0)	0.2 (0.8)	1.4 (1.6)	0.2 (0.2)	0 (0)	0 (0)
Ni	0.11 (0.11)	0.07 (0.04)	0.19 (0.03)	0.18 (0.11)	0.20 (0.07)	0.95 (0.27)	0.49 (0.15)	0.46 (0.09)
Zn	0 (0)	0.05 (0.10)	0.24 (0.15)	0.11 (0.12)	0.4 (0.3)	2.1 (2.5)	0.09 (0.13)	0.07 (0)
I	0.26 (0.19)	0.5 (0.4)	0.33 (0.15)	0.6 (0.5)	0.47 (0.19)	0.87 (0.26)	0.35 (0.28)	0.3 (0.3)
Co	0.036 (0.023)	0.1 (0.06)	0.27 (0.05)	0.19 (0.11)	0.31 (0.13)	0.5 (0.5)	0.12 (0.07)	0.19 (0.05)
Sc	0.03 (0.01)	0.10 (0.04)	0.09 (0.02)	0.10 (0.04)	0.07 (0.04)	0.07 (0.03)	0.14 (0.06)	0.16 (0.11)
As	0.23 (0.22)	0.06 (0.04)	0 (0)	0.10 (0.14)	0.03 (0.05)	0.23 (0.17)	0.08 (0.10)	0 (0)
Cu	0.02 (0.01)	0.05 (0.03)	0.06 (0.06)	0.09 (0.05)	0.11 (0.10)	0.10 (0.06)	0.06 (0.04)	0.07 (0.07)
Cr	0.02 (0.02)	0.03 (0.03)	0.02 (0.01)	0.04 (0.06)	0.01 (0.01)	0.02 (0.01)	0.21 (0.16)	0.08 (0.08)
Bi	0.04 (0.07)	0.14 (0.09)	0.16 (0.04)	0.11 (0.09)	0.07 (0.11)	0.08 (0.13)	0.20 (0.12)	0.14 (0.19)
Ag	0.004 (0.009)	0.026 (0.019)	0.030 (0.010)	0.027 (0.017)	0.025 (0.008)	0.015 (0.010)	0.042 (0.019)	0.055 (0.035)
Au (μg/L)	0.10 (0.06)	0.24 (0.23)	0.14 (0.13)	0.46 (0.8)	0.11 (0.12)	0.81 (1.0)	0.25 (0.22)	0.14 (0.13)

$: See Section 3.2 for description of lithological groups
* : Shallow
# : Deep
@: Dissolved Oxygen

[ ] : Number of Samples
( ) : Standard Deviation
nd : not determined

(iii) possible low concentrations of I (Fig. 46), Ag (Fig. 56), and Bi (Fig. 57), relative to the other groups of waters.

The lowered Br/TDS ratio suggests that the shale system is hydrologically separate from the northern (mafic and ultramafic rocks) system. The lower concentrations of base metals, despite a number of the shale waters being acid and therefore capable of dissolving these metals, suggests that the shale system is strongly depleted in "available metals". Analyses of solid shale, mafic and ultramafic samples (Scott, 1989a,b, 1990) indicate that unweathered and weathered shales are lower in Mn, Ni, Zn, Co, Sc, Cu and Cr, relative to the mafic and ultramafic materials. Data for As, Bi, Ag and Au are not clear, due to low abundances and sample variation. However, the lower concentrations of base metals in shale materials appear to offer a simple explanation for the lower concentrations in the shale waters.

Comparison of the mafic and ultramafic waters (Table 5) indicates that each group has a particular 'signature'. The mafic waters are enriched in Mn (Fig. 48), Co (Fig. 49) and Zn (Fig. 51), and depleted in Ni (Fig. 53), Cr (Fig. 54), Sc (Fig. 55), Ag (Fig. 56) and Bi (Fig. 57), relative to the ultramafic waters. These characteristics are in accordance the known chemistry of mafic and ultramafic element abundances, and in general agree with the observations by Scott (1989a,b, 1990). The implications of the high concentrations of iodide have been discussed previously (Section 3.5). The relative enrichment of Bi in waters from the ultramafics may indicate the presence of an additional source of Bi in these rocks.

There are two groups of waters associated with ultramafic lithologies. These are the U waters, which were sampled between 4000 and 4300 N and represent the principal ultramafic unit (Fig. 5); and the M-U waters, which appear to be located close to the interface between mafic and ultramafic rocks. These waters differ markedly in pH. The M-U waters have a pH of 3.3 - 4.8, a similar range to the shallow mafic waters (3.2 - 5.7). However the U waters are more neutral than any other surface water groups (pH 5.7 - 6.3), presumably as a result of the more basic nature of the rocks.

The pH differences may also be related to differing degrees of weathering. Scott (1990) observed that the ultramafic rocks in the east are sheared and more weathered than those in the west. A similar hypothesis may explain the pH and chemical differences between the U waters and the M-U waters to the north-east.

Specific chemical differences are also observed between the U and M-U waters. The U waters are strongly enriched in Si (Fig. 44), Cr (Fig. 54) and Ni (Fig. 53), consistent with the known compositions of ultramafic rocks and their weathering products at this site (Scott, 1989b, 1990). The M-U waters have higher Ni concentrations than the U waters (Fig. 53), but have relatively low Cr concentrations (Fig. 54). In addition the high Si content of these waters may be from a different source than for the U waters: the M-U waters are very acid and may be enriched in Si due to kaolinite dissolution (Section 3.4.4). Such an explanation cannot, however, explain the high Si contents of the near neutral U waters. One feasible explanation of these data is that 'accessible' Cr in ultramafic rocks occurs in a readily dissolved form, whereas the 'accessible' Ni is not depleted during acid weathering. This correlates with the observations of Scott (1990), that both Cr and Ni occur in chlorite, which is readily weathered. However Ni is also found in talc, which is resistant to weathering. Thus it is conceivable that the high Cr and Si in the U waters results from weathering of chlorite. The acidic M-U waters are contacting more intensely weathered materials, from which all of the chlorite has been removed, so that no Cr is dissolving. However appreciable Ni may still be dissolving due to the weathering of talc.

The clear chemical differences between the water groups can be used for classification. Even a simple plot such as Co (enriched in mafic rocks) vs. Ni (enriched in ultramafic rocks) gives a reasonable separation between the three major geological groups (Fig. 61). In general plotting any of the "mafic elements" such as Mn, Co or Zn, with the "ultramafic elements" Ni or Cr, gives a good separation. The best classification was obtained by using multi-variate plots, as illustrated in Fig. 62. In this plot the X-axis (Ni + 2Cr) represents an index that efficiently separates the ultramafic rocks from the other rock types. The other ultramafic 'indicators', Bi, Sc and Ag, were not used because the precision of analysis for those elements was low. The Y-axis (Mn + 13Co + 9Zn + 36Cu) was obtained by calculating the parameters for the mafic enriched elements Mn, Co, Zn and Cu, such that they have normalized means, *i.e.* the mean Mn value for the 50 samples equals 36 times the mean Cu value. The three water groups are clearly resolved using this plot.

Several features and mis-classifications can be observed on Fig. 62. One mafic sample (P18) has metal concentrations at or below those of the shale waters. This sample is high in HCO_3 (260 mg/L compared with the next highest sample with 170 mg/L; Fig 28) and has the highest pH of the shallow mafic waters. Thus, this low metal content could be pH controlled. Two shallow waters (P14 and P15) and three deep waters (P46, P47 and P50), previously classified as intermediate are here classed as mafic waters. This reclassification is possible, as indicated by the location of the sample sites (Figs. 1 and 4)

The single water sample (P5) that lies between the mafic and ultramafic fields (Fig. 62) [7] is located close to the mafic - ultramafic boundary (Fig. 1 and 4) and is thus reclassified as being intermediate. Similarly, sample P10, previously classified as mafic (Fig. 62), lies within the ultramafic domain. These classifications are further supported by the strong (P10) and moderate (P5) enrichments with Cr, Sc, Ag and Bi (Fig. 54 - 57). The geology map (Figs. 1 and 3) suggests that P10 was sampled in a mafic area, about 70 m from any ultramafic rocks. However, it is possible that there may be some unobserved ultramafic rocks in this area or, alternatively, there may be an aquifer allowing essentially unaltered ultramafic waters to flow the 70 m distance.

The spatial distributions of the calculated values of the mafic and ultramafic indices [(Mn + 13Co + 9Zn + 36Cu) and (Ni + 2Cr)] are shown in Figs. 63 and 64. High values for the mafic index occur across the northern part of the study area (north of 4300N; Fig. 63), particularly in P39 and P40, which are located at 2500E, 4700N (Fig. 63). These two samples, which plot in the top right hand corner of the multi-variate plot (Fig. 62), have high concentrations of both mafic (*e.g.* Zn $>$ 3 μg/L) and ultramafic (*e.g.* Ni $\geq$ 1 μg/L) elements, and may represent intensely weathered ultramafic or mafic environments. The most metal rich mafic water P41 (Fig. 62), is spatially close to these two waters (Fig. 1).

These observations suggest that the northern region of the study area is the zone of the most pronounced acid/oxidative weathering. This is consistent with the high Au solutions occurring in this area (Fig. 27). It would seem that the area may be worthy of further geochemical and mineralogical investigation.

[7] Note that in all the Figures used in this discussion of the chemistry of samples P5 and P10 (namely Figs. 54 - 57 and 62) the relevant sample points are numbered on the plots for clarity.

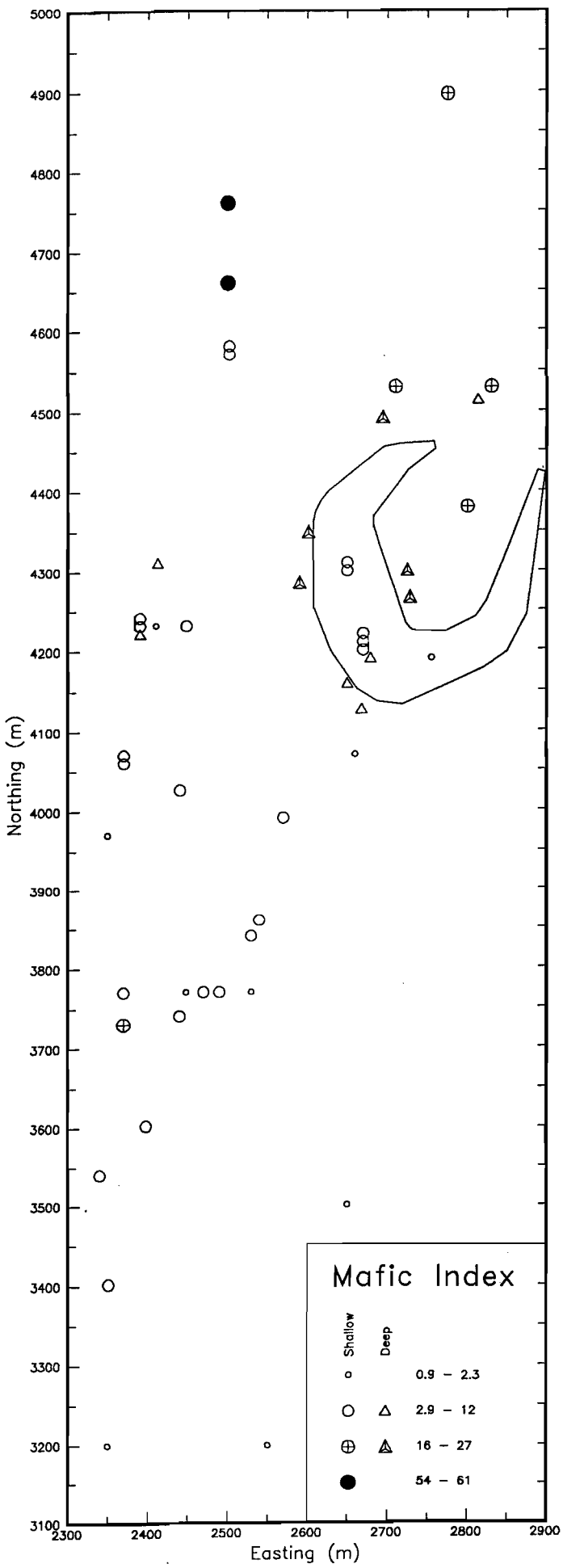

Fig. 63 Spatial Distribution of the Mafic Index (Mn + 13Co + 9Zn + 36Cu).

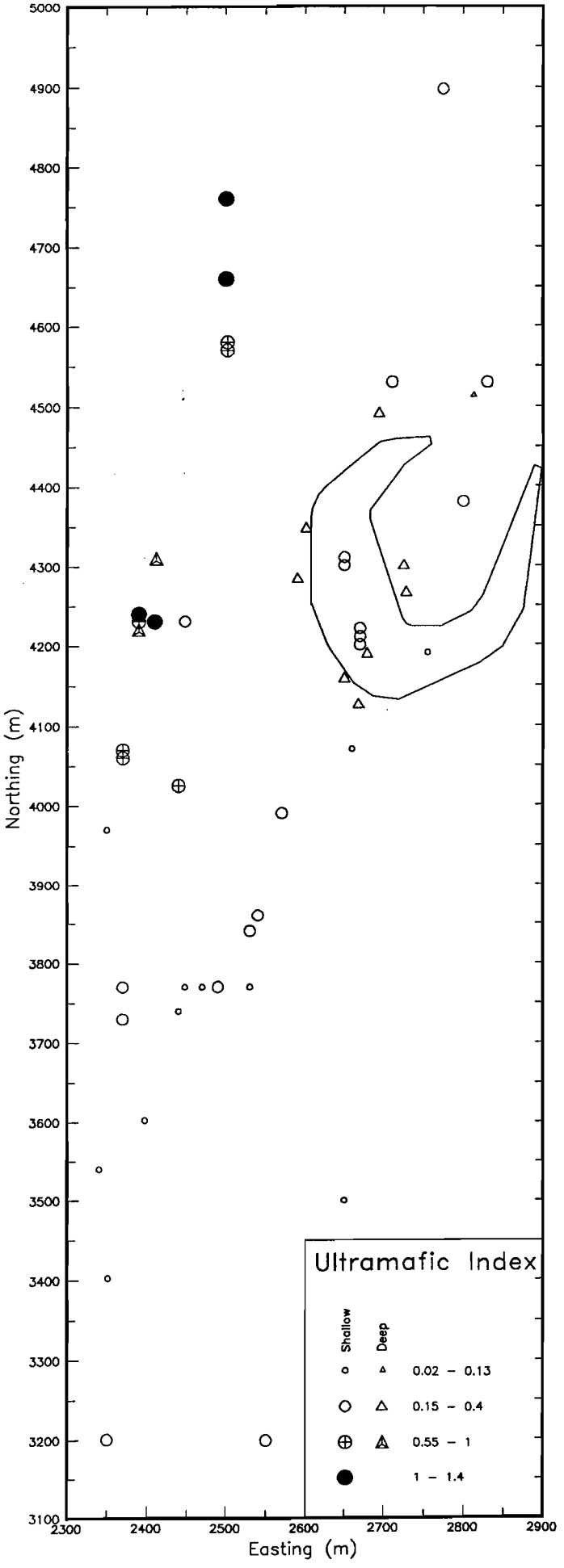

Fig. 64 Spatial Distribution of the Ultramafic Index (Ni + 2Cr).

It should be noted that these minor reclassifications are sensible in terms of the spatial location of the reclassified samples and are successful in terms of understanding the hydrogeochemistry of this area. However one should not assume that waters from another site will plot in the domains given in Fig. 62. Solution metal concentrations can be dependant on a number of site dependant factors such as pH, salinity and Eh, in addition to the metal concentrations in the rocks or weathering minerals. Thus waters from sites under similar climatic conditions to Panglo may be lithologically distinguished by a similar plot to Fig. 62, whereas sites with significant climatic or other differences may show major differences in the solution parameters, even where the rocks themselves have similar geochemistries. However a similar methodology may still yield a comparable multi-element plot that would enable a site specific water classification.

3.8. Speciation Analysis

The speciation of the analysed elements, and their potential solid phases, was investigated using the speciation programme PHREEQE (Parkhurst *et al.*, 1980). In this program the concentration of the elements is entered, along with other relevant parameters such as temperature (assumed to be 25°C), pH, Eh and density (calculated from TDS). Using data for association constants for all the potential complexes the programme calculates, by a system of iterations, the activities and concentrations of all phases [8] . In addition, it calculates whether the solution is oversaturated with respect to specified solid phases. For a particular solid phase, the Ion Activity Product (IAP) is calculated: *e.g.* for calcite, which precipitates according to:

$$Ca^{2+} + CO_3^{2-} \Rightarrow CaCO_{3(S)} \qquad \ldots(12)$$

the IAP is equal to $[Ca^{2+}] \times [CO_3^{2-}]$, where $[Ca^{2+}]$ denotes the activity of the free Ca^{2+} ion. This is then related to the activity product of these ions required for equilibrium (K_T) by calculation of the parameter $\log(IAP/K_T)$. In common with a number of other texts, this parameter is referred to here as the solubility index (SI). If the SI parameter equals zero the water is in equilibrium with the solid phase, under the conditions specified. Where the SI is less than zero the solution is under-saturated with respect to the phase and the phase, if present, may dissolve. If the SI is greater than zero the solution is over-saturated with respect to this phase and the phase can precipitate.

Note that this analysis only specifies possible reactions. Kinetic constraints may rule out reactions that are thermodynamically allowed. Thus, for example, waters are commonly in equilibrium with calcite, but may become over-saturated with respect to dolomite, due to the slow speed of solution equilibration with this mineral (Drever, 1982). Additionally, waters tend to be in equilibrium with the first phase that precipitates from solution, rather than the final recrystallized form. Thus, for example, waters are commonly in equilibrium with amorphous forms of Fe (Schwab and Lindsay, 1983) such as ferrihydrite $[Fe(OH)_3 \cdot xH_2O]$ or $Fe_3(OH)_8$ rather than goethite (FeOOH) or hematite (Fe_2O_3), even where these crystalline iron oxides are present at high concentrations.

The total output from the speciation analysis of all of the groundwaters is voluminous, and the output from only a single sample is shown in Appendix 2. The general speciation of the elements is given in Table 6.

Data from this analysis have been utilized in earlier discussions. The non-metals C, Si, N, O, S, Cl, Br and I are present in their standard forms: namely HCO_3^-, $H_4SiO_4^0$, NO_3^-, H_2O, SO_4^{2-}, Cl^-, Br^- and I^-. Metals are commonly present in solution as the uncomplexed ions or as chloride

[8] Generally the activity of a phase is similar to its concentration; further details are available from a number of standard texts, *e.g.* Garrels and Christ (1965).

complexes: with the exception of Cr^{3+}, which is complexed by OH^- above pH 4, and Bi, which is present as BiO^+.

Speciation analyses for Au indicates that it will occur in most of the waters as AuI_2^- rather than $AuCl_2^-$. This is a consequence of the high abundance of I in the Panglo groundwaters: the average I concentration in these waters is 0.5 mg/L, in comparison to an average Cl content of 49000 mg/L. This gives an average I enrichment factor of about 3 times, relative to sea water, with enrichments ranging up to 13 times. Although the possibility of Au mobilization as the iodide complex has been suggested by previous investigators (*e.g.* Lakin *et al.*, 1974), this mechanism was only thought to be of importance in soil solutions enriched in I by biological processes. Implications of this hypothesis of AuI_2^- mobilization within the Panglo groundwater system are not clear: it is possible that Au at Panglo may be more mobile than in a comparatively I poor environment, as a consequence of the high stability of the AuI_2^- complex, relative to $AuCl_2^-$.

Table 6: Solution Speciation of Elements.

Element	Major Species	Additional Species
Na	Na^+	
K	K^+	
Mg	Mg^{2+}	
Ca	Ca^{2+}	
Sr	Sr^{2+}	
Cr	$CrOH^{2+}$	Cr^{3+} (pH < 4)
Mn	Mn^{2+} (TDS<60,000mg/L)	$MnCl^+$ (TDS>60,000mg/L)
Fe	Fe^{2+}, $FeCl^+$	
Co	$CoCl^+$, Co^{2+}	$CoCl^+$ (TDS>80,000mg/L)
Ni	Ni^{2+}, $NiCl_2^0$ (TDS>50,000mg/L)	
Cu	Cu^{2+},$CuCl^+$,$CuCl_3^{2-}$	
Ag	$AgCl_2^-$,$AgCl_3^{2-}$,$AgCl_4^{3-}$	
Au	AuI_2^- / $AuCl_2^-$ (depending on I/Cl ratio)	$AuClOH^-$ (pH > 6.5)
Zn	Zn^{2+} (TDS<72,000mg/L)	$ZnCl^+$ (72,000<TDS<105,000mg/L) $ZnCl_3^-$ (105,000mg/L<TDS)
C	HCO_3^-	
Si	$H_4SiO_4^0$	
N	NO_3^-	
O	H_2O	
S	SO_4^{2-}	
Cl	Cl^-	
Br	Br^-	
I	I^-	

The SI values for a number of relevant phases are shown graphically in Figs. 65 - 76. Note that these values are in general plotted against the variable that most strongly controls the solubility of the solid phase (*e.g.* TDS for halite, pH for calcite). The sample points will commonly tend to lie on a well defined line. This line will be curved where SI is plotted against TDS (logarithmic parameter *vs.* a linear variable; Fig. 65), and straight where SI is plotted against pH (logarithmic parameter *vs.* a logarithmic variable; Fig. 66). Major controls on solubility of the particular phase are indicated where the samples show a break in this curve and instead tend to a SI of zero (*e.g.* Fig. 67). This suggests that active dissolution or precipitation of the mineral is occurring: *i.e.* that the particular solid phase is tending to equilibrium with the solution. The SI data for particular minerals are discussed below, in terms of the cations involved.

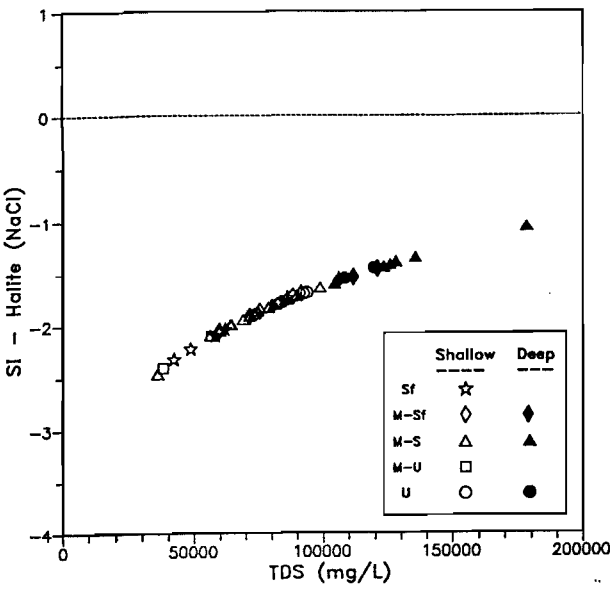

Fig. 65 SI for Halite vs. TDS.

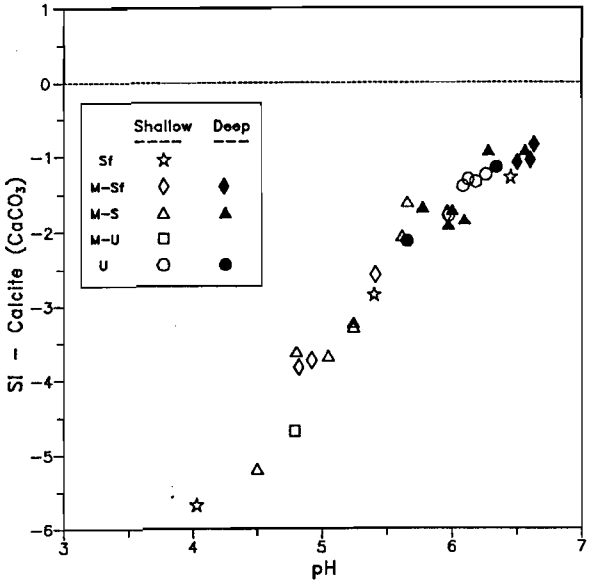

Fig. 66 SI for Calcite vs. pH.

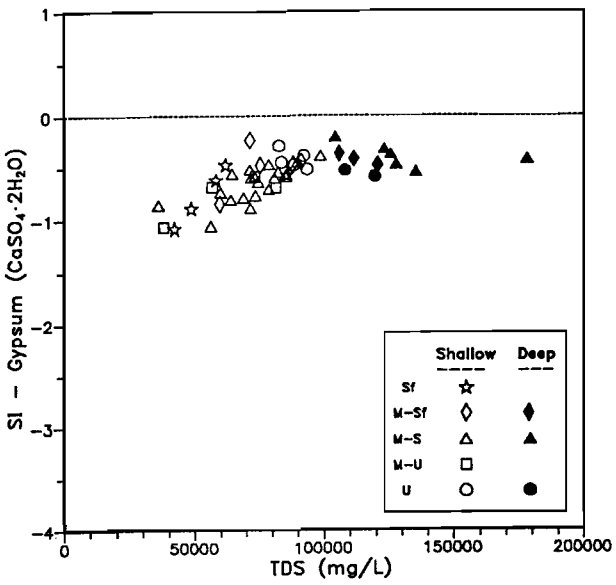

Fig. 67 SI for Gypsum vs. TDS.

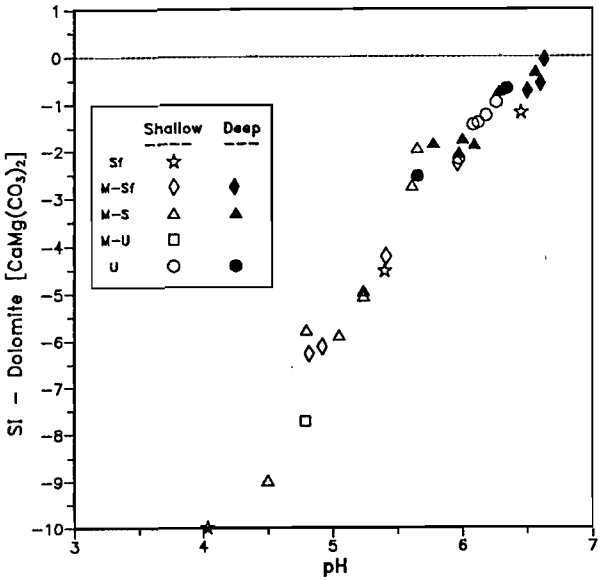

Fig. 68 SI for Dolomite vs. pH.

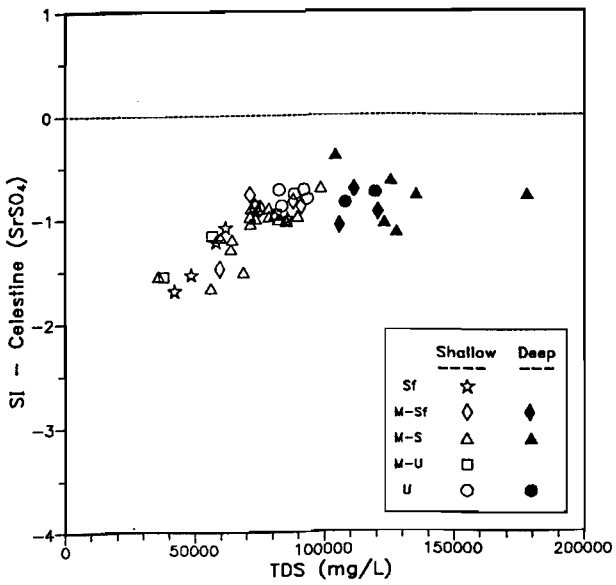

Fig. 69 SI for Celestine vs. TDS.

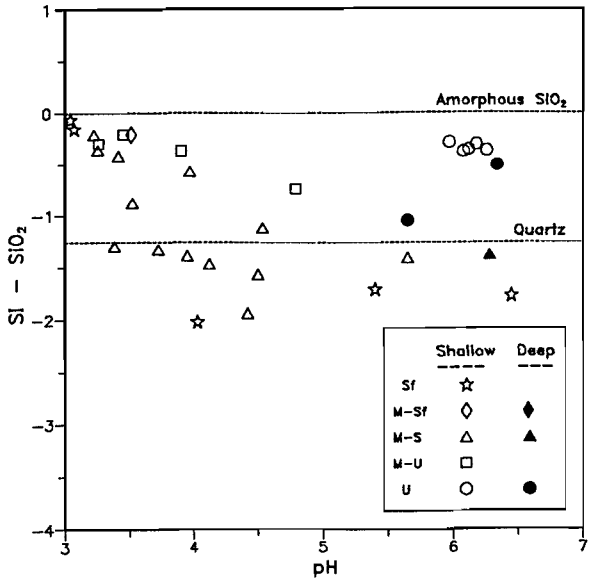

Fig. 70 SI for SiO_2 minerals vs. pH.

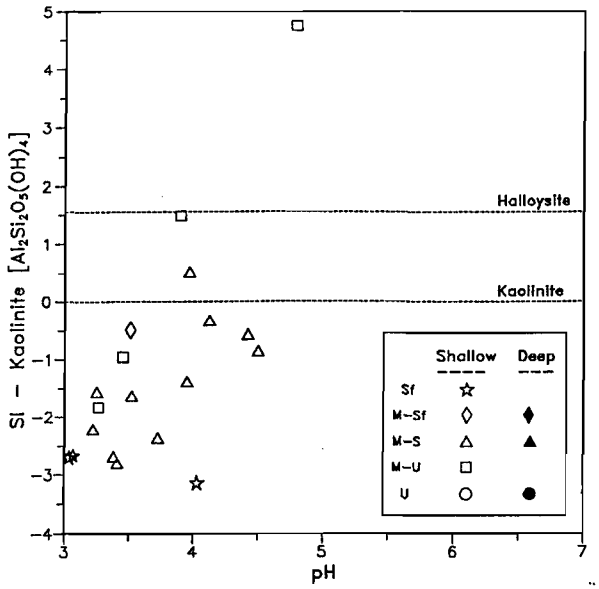

Fig. 71 SI for Kaolinite vs. pH.

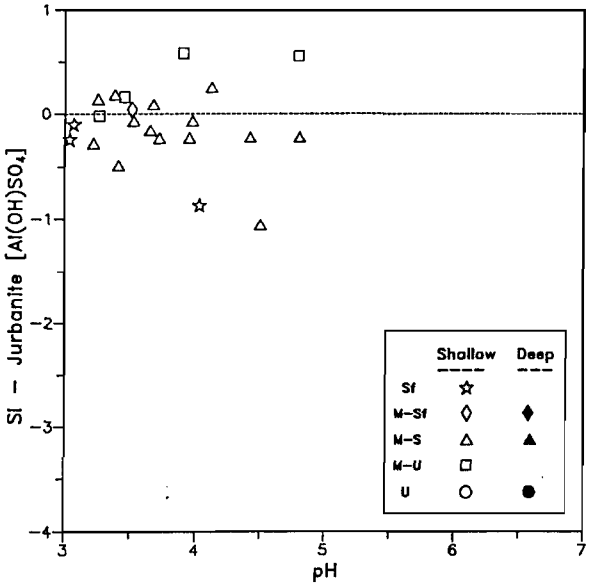

Fig. 72 SI for Jurbanite vs. pH.

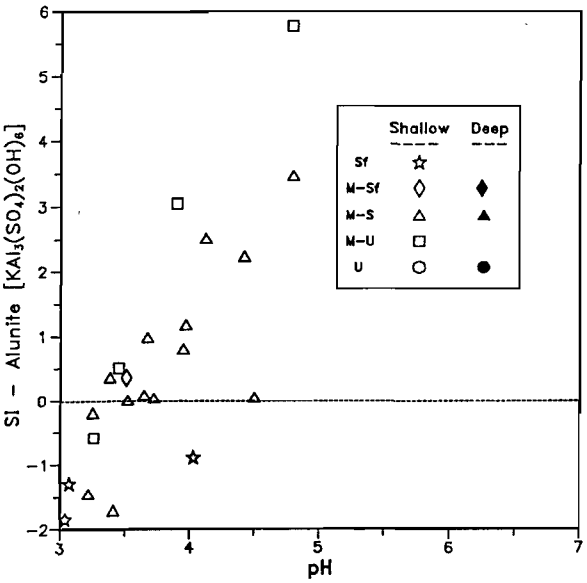

Fig. 73 SI for Alunite vs. pH.

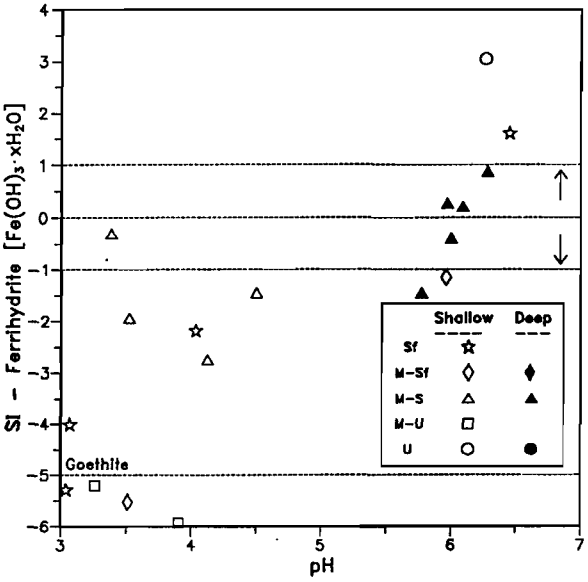

Fig. 74 SI for Fe minerals vs. pH.

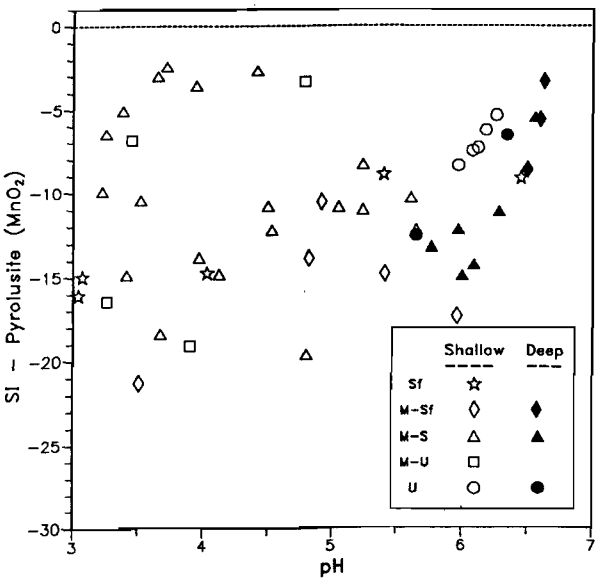

Fig. 75 SI for Pyrolusite vs. pH.

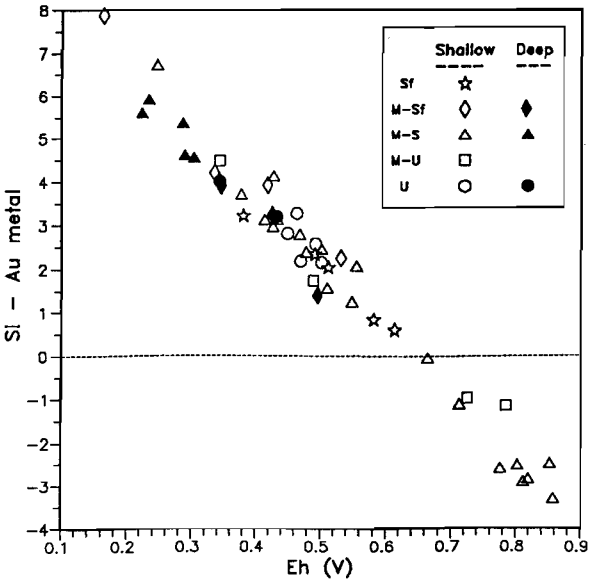

Fig. 76 SI for Au Metal vs. Eh.

Sodium

All solutions are undersaturated with respect to halite (NaCl; Fig. 65). As can be seen, the SI parameter is strongly correlated with TDS. Given that the Panglo groundwaters primarily contain Na and Cl ions, this is as expected.

Calcium

The SI data for calcite ($CaCO_3$; Fig. 66) indicate that all of the groundwaters are undersaturated with respect to calcite. At TDS values above 90000 mg/L groundwaters become saturated with respect to gypsum ($CaSO_4 \cdot 2H_2O$; Fig. 67). Note that the deeper groundwater samples all appear to be at equilibrium with gypsum.

Magnesium

All of the solutions are significantly undersaturated with respect to magnesite ($MgCO_3$) or epsomite ($MgSO_4 \cdot 7H_2O$). The SI data for dolomite (Fig. 68) suggest that the deeper, neutral groundwaters approach dolomite saturation. Unfortunately, in the absence of any samples at higher pH, it is not clear whether this is coincidental, as waters equilibrate with this mineral slowly.

Strontium

All of the solutions are significantly undersaturated with respect to the strontianite ($SrCO_3$; not shown). Data for celestine (Fig. 69) indicate that Sr concentrations are generally too low for saturation. However, the plot shows a 'plateau' in the SI data that is similar to that observed for gypsum (Fig. 67), and chemical data (Section 3.3; Fig. 31) suggest that Sr concentration is being controlled in a similar manner to Ca. Strontium concentration is approximately 100 times less than that of Ca (Appendix 1), . It is possible that Sr concentration is being controlled, not by a separate Sr phase, but by (approximately) one percent Sr substituted gypsum.

Silicon

Silica can precipitate as amorphous SiO_2, the less soluble quartz (SiO_2), or as range of phases with solubility between these two extremes. The lines for solution equilibration with amorphous SiO_2 or with quartz are shown in Fig. 70. A number of the waters are approximately in equilibrium with quartz. However, several have very high Si concentrations and approach saturation with amorphous SiO_2 (Fig. 70). These are the neutral ultramafic waters, where dissolution of a Si-containing mineral (such as chlorite) is presumably occurring (Section 3.7), and the acidic waters (pH $<$ 4), where Si is possibly being released by dissolution of kaolinite or another silicate mineral (Section 3.4.4). The Al-containing waters are generally strongly undersaturated with respect to kaolinite (Fig. 71), indicating that this mineral could be actively dissolving.

Aluminium

The Al-containing waters appear to be equilibrated with jurbanite (Fig. 72), as suggested previously (Section 3.4.4). These waters show little tendency to equilibrate with alunite (Fig. 73), and are in many instances highly oversaturated with respect to this mineral phase. Note that a composite diagram for Al minerals was shown in Fig. 40.

Iron

The K_T value for the amorphous iron oxide ferrihydrite is not well defined and has an uncertainty of about one order of magnitude. This is demonstrated in Fig. 74 by the lines for SI equals 1 and -1, which indicate the uncertainty for calculating equilibration with this phase. Also shown is the line for solution equilibration with respect to the crystalline iron oxide goethite, which occurs at a much lower K_T, due to the much lower solubility of this phase. The deep waters appear to be approximately at equilibrium with ferrihydrite, whereas some of the acid waters are strongly undersaturated with respect to ferrihydrite, and have SI values that suggest that they are at

equilibrium, or even understaturated, with respect to goethite. These waters could possibly be actively dissolving Fe from goethite or other Fe oxides.

Other Metals

The other metals (*e.g.* Cr, Mn, Co, Ni, Cu, Zn and Ag) are generally undersaturated with respect to their relevant solid phases (*e.g.* Fig. 75). Thus the solution concentration of these metals is presumably controlled by adsorption on iron oxides or other oxide surfaces, and/or the kinetics of dissolution during weathering.

Gold

Gold metal is the important solid phase of Au. The calculated SI for Au metal is dominantly controlled by the Eh (Fig. 76). Indeed, the highly oxidized waters (Eh > 0.65 V) are theoretically significantly undersaturated with respect to Au metal. In these waters Au concentration could be limited by sorption reactions or by kinetic constraints (*i.e.* Au is still actively dissolving in these high Eh waters, and could reach higher concentrations if the oxidized waters remained in contact with a Au source).

Waters at low Eh are calculated as being up to 8 orders of magnitude oversaturated with respect to Au metal (Fig. 76). This may not be correct because it does not include other ligands such as thiosulphate, which complex Au very strongly. The low Eh waters are generally contain low concentrations of Au (Fig. 60). In such circumstances, thiosulphate at levels below detection could still complex the Au present (Gray, 1990). The speciation program used to derive the SI values for Au metal only included the concentration of ligands such as chloride or iodide (as thiosulphate was, in all cases tested, below detection). Given the absence of data, the effect of thiosulphate cannot presently be tested.

The effects of complexation by ligands at low concentrations is nowhere near as pronounced for the other elements, as the strength of bonding of ligands such as $S_2O_3^{2-}$ is much weaker than for Au, and major constituents such as Cl^-, HCO_3^- or OH^- are more important. The conclusions on the other elements described above would not be invalidated by assuming the presence of ligands such as thiosulphate at concentrations below the analytical detection limit.

In general the speciation results supported conclusions from previous Sections. In particular Au was observed to be complexed by either chloride or iodide, whereas the solution concentrations of other elements appeared to be controlled by a number of phases, namely:

Ca: gypsum
Sr: Sr-substituted gypsum (?)
Si: quartz, amorphous SiO_2, kaolinite
Al: jurbanite, kaolinite
Fe: ferrihydrite (?), goethite (?)
other metals: adsorption (?), dissolution reactions (?)

3.9. Statistical Analyses

3.9.1. Introduction

Analyses of correlation coefficients were used to investigate element associations in groundwaters, and to determine additional information concerning the relationships between groundwater masses.

The analyses examined the data sets identified in the multi-variate plots (Fig. 62), namely:

(i) the entire data set;

(ii) the shale waters (P1, P9, P25, P27, P28);
(iii) the mafic waters (P2 - P4, P13 - P17, P19, P20, P22 - P24, P26, P32 - P36, P41);
(iv) the ultramafic waters (P6 - P8, P10 - P12, P30, P31, P37, P38);
(v) the deep waters (P42 - P50).

Note that a number of the data sets (and in particular, the shale waters data set) contained a small number of samples, which will significantly reduce the number of significant correlations.

For simplicity, the TDS value was used instead of the elements Na, Mg, Cl and SO_4. These elements were all highly correlated with TDS.

Correlation matrices for each data set are shown in Appendices 3a - 3e. This information was analysed by relating the correlation value for each variable pair to the probability that it represents a significant correlation. Those correlations were then displayed according to their significance. Thus a correlation significant to the 99.9 % level is displayed in bold type; a correlation significant to the 99 - 99.9 % level is displayed in italics; a correlation significant to the 95 - 99 % level is displayed in normal type; and insignificant correlations are displayed in small type to only one digit. Results for each data set are discussed separately in the following Sections.

3.9.2. Entire Data Set

Correlations for the entire set of waters (Appendix 3a) are strongly affected by the differences between the saline/neutral deep waters, and the (relatively) fresher/acidic shallow waters. Thus pH is highly correlated with TDS (r = 0.67), and other TDS dependant elements such as Br. Potassium, unlike TDS, is only weakly correlated with pH (r = 0.30), due to the enrichment of K in highly acid waters (Section 3.4.4). The species HCO_3, Ca and Sr were also highly correlated with pH, suggesting enrichment of these elements in the neutral waters. The poorer correlation of Ca and Sr with TDS for this and other data sets is presumably because they precipitate at high TDS (Sections 3.3 and 3.8).

The strong negative correlation observed between pH and Eh (r = -0.60) is consistent with the tendency of solutions to have lower Eh values with increasing pH (Fig. 34). Aluminium has a particularly marked negative correlation with pH (r = -0.73), due to dissolution of Al and Al/Si minerals at low pH (Section 3.4.4; Fig. 43). A weaker negative correlation between pH and Si is also observed, for similar reasons. The negative correlation between As and pH is possibly due to release of adsorbed As in acidic conditions. The negatively correlation with pH is the strongest correlation for I (r = -0.45)and is possibly due to its increased dissolution and/or desorption in acidic conditions.

Correlations with Eh tend to be the inverse of the pH correlations discussed above, due to the negative correlation between Eh and pH. There are some additional correlations, the most important of which is the strong correlation between Au and Eh (r = 0.50), supporting the hypothesis that Au mobilization is primarily controlled by oxidation conditions (Section 3.6; Figs. 59 and 60). Note that this correlation is the strongest for either of these variables. In addition, Eh is positively correlated with NO_3 (possibly due to ammonia oxidation at high Eh) and negatively correlated with Fe (Section 3.5; Fig. 37).

Other important correlations include:
(i) Ca with Sr (r = 0.78);
(ii) Al, Si and As, due to the tendency of these elements to be enriched in acidic waters;
(iii) Cr, Ag, Bi and Sc, due to their strong enrichment in the ultramafic waters (Section 3.7);
(iv) Mn with Co (r = 0.64; also see Fig. 50);

(v) Co with Ni, Zn and, more weakly, Cu, possibly due to their strong enrichment in groundwaters from the northern section of the study area (Section 3.7; Fig. 62).

3.9.3. Shale Waters Subset

Comparison of the correlation matrix for the shale waters (Appendix 3b) with the entire data set shows several differences. These waters have lower concentrations of a number of trace elements (Section 3.7) and show fewer significant correlations, in part due to lower analytical precision.

Due to the absence of any deep water samples, TDS no longer correlates with pH. Elements correlating (weakly) with TDS are Sr, Mn, Ag, Fe and Ca which tend to increase in the more saline waters. As previously, pH and Eh are negatively correlated ($r = -0.91$). Elements correlated negatively with pH are I, Ni, Al and Si. Aluminium, Si and Ni are also very strongly correlated ($r = 0.99$). As observed for the entire data set, Ca and Sr are correlated together ($r = 0.90$).

3.9.4. Mafic Waters Subset

More significant correlations were observed for the mafic waters data set (Appendix 3c) than for the shale waters, possibly as a consequence of the larger number of samples, and of the higher minor element concentrations.

Important correlations observed include:

(i) pH with TDS ($r = 0.68$);
(ii) TDS with Ca, Sr and Ag;
(iii) Ca with Sr ($r = 0.79$)
(iv) Ca and HCO_3 with pH
(v) Al negatively with pH ($r = -0.71$), and positively with As ($r = 0.76$);
(vi) Al, weakly, with Si ($r = 0.57$)
(vii) I negatively with pH ($r = -0.56$)
(viii) Au with Cu ($r = 0.55$) and Eh ($r = 0.38$), with the Au - Cu correlation possibly due to Cu enrichment with Au mineralization;
(ix) Co with Ni ($r = 0.93$) and, moderately, with Mn ($r = 0.67$);
(x) Fe negatively with Eh ($r = -0.54$);
(xi) Zn with Cu ($r = 0.62$);
(xii) Cu, moderately, with Eh, Au and Ni.

Neither K or Br have any significant correlation with TDS. Bromine is significantly correlated with Co ($r = 0.77$) and Ni ($r = 0.80$), suggesting enrichment with mineralization. This is consistent with the discussed potential for use of Br as an indicator for mineralization (Section 3.5, under Iodide). Note however that this result is only observed for the mafic data set, suggesting that this Br enrichment may only be a useful exploration tool where the geology of the site being investigated is known. No clear correlations are observed for K, suggesting K may be controlled by a number of factors, such as increases with salinity or acidity (Section 3.4.4; Fig 38).

The ultramafic indicators Cr, Ag, Bi and Sc (Section 3.7) are all correlated with each other, indicating an "ultramafic influence", even in this set of selected mafic waters. This presumably arises from some of the waters having had some minor contact with ultramafic material. Although the minor element chemistry is still dominated by the mafic interactions the "ultramafic signature" can still be observed in terms of the elements strongly enriched in ultramafic waters (*i.e.* Cr, Ag, Bi and Sc), but only weakly affected by interaction with mafic materials.

3.9.5. Ultramafic Waters Subset

Correlations within the ultramafic data sets (Appendix 3d) yield some important differences with the other data sets. Bromide is highly correlated with TDS (r = 0.96), unlike the shale and mafic waters, which show little or no correlation. However Ca and Sr are only poorly correlated with TDS, though well correlated with each other (r = 0.85), as with previous data sets. As with the mafic data set, no clear correlations are observed for K, suggesting K may be controlled by a number of factors.

As previously, pH is positively correlated with HCO_3 (r = 0.90) and negatively correlated with Al (r = -0.80). Elements most strongly positively correlated with Eh are NO_3 (r = 0.91) and Au (r = 0.87), presumably due to the redox control over the mobility of these two species.

Interestingly, though Cr and Ni were good indicators of ultramafic waters, these two elements did not correlate with each other (r = -0.5), nor with the other ultramafic indicators, within the ultramafic data set. This is possibly due to the influence of acidity and weathering intensity (Section 3.7) on the dissolution of these elements. The other ultramafic indicators Ag, Bi and Sc are highly correlated with each other (correlation coefficients between 0.83 and 0.95). If detection limits can be improved, these three elements appear to be better indicators (in groundwater) of ultramafic rocks at this site than Cr or Ni.

Other trace elements give no strong correlations, and those present are not very sensible. Manganese shows a moderate correlation with K (r = 0.74), Co with Al (r = 0.72), and Zn with Ca (r = 0.73), while Cu appears to be weakly associated with the ultramafic elements Ag (r = 0.57) and Sc (r = 0.66).

3.9.6. Deep Waters Subset

The deep water data set represents the highly saline waters that were sampled at depth. The samples were all within the Trial Pit area. Their location (Fig. 4) and chemistry (Fig. 62; Appendix 1) suggest they are primarily mafic waters. Correlation analysis (Appendix 3e) shows that K and Br are highly correlated with TDS. This suggests that the geological and chemical effects on the distribution of these elements, as described previously (Sections 3.3 and 3.4.4), primarily occurs in the shallow waters.

Aside from these correlations, few important associations could be delineated. Data for NO_3, Au, Si and As are discounted because values are generally at the detection limit for these elements. Iodide appeared to be negatively correlated with Eh (r = -0.76). As with the other data sets, Ca and Sr were correlated together (r = 0.83). However, Mn and Co were also correlated with these elements. This suggests that at depth all four elements may have similar geochemistries.

3.9.7. Summary

In general, each data set had correlations dependent on the chemistries of the particular group. Thus differences in correlations between groups gives information of how the element associations change. Thus, mafic indicators such as Zn and Cu tend to be highly correlated within the mafic data set but not in the shale or ultramafic sets. Bromide tends to be associated with Cu in the shale data set, with Co and Ni in the mafic data set, and with TDS in the ultramafic and deep data sets. Gold is enriched in the mafic and ultramafic waters: in the mafic waters it is correlated with Cu, whereas in the ultramafic waters it is correlated with Al and Co. The correlations of Cr and Ni are particularly complicated, owing to the specific pattern of enrichment in ultramafic waters (*i.e.* neutral ultramafics are high in Cr and moderate in Ni, while acid ultramafic waters have high Ni and low Cr; Section 3.5), and the fact that Ni is also moderately enriched in mafic waters.

Other elements showed similar correlations for different data sets. Potassium shows no significant correlations with TDS for the shale, mafic or ultramafic data sets, due to the major influence of K enrichment in acid waters. Gold is generally strongly correlated with Eh, supporting previous conclusions (Section 3.6). Calcium and Sr are correlated in all data sets, indicating major similarities in their geochemical dispersion patterns. The cause of the negative correlations between I and pH are not clear, but presumably represent some hydrogeochemical effect. Nickel and Cr are only poorly correlated, due to their complex chemistry (Section 3.7). The other ultramafic indicators, Ag, Bi and Sc, are strongly correlated for the entire data set, mafic and ultramafic subsets, and to a lesser degree the deep water subset.

The statistical data support the previous conclusions about the various controls on distributions (*e.g.* effect of Eh on Au), on element associations (*e.g.* Ca - Sr correlations), and on the water groupings. Observations of ultramafic correlations in the mafic and deep data sets suggest a minor "ultramafic influence" in the waters that had previously been distinguished as mafic (Section 3.7).

4. General Discussion

4.1. Key Observations

Waters were classified in terms of the geological environment in which the bore hole was located (Table 1; Fig. 4). Classes were:

Sf: Waters from the shale/siltstone system in the south-east part of the study area.
M-Sf: Waters close to the interface of the mafic/sediment and shale/siltstone systems.
M-S: Waters from the mafic/sediment system. This is the system hosting the gold mineralization.
M-U: Waters close to the interface of mafic and ultramafic rocks. These waters are situated at 2500E / 4600-4800N.
U: Waters within a major band of Ultramafic rocks, situated at about 2400E / 4050-4300N.

Water were also distinguished as shallow or deep. Deeper water are highly saline (TDS > 100,000 mg/L) and less acid (pH > 5.5) than the shallow waters. These deeper waters appear to be basically homogeneous (Sections 3.3 and 3.5), suggesting only minor groundwater/rock interactions, whereas shallow waters in contact with the oxidized, weathered rocks have compositions highly dependent on the lithology. Thus the shallow waters contact the weathered lithologies for sufficient periods to enable major interactions of the groundwater with the weathered or weathering phases.

Waters are divided into two sub-groups by virtue of their pH-alkalinity characteristics (Fig. 28). The first sub-group comprises the acid (pH < 5.5; HCO_3 < 30 mg/L) waters, which include almost all of the surface Sf, M-Sf, M-S and M-U waters. The second sub-group comprises the more neutral waters (pH > 5.5; HCO_3 > 45 mg/L), which include all of the U waters and deep waters.

Calcium and Sr concentrations correlate well with each other, but only weakly with TDS, presumably due to precipitation reactions involving these elements (Sections 3.3 and 3.8). The other major elements Cl, SO_4, Na, Mg, and to a lesser degree K and Br, correlate closely with TDS. Panglo waters are slightly enriched with respect to Na and Cl, slightly depleted with respect to Mg and SO_4, and strongly depleted with respect to K and Br (Table 2). This suggests that halite (NaCl) is actively dissolving under present day conditions (Section 3.3.)

The redox characteristics of the Panglo waters differ from the standard model for groundwaters (Section 3.4). Water samples were divided into four pH/Eh groups (Table 3; Fig. 35):

group Fe: waters containing Fe;
group HO: waters fitting the "weathering environment" category as given by Sato (1960);
group Al: acid waters;
group Mn: waters with pH/Eh controlled by the redox chemistry of Mn.

The acid waters are dominated by the chemistry of Al sulphate minerals such as alunite and jurbanite (Section 3.4.4). It appears that highly acid waters (pH < 3.5) are dissolving alunite and precipitating jurbanite (eqn. 9), leading to anomalously high K concentrations (Section 3.4.4; Fig. 39). It is feasible that waters with pH < 4.5 are also actively dissolving kaolinite (Fig. 40), leading to high concentrations of Si (Fig. 44).

The upper limit for the Eh of the Panglo groundwaters appears to be set by the Mn^{2+}/Mn_xO_y redox couple (Section 3.4.5; Fig. 41). This is particularly important for the acid-oxidizing waters (pH < 5; Eh > 0.7 V), where this has allowed the generation of sufficiently high Eh values for oxidative dissolution of Au (Fig. 60).

The concentrations of the base metals Cr, Mn, Co, Ni, Cu, Zn and Ag appear to be influenced by geological and chemical controls (Sections 3.5 and 3.7). Shale waters are relatively low in these elements (as well as Br, Sr, Sc and As), while mafic waters are enriched in Mn, Zn and Co (as well as I), and ultramafic waters are enriched in Ni, Cr and Ag (as well as Bi and Sc). In addition these base metals tend to be enriched in the deeper waters and in the acid waters, being depleted in the near-neutral shallow waters. This is consistent with these elements being primarily removed from solution by adsorption on surfaces of secondary minerals, particularly iron oxides, which will be strongest in neutral oxidized conditions. This is also inferred by speciation analysis (Section 3.8), which suggests that concentrations of these metals is not controlled by any particular separate mineral phase.

Arsenic was strongly enriched in acid waters (Fig. 58), again consistent with control by sorption reactions. No clear controls on I concentrations were observed, though there appears to be some enrichment in acid waters (Section 3.9). However, the most important observation for this element was its generally high abundance (average concentration 0.5 mg/L), even in the highly oxidized waters (Fig. 46), where in theory I should volatilize as I_2. This high concentration of I may be consistent with I behaving as a chalcophile element (Section 3.5).

It was found that waters could be effectively classified by using their base metal concentrations. Plotting the water samples using ultramafic 'indicators' as the X-axis and mafic 'indicators' as the Y-axis gave a very good separation between the water groups (Fig. 62). Some sensible mis-classifications were observed by this procedure (Section 3.7).

One attribute indicated by this multi-variate plot was the high metal ion content in the northern water samples (north of 4300N; Fig 63; Section 3.7). Additionally the major Au anomalies were observed in this area (Fig. 27). This suggests this northern area of Panglo to be actively weathering, possibly as a consequence of shear zones or other causes of enhanced groundwater flows.

Speciation analysis (Section 3.8) indicates that at TDS > 90000 mg/L groundwaters become saturated with respect to gypsum (Fig. 67). The deeper groundwater samples all appear to be at equilibrium with gypsum. A number of the waters are approximately in equilibrium with quartz (Fig. 70), and several, with very high Si contents, approach saturation with amorphous SiO_2. These samples are the ultramafic waters, where dissolution of a silicate such as chlorite is presumably occurring, and the low pH waters (pH < 4), where Si is possibly being released by kaolinite dissolution. The Al containing waters are generally strongly undersaturated with respect to kaolinite (Fig. 71).

The important solid phase of Au is the metal, and the primary control on the calculated SI parameter is Eh (Fig. 74). Indeed, the highly oxidized waters (Eh > 0.65 V) are theoretically significantly undersaturated with respect to Au metal. In these waters Au concentration could be limited by sorption reactions or by kinetic constraints (*i.e.* Au is still actively dissolving in these high Eh waters and could reach higher concentrations if the oxidized waters remained in contact with a Au source). Speciation calculations (Section 3.8) indicate that Au may be present in solution as AuI_2^-, rather than $AuCl_2^-$, as a consequence of the relatively high concentration of I. This has not, in the author's experience, been previously observed for groundwaters. It is possible that Au mobilized as AuI_2^- would be redistributed differently during weathering than if mobilized as $AuCl_2^-$.

Statistical analysis (Section 3.9) strongly supported a number of the observations given above. Particular observations were:

(i) Au and Eh were correlated with each other;
(ii) Fe and Eh were commonly negatively correlated;
(iii) I was commonly negatively correlated with pH;
(iv) Ca and Sr were highly correlated in all data sets, with additional correlations with Mn and Co for the deep waters;
(v) Mn, Co, Ni, Zn, and to a lesser degree Cu are strongly correlated in the entire data set, possibly due to strong enrichment of these elements in the northern part of the study area;
(vi) K and Br in many circumstances correlated poorly with TDS, due to influences such as K enrichment in acid water;
(vii) Br was correlated with Co and Ni in the mafic data set, suggesting some Br enrichment with mineralization;
(viii) the ultramafic indicators, Ag, Bi and Sc, were strongly correlated with each other and, in the entire data set, with Cr;
(ix) observations of Ag, Bi and Sc correlations in the mafic and deep water data sets suggest some mixing of ultramafic and mafic waters.

4.2. Outstanding Questions

Several points of interest are still unresolved. These include:

(i) How extensive and homogeneous is the lower saline aquifer in the study area?

(ii) What are the geochemical events that have lead to the strong metal (including Au) enrichment in the northern part of the study area?

(iii) Does the I (and Br?) enrichment in the mineralized waters indicate a usefulness for these elements as pathfinders for Au (or other minerals)?

(iv) Is the multi-element classification scheme described in this report relevant for other sites?

4.3. Implications for Exploration

One complexity in studying the hydrogeochemistry of this site is that the Panglo area may have been disturbed within the immediate past by clearing operations. This may have resulted in rising of the watertable and changes in the chemistry of the groundwater. Thus, while this investigation is useful in terms of giving information on the hydrogeochemistry of Au and other elements and on the processes of anomaly formation, present-day observations may not be directly related to the particular anomalies observed at this site.

The area of Au mineralization investigated in this report includes many interesting features. In general, the concentrations of soluble Au within the mafic and ultramafic waters are well above analytical detection limits, and are anomalously high. Thus, Au in water would be a perfectly adequate indicator for Au mineralization in this area. The principal anomalies in dissolved Au occur in the northern part of the study area (Fig. 27). These anomalies appear to be related to an intense degree of weathering in this northern region, which has resulted in enhanced redox activity (Figs. 10 and 36), and anomalously high concentrations of Br, Mn, Co, Zn, Cu and Ni (Figs. 12, 16 - 20). Further investigation of such an effect would be of value. Clearly, it would be advantageous to determine the mechanism of Au dispersion in weathered material, based on groundwater and/or other information. Unfortunately, though there is now a reasonable theoretical

understanding of the aqueous chemistry of Au, little is known how this is related to geochemical dispersion patterns.

Based on the information obtained at this site, there may be some advantage in water sampling during drilling operations. Separate samples may be taken for Au analysis and for water quality measurements. The later sample could be sent for commercial analysis for Conductivity/TDS, pH, Fe^{2+}, and a suite of elements of interest, such as Cr, Mn, Fe, Co, Ni, Cu and Zn. Such a procedure could provide a low cost adjunct to petrological information. The observation of the Au anomaly at this site suggests such a method could be successful in giving information on the location of buried mineralization in an area under investigation.

Acknowledgements

I would like to thank CSIRO staff for their support in the preparation of this report. C.R.M. Butt and M.J. Lintern assisted in giving advice and in sample collection. Staff who assisted in the analysis of waters included G.D. Longman and M.J. Lintern, who were primarily involved in gold analysis; M.J. Willing, D.C. Wright and A.K. Howe, who provided AAS and Ion Chromatography analyses; and J.W. Wildman who provided ICP analyses. Some of the statistical programs were provided by E.C. Grunsky. Thanks also go to C.R.M. Butt and I.D.M. Robertson for critical comments.

In addition I would like to thank the staff of Pancontinental for their assistance during the sample collection period, with particular mention of R.W. Howard and I.G. Robertson, for their assistance in sample collection, advice, and provision of maps.

References

Andrews, M.J., Bibby, J.M., Fuge, R. and Johnson, C.C., 1984. The distribution of iodine and chlorine in soils over lead-zinc mineralisation, east of Glogfawr, mid-Wales. *J. Geochem. Explor.*, **20**:19-32.

Baas Becking, L.G.M., Kaplan, I.R. and Moore, D., 1960. Limits of the natural environment in terms of pH and oxidation-reduction potentials. *J. Geol.*, **68**:243-84.

Blowes, D.W. and Jambor, J.L., 1990. The pore-water geochemistry and the mineralogy of the vadose zone of sulfide tailings, Waite Amulet, Quebec, Canada. *App. Geochem.*, **5**:327-46.

Van Breeman, N., 1973. Dissolved aluminium in acid sulfate soils and in acid mine waters. *Soil Sci. Soc. Amer. Proc.*, **37**:694-7.

Bricker, O., 1965. Some stability relations in the system $Mn\text{-}O_2\text{-}H_2O$ at 25° and one atmosphere total pressure. *Am. Minera.* **50**:1296-354.

Brinkman, R., 1977. Surface-water gley soils in Bangladesh: Genesis. *Geoderma*, **17**:111-44.

Chitayeva, N.A., Miller, A.D., Grosse, Yu.I. and Christyakova, N.I., 1971. Iodine distribution in the supergene zone of the Gay chalcopyrite deposit. *Geochem. Int.*, **8(3)**:426-36.

Cloke, P.L. and Kelly, W.C., 1964. Solubility of gold under inorganic supergene conditions. *Econ. Geol.*, **59**:259-70.

Dionex, 1985. Technical Note 16. (PO Box 3603 Sunnyvale, California, USA).

Doyle, R.W., 1968. The origin of the ferrous ion-ferric oxide Nernst potential in environments containing dissolved ferrous iron. *Am. J. Sci.*, **266**:840-59.

Drever, J.I., 1982. "The Geochemistry of Natural Waters." (Prentice-Hall, Inc., Englewood Cliffs, N.J. U.S.A.). 388 p.

Frick, C., Strauss, S.W. and Dixon, R., 1989. The use of chlorine, bromine and fluorine in detecting a buried Cu-Zn orebody along the zinc-line in the Murchison Range, South Africa. *J. Geochem. Explor.*, **34**:83-102.

Fuge, R., 1990. The role of volatility in the distribution of iodine in the secondary environment. *Appl. Geochem.*, **5**:357-360.

Fuge, R. and Johnson, C.C., 1984. Evidence for the chalcophile nature of iodine. *Chem. Geol.*, **43**:347-52.

Fuge, R. and Johnson, C.C., 1986. The geochemistry of iodine - a review. *Environ. geochem. Hlth.*, **8**:31-54.

Fuge, R., Andrews, M.J. and Johnson, C.C., 1986. Chlorine and iodine, potential pathfinder elements in exploration geochemistry. *Appl. Geochem.*, **1**:111-6.

Fuge, R., Andrews, M.J., Clevenger, T.E., Davies, B.E., Gale, N.L., Pavely, C.F. and Wixson, B.G., 1988. The distribution of chlorine and iodine in soil in the vicinity of lead mining and smelting operations, Bixby area, S.E. Missouri, U.S.A. *Appl. Geochem.*, **3**:517-21.

Garrels, R.M. and Christ, C.L., 1965. "Solutions, Minerals and Equilibria." (Harper and Row, New York). 450 p.

Gray, D.J. 1990. Hydrogeochemistry in the Mount Gibson Gold District. (AMIRA P240: Laterite Geochemistry). CSIRO Division of Exploration Geoscience Restricted Report 120R.

Gundersen, P. and Beier, C., 1988. Aluminium sulphate solubility in acid forest soils in Denmark. *Water, Air, and Soil Pollut.*, **31**:247-261.

Hostettler, J.D., 1984. Electrode electrons, aqueous electrons, and redox potentials in natural waters. *Amer. J. Sci*, **284**:734-59.

Karathanasis, A.D., Evangelou, V.P. and Thompson, Y.L., 1988. Aluminum and iron equilibria in soil solutions and surface waters of acid mine watersheds. *J. Environ. Qual.*, **17**:534-43.

Lakin, H.W., Curtin, G.C. and Hubert, A.E., 1974. Geochemistry of gold in the weathering cycle. U.S. Geol. Surv. Bull. 1330, 80 p.

Lintern, M.J and Scott, K.M., 1990. The distribution of gold and other elements in soils and vegetation at Panglo, Western Australia. (AMIRA P241: Weathering Processes). CSIRO Division of Exploration Geoscience Restricted Report.

Miller, A.D. and Fisher, E.I., 1973. Dissolution of gold during oxidation by MnO_2. *Geochem. Int.*, **10**:656-63.

Nordstrom, D.K., 1982. The effect of sulfate on aluminum concentrations in natural waters: some stability relations in the system Al_2O_3-SO_3-H_2O at 298 K. *Geochim. Cosmochim. Acta,* **46**:681-92.

Parkhurst, D.L., Thorstenson, D.C. and Plummer, L.N., 1980. PHREEQE, a computer program for geochemical calculations. U.S. Geol. Surv. Water Resources Investigations 80-96, 210p.

Sato, M., 1960. Oxidation of sulfide ore bodies, 1. Geochemical environments in terms of Eh and pH. *Econ. Geol.*, **55**:928-61.

Schwab, A.P. and Lindsay, W.L., 1983. Effect of redox on the solubility and availability of iron. *Soil Sci. Soc. Am. J.*, **47**:201-5.

Scott K.M. 1989a. Mineralogy and geochemistry of weathered shale profiles at the Panglo Gold Deposit, Eastern Goldfields, W.A. (AMIRA P241: Weathering Processes). CSIRO Division of Exploration Geoscience Restricted Report 32R.

Scott K.M. 1989b. Mineralogy and geochemistry of weathered mafic/ultramafic volcanics from Section 4200N at Panglo, Eastern Goldfields, W.A. (AMIRA P241: Weathering Processes). CSIRO Division of Exploration Geoscience Restricted Report 42R.

Scott K.M. 1990. The mineralogical and geochemical effects of weathering on volcanics from the Panglo Deposit, Eastern Goldfields, W.A. (AMIRA P241: Weathering Processes). CSIRO Division of Exploration Geoscience Restricted Report 143R.

Weast, R.C., Astle, M.J. and Beyer, W.H., 1984. "CRC Handbook of Chemistry and Physics." F-154 Elements in Sea Water. (64th Edition; CRC Press Inc., Florida, USA).

Xie Xuejing, Sun Huanzhen and Li Shanfang, 1981. Geochemical exploration in China. *J. Geochem. Explor.*, **15**:489-506.

Appendix 1: Tabulated Water Data

Sample Number	Hole Name	Geology Group	pH/Eh Group	Easting (m)	Northing (m)	RL (m)	WT (m RL)	SD (m RL)	Eh (V)	pH	Fe2+ mg/L
P1	ARP419-1	Sf	HO	2755	4190	343.6	336.7	332.8	0.38	6.45	0
P2	ARM421-2	M-S	HO	2670	4210	343.5	338.3	328.3	0.47	5.05	0
P3		M-S	HO	2670	4210	343.5	338.3	318.5	0.43	5.24	0
P4		M-S	HO	2670	4210	343.5	338.3	309.5	0.51	5.24	0
P5	ARP423-5	M-S	HO	2448	4230	343.4	338.5	333.9	0.56	4.5	0
P6	ARP423-2	U	HO	2390	4230	343.2	337.7	327.7	0.50	6.18	0
P7		U	HO	2390	4230	343.2	337.7	308.2	0.49	6.26	0
P8		U	HO	2390	4230	343.2	337.7	293.2	0.43	6.34	0
P9	ARP407-2	Sf	HO	2660	4070	342.7	338.7	328.7	0.51	5.4	0
P10	PSRC367	M-S	HO	2440	4025	343.4	337.4	334.4	0.50	4.53	0
P11	ARP407-5	U	HO	2370	4070	342.9	337.4	327.4	0.47	6.12	0
P12		U	HO	2370	4070	342.9	337.4	302.9	0.45	6.08	0
P13	ARP399-1	M-S	HO	2570	3990	342.3	336.5	326.5	0.43	5.61	0
P14	ARP384-3	M-Sf	HO	2530	3840	342	336	326	0.42	4.82	0
P15	ARP386-5	M-Sf	HO	2540	3860	342	336	326	0.53	4.92	0
P16	ARP373-1	M-S	Mn	2370	3730	344.8	335.3	325.3	0.82	3.38	0
P17	ARP377-10	M-S	Al1	2370	3770	345.8	335	325.8	0.41	3.67	0
P18	ARP377-6	M-S	HO	2448	3770	345.7	335.9	331.2	0.38	5.65	0
P19	ARP377-5	M-S	L	2470	3770	345.5	335.9	325.9	0.25	4.8	0
P20	ARP377-4	M-S	Al2	2490	3770	345.5	335.7	326.5	0.66	3.52	0
P21	ARP377-2	M-Sf	HO	2530	3770	342	336	331	0.34	5.41	0
P22	ARP374-10	M-S	Mn	2440	3740	345.1	335.9	327.1	0.81	3.25	0
P23	PSR491	M-Sf	Fe2	2398	3602	342	335	333	0.34	3.51	8
P24	ARP342-2	M-S	Al2	2340	3540	341.7	334.7	330.2	0.71	3.22	0
P25	PSR627	Sf	Fe2	2650	3500	341.9	332.9	331.9	0.49	4.03	1.8
P26	PSR495	M-Sf	Fe1	2351	3402	340	334	331.7	0.16	5.96	12.5
P27	PSR616	Sf	Al2	2350	3200	342	335.8	335	0.61	3.07	0
P28	PSR620	Sf	Al2	2550	3200	342.1	336.6	333.6	0.58	3.04	0
P29	ARP397-2	M-S	Al1	2350	3970	345	337	335.5	0.55	3.41	0
P30	ARP423-3	U	HO	2410	4230	343.2	337.7	327.7	0.46	5.97	0
P31	ARP431-3	U	HO	2412	4310	343.7	338.2	328.2	0.34	5.65	0
P32	ARM431-2	M-S	Mn	2650	4310	344.3	338.8	328.8	0.80	3.95	0
P33		M-S	Mn	2650	4310	344.3	338.8	318.8	0.78	4.42	0
P34	ARP438-12	M-S	Mn	2800	4380	345.4	337.4	327.4	0.85	3.65	0
P35	ARP453-1	M-S	Mn	2830	4530	347.2	339.2	329.2	0.86	3.72	0
P36	ARP453-7	M-S	Al1	2710	4530	345.8	339.3	336.8	0.48	3.97	0
P37	ARP458-1	M-U	Mn	2502	4580	345.4	338.4	327.4	0.79	3.45	0
P38		M-U	Mn	2502	4580	345.4	338.4	302.4	0.73	4.79	0
P39	ARP466-1	M-U	Al1	2500	4660	345.6	337.6	333.6	0.49	3.26	0.35
P40	ARP476-1	M-U	Al1	2500	4760	345.8	339.8	334.8	0.34	3.9	0.35
P41	PSR402	M-S	Fe2	2775	4897	347.8	339.3	332.8	0.43	4.12	3.5
P42	Bore 2	M-S	Fe1	2813	4514	nd	nd	nd	0.23	6.09	nd
P43	Bore 4	M-S	Fe1	2725	4301	nd	nd	nd	0.30	5.97	nd
P44	Bore 5	M-S	Fe1	2694	4492	nd	nd	nd	0.29	6.28	nd
P45	Bore 7	M-S	HO	2601	4349	nd	nd	nd	0.43	6.56	nd
P46	Bore 8	M-Sf	HO	2650	4159	nd	nd	nd	0.50	6.63	nd
P47	Trial Pit	M-Sf	HO	2679	4190	nd	nd	nd	0.43	6.6	nd
P48	Pipe A	M-S	Fe1	2728	4267	nd	nd	nd	0.22	6	nd
P49	Pipe B	M-S	HO	2590	4285	nd	nd	nd	0.29	5.77	nd
P50	Pipe C	M-Sf	HO	2668	4127	nd	nd	nd	0.35	6.5	nd

All holes vertical
nd: not determined

RL: Reduced Level
WT: Watertable
SD: Sampling Depth

	DO (#) mg/L	HCO3 mg/L	SO4 mg/L	S2O3 mg/L	Cl mg/L	Br mg/L	I mg/L	NO3 mg/L	Na mg/L	K mg/L	Mg mg/L
1	4.5	106	3480	nd	33300	23.8	0.08	3.3	18547	32.8	1999
2	5.6	11	4500	nd	47700	40	*<0.05*	3.3	26547	59	2856
3	5.4	21	4530	nd	49280	40.2	0.11	9	27711	64	2968
4	5	19	4460	nd	49300	39.4	*<0.05*	*<3.2*	27784	67	2989
5	6.5	1	4720	nd	51900	47.8	0.10	*<4*	29020	74	3060
6	4	131	4730	nd	48400	41.9	0.10	*<4*	26402	42	3040
7	2.9	154	5130	nd	54300	44.1	0.35	*<4*	29820	60	3254
8	2.6	166	5740	nd	63300	46.3	*<0.07*	*<4*	34475	85	3662
9	5.8	24	3450	nd	35800	16.8	*<0.04*	5.3	19783	51	1775
10	7.1	0	5320	nd	57900	47.8	0.27	*<4*	31057	58	3264
11	5.7	113	4850	nd	47900	40.5	0.23	*<4*	25747	28.1	2713
12	4.3	121	5030	nd	54100	41.9	0.82	*<4*	28875	52	2958
13	3	103	4610	nd	45900	26.5	0.11	7	24729	44	2509
14	3.9	10	4500	nd	53900	24.4	0.33	*<4*	28802	54	2887
15	3.5	10	4320	nd	51600	23	*<0.05*	*<4*	28220	54	2774
16	2.9	0	3610	nd	41800	31.8	0.41	*<3.2*	23274	63	2275
17	2	0	4210	nd	46100	33.5	1.90	*<3.2*	25165	70	2448
18	3.2	264	3340	nd	37500	27.3	0.84	20.4	20583	63	1989
19	2.9	23	4050	nd	47600	31.7	0.23	31.7	25747	68	2550
20	4.5	0	3560	nd	43600	25.8	0.20	8.8	24002	58	2397
21	4.1	27	4040	nd	40800	12.9	0.27	*<2.4*	23202	47	1703
22	3.7	0	2570	nd	32700	25.2	0.50	15.8	18401	53	1816
23	2.25	0	2890	nd	35000	26	1.10	*<2.4*	19129	65	1877
24	5.4	0	3180	nd	37400	28.3	1.60	22.4	20511	67	1999
25	3.3	1	3660	nd	50600	27.3	0.40	*<4*	28075	47	2601
26	1.35	76	3860	nd	44200	23	0.61	*<3.2*	24074	50	2173
27	5	0	2680	nd	27800	21.6	0.37	3.4	15928	86	1499
28	2	0	1550	nd	25000	21.3	0.43	3.5	13892	51	1071
29	3.65	0	1730	nd	21000	17.2	0.57	13.6	11637	37.4	956
30	3.8	77	4670	nd	51800	46.3	0.09	*<4*	28075	61	2846
31	2.2	115	6390	nd	68800	51	0.53	*<5*	39639	102	3907
32	6.2	0	3510	nd	42100	35.9	0.39	*<3.2*	22983	55	2213
33	6.9	0	3610	nd	42900	35.2	0.52	*<4*	23565	56	2264
34	5.3	0	3950	nd	42500	39	0.85	*<4*	23929	60	2438
35	5.15	0	3770	nd	40000	35.9	0.60	*<3.2*	22038	54	2315
36	2.1	0	3960	nd	41400	38.2	1.25	*<3.2*	22838	43	2142
37	6.8	0	1980	nd	21900	25.6	0.61	190	12583	59	1007
38	4.2	3	4790	nd	47400	40.5	0.74	97	25966	85	2662
39	2.8	0	4630	nd	42400	39.4	1.20	12.8	23129	81	2356
40	2.6	0	3420	nd	32800	37.5	0.94	3.4	18038	62	1663
41	3.5	0	3320	nd	34900	36.5	0.82	*<2.8*	19274	36.1	1734
42	nd	49	8450	*<0.12*	107000	60	0.43	*<9*	56586	167	5131
43	nd	74	7210	*<0.08*	82100	56	0.48	*<6.4*	41312	116	4070
44	nd	105	4330	*<0.08*	64700	53	0.65	*<6*	30475	68	2999
45	nd	108	6610	*<0.08*	75500	53	0.20	*<6*	38257	100	4070
46	nd	145	6380	*<0.08*	72000	53	0.28	*<6*	37312	98	4009
47	nd	83	5990	*<0.08*	67100	52	0.22	*<5.5*	33675	85	3692
48	nd	99	7000	nd	74000	55	0.70	*<10*	41320	109	4600
49	nd	133	6660	nd	72000	52	0.35	*<10*	38950	102	4300
50	nd	89	5750	nd	61500	47.5	0.50	*<10*	33760	84	3700
SW		142	2652		19000	65	0.06		10500	380	1350

nd: not determined
#: dissolved oxygen

Numbers in italics denote values below the calculated detection limit

SW: sea water

	Ca mg/L	Sr mg/L	% Ion (#) Balance	TDS mg/L	Au ug/L	Si mg/L	Al mg/L	Cr mg/L	Mn mg/L	Fe mg/L	Co mg/L
1	558	3.7	-1	57994	*0.02*	0.8	*0.0*	*0*	0.13	0.03	*0.00*
2	684	6.2	0	82392	0.15	*0*	*0.1*	0.06	1.14	*0*	0.25
3	648	6.2	0	85252	0.09	*0*	*0.1*	0.04	1.95	*0*	0.28
4	635	6.1	0	85283	*0.05*	*0*	*0.1*	0.04	2.49	*0.01*	0.33
5	863	6.7	0	89688	0.92	1.1	0.2	0.12	0.24	0.02	0.07
6	814	8.1	-1	83578	0.20	20.4	*0.1*	0.35	0.10	*0*	0.07
7	685	9.3	-1	93407	0.48	17.2	*0.1*	0.24	0.82	0.04	0.08
8	646	8.2	-2	108061	0.23	11.7	*0.1*	0.14	2.64	*0*	0.15
9	822	5.3	-2	61712	0.11	0.9	*0*	*0.03*	0.12	*0*	0.05
10	918	12.0	-2	98571	0.34	3.0	*0.0*	0.25	0.50	*0*	0.10
11	1142	11.3	-2	82517	0.06	18.6	*0.1*	0.10	0.18	*0*	0.11
12	921	11.3	-3	92073	0.17	16.9	*0*	0.10	0.85	*0*	0.19
13	748	7.4	-3	78617	0.73	*0*	*0.0*	0.05	0.58	*0*	0.13
14	886	8.7	-2	91058	0.37	*0*	*0.0*	0.05	0.49	*0*	0.14
15	864	9.9	-1	87860	0.56	*0*	*0*	0.07	0.06	*0*	0.17
16	334	6.1	-1	71471	0.30	2.2	41.7	0.04	4.40	0.02	0.18
17	455	6.6	-2	78510	0.15	*0*	15.0	0.03	0.84	*0*	0.08
18	702	4.3	-2	64339	*0.05*	1.8	*0*	*0*	0.23	*0.00*	*0.04*
19	625	7.2	-2	80685	0.25	*0*	0.7	*0.01*	0.67	*0*	0.13
20	615	8.9	-1	74304	0.40	5.8	18.0	*0.01*	1.05	0.08	0.18
21	1377	10.8	-1	71195	*0.02*	*0*	*0*	*0*	0.13	*0*	*0.04*
22	259	1.7	0	55979	0.15	20.5	58.7	*0.02*	1.00	*0*	0.10
23	385	2.4	-2	59474	*0.03*	28.7	22.3	*0.01*	1.00	5.45	0.09
24	410	3.6	-2	63695	0.73	28.6	20.6	*0*	1.15	*0*	0.10
25	777	7.8	-1	85791	0.16	0.4	1.0	*0*	0.32	1.11	*0.03*
26	814	8.3	-2	75232	0.20	*0*	*0*	*0.01*	1.59	6.78	0.05
27	323	2.0	0	48495	0.15	34.7	43.3	0.05	0.09	0.10	*0.04*
28	301	2.0	-2	42065	0.07	43.6	45.0	*0.02*	0.11	0.02	*0.06*
29	395	2.2	-2	35830	*0.05*	20.0	8.1	*0.00*	0.73	*0*	*0.03*
30	784	10.8	-2	88365	0.56	21.1	*0*	0.43	0.10	*0*	*0.05*
31	551	10.2	0	119503	*0.04*	3.2	*0*	*0.02*	1.63	*0*	0.22
32	663	8.8	-2	71572	0.33	1.8	4.4	*0.03*	2.59	*0*	0.26
33	669	9.8	-2	73104	0.11	0.5	1.6	*0.02*	2.48	*0*	0.19
34	412	6.5	-1	73347	3.73	*0*	9.9	*0.01*	3.21	*0*	0.32
35	387	2.0	-2	68617	0.51	2.1	6.7	*0.03*	4.61	*0*	0.30
36	719	6.5	-2	71177	0.18	12.1	5.4	*0.01*	12.39	*0*	0.29
37	227	2.0	-1	37909	2.26	32.1	31.1	0.04	0.50	*0*	0.30
38	434	6.3	-2	81401	0.85	7.8	3.6	*0.01*	0.89	*0*	0.16
39	544	7.4	-2	73276	0.06	22.2	26.1	*0.01*	8.41	0.23	1.17
40	459	4.1	-2	56568	0.07	20.1	24.6	*0.02*	4.32	0.14	0.38
41	438	4.2	-2	59756	*0.05*	1.6	7.7	*0.02*	17.85	1.89	0.42
42	620	7.7	-4	178038	0.08	*0*	*0*	*0*	3.72	3.75	0.13
43	524	8.2	-6	135425	*0.04*	*0*	*0*	*0*	4.75	0.67	0.26
44	1703	29.9	-7	104384	0.14	1.6	*0*	*0.01*	10.82	0.63	0.42
45	862	12.5	-5	125505	0.33	*0*	*0*	*0.01*	8.26	*0*	0.39
46	677	6.3	-4	120600	0.07	*0*	*0*	*0.01*	2.81	*0*	0.25
47	789	10.4	-5	111425	0.29	*0*	*0*	*0.02*	4.28	*0*	0.33
48	700	4.0	0	127833	*0.02*	*0*	*0*	*0.03*	3.24	3.19	0.19
49	1000	5.1	-2	123129	*0.02*	*0*	*0*	*0.03*	7.90	0.10	0.46
50	955	5.0	-1	105840	*0.05*	*0*	*0*	*0.03*	3.83	*0*	0.24
SW	400	8.1	0	34417	0.00001	3	0.01	0.00005	0.002	0.01	0.00027

nd: not determined
#: = 100 x (cations-anions)/total ions

Numbers in italics denote values below the calculated detection limit

SW: sea water

	Ni mg/L	Cu mg/L	Zn mg/L	Ag mg/L	As mg/L	Bi mg/L	Sc mg/L
1	*0.02*	*0.03*	*0*	*0.00*	*0.03*	*0.03*	*0.02*
2	0.21	0.06	*0.17*	0.03	*0.04*	*0.15*	0.08
3	0.23	0.07	*0.07*	0.04	*0*	*0.10*	0.09
4	0.24	0.06	*0.10*	0.03	*0*	*0.16*	0.12
5	0.10	0.08	*0*	0.05	*0*	*0.13*	0.16
6	0.70	0.08	*0*	0.05	*0.1*	0.26	0.14
7	0.50	0.11	*0*	0.06	*0*	0.27	0.20
8	0.39	0.12	*0.07*	0.08	*0*	0.27	0.23
9	*0.03*	*0.01*	*0*	*0*	*0.2*	*0.17*	*0.02*
10	0.10	0.10	0.29	0.05	*0.2*	0.34	0.21
11	0.42	0.09	0.31	0.06	*0.2*	0.32	0.19
12	0.55	0.06	*0.17*	0.04	*0.2*	0.23	0.16
13	0.11	0.08	*0.12*	0.05	*0.04*	0.19	0.13
14	0.10	0.08	*0*	0.05	*0.1*	0.26	0.16
15	0.13	0.08	*0.23*	0.04	*0.05*	0.22	0.12
16	0.18	0.20	0.25	0.05	*0.2*	*0.06*	0.16
17	0.13	0.10	*0.15*	0.05	*0*	*0.09*	0.11
18	*0.01*	*0.01*	*0*	*0*	*0.03*	*0.17*	*0.07*
19	0.09	0.05	*0*	0.02	*0*	*0.06*	0.08
20	0.13	0.09	0.37	0.02	*0.2*	*0.09*	0.08
21	*0.02*	0.04	*0*	0.02	*0.04*	*0.09*	*0.05*
22	0.09	0.10	*0*	*0.01*	0.5	*0*	*0.11*
23	*0.08*	*0.02*	*0*	*0.00*	*0.1*	*0.04*	*0.07*
24	*0.06*	0.04	*0*	*0*	*0.2*	*0*	*0.07*
25	*0.05*	0.03	*0*	0.02	*0*	*0.01*	*0.02*
26	*0.04*	0.03	*0*	0.02	*0*	*0.11*	0.08
27	0.20	*0.02*	*0*	*0*	0.4	*0*	*0.05*
28	0.25	*0.01*	*0*	*0*	0.5	*0*	*0.02*
29	*0.07*	0.03	*0.01*	*0.01*	*0.1*	*0.10*	*0.04*
30	0.25	*0.00*	*0*	*0.01*	*0*	*0.10*	*0.05*
31	0.52	*0.02*	*0.07*	0.03	*0*	*0*	*0.08*
32	0.27	0.07	*0.17*	0.03	*0*	*0.03*	0.08
33	0.21	0.03	*0*	0.02	*0*	*0*	*0.05*
34	0.38	0.20	0.25	0.02	*0*	*0*	*0.02*
35	0.33	0.17	0.27	0.02	*0*	*0.09*	*0.08*
36	0.31	0.11	*0*	*0.01*	0.3	*0.14*	*0.08*
37	0.79	0.13	*0*	*0.01*	*0.3*	*0.02*	*0.07*
38	0.69	0.03	*0*	0.01	*0*	*0*	*0.05*
39	1.30	0.16	3.45	*0.01*	*0.2*	*0.03*	0.11
40	1.00	0.06	4.84	0.03	0.4	0.27	*0.06*
41	0.36	0.07	*0.07*	0.02	*0.2*	0.25	*0.11*
42	0.09	0.05	*0*	0.03	*0*	*0*	*0.04*
43	0.14	0.21	0.78	*0.01*	*0*	*0*	*0.03*
44	0.19	*0.02*	*0*	0.02	*0.1*	*0.24*	0.09
45	0.27	*0.02*	0.64	0.03	*0*	*0.05*	0.12
46	0.17	0.13	*0.08*	0.04	*0*	*0.13*	*0.07*
47	0.22	0.03	0.26	0.02	*0*	*0.19*	0.10
48	0.21	0.26	0.60	*0.03*	nd	nd	nd
49	0.27	0.07	0.52	*0.03*	nd	nd	nd
50	0.19	0.03	0.38	*0.03*	nd	nd	nd
SW	0.0054	0.003	0.01	0.0003	0.003	2E-05	nd

nd: not determined
SW: sea water

Numbers in italics denote values below the calculated detection limit

Appendix 2: Sample PHREEQE Output

PAN1 Hole No. ARP419-1

TOTAL MOLALITIES OF ELEMENTS

ELEMENT	MOLALITY	LOG MOLALITY
Br	2.863063D-04	-3.5432
TOT ALK	1.669847D-03	-2.7773
Ca	1.338224D-02	-1.8735
Cl	9.028461D-01	-.0444
Fe	5.163496D-07	-6.2871
I	6.059486D-07	-6.2176
K	8.063013D-04	-3.0935
Mg	7.903411D-02	-1.1022
Mn	2.274537D-06	-5.6431
N	5.115763D-05	-4.2911
Na	7.754628D-01	-.1104
SO4	3.482186D-02	-1.4581
Si	2.398551D-05	-4.6201
Sr	4.059018D-05	-4.3916
Au	9.760231D-11	-10.0105

----DESCRIPTION OF SOLUTION----

PH =	6.45
PE =	6.4233
ACTIVITY H2O =	.9696
IONIC STRENGTH =	1.0383
TEMPERATURE =	25.0000
ELECTRICAL BALANCE =	-1.3235D-02
THOR =	2.1768D-01
TOTAL ALKALINITY =	1.6698D-03
ITERATIONS =	13
TOTAL CARBON =	2.2088D-03

DISTRIBUTION OF SPECIES

I	SPECIES	Z	MOLALITY	LOG MOLALITY	ACTIVITY	LOG ACTIVITY
1	H+	1.0	1.18D-06	-5.93	3.55D-07	-6.45
2	E-	-1.0	3.77D-07	-6.42	3.77D-07	-6.42
3	H2O	.0	9.70D-01	-.01	9.70D-01	-.01
9	Br-	-1.0	2.86D-04	-3.54	2.28D-04	-3.64
10	CO3 2-	-2.0	2.85D-07	-6.55	1.15D-07	-6.94
11	Ca 2+	2.0	1.22D-02	-1.91	3.67D-03	-2.44
13	Cl-	-1.0	9.03D-01	-.04	5.15D-01	-.29
17	Fe 2+	2.0	2.28D-07	-6.64	4.64D-08	-7.33
18	I-	-1.0	6.06D-07	-6.22	4.83D-07	-6.32
19	K+	1.0	7.98D-04	-3.10	4.55D-04	-3.34
21	Mg 2+	2.0	6.94D-02	-1.16	2.48D-02	-1.61
22	Mn 2+	2.0	9.61D-07	-6.02	3.87D-07	-6.41
23	NO3 -	-1.0	2.14D-08	-7.67	1.71D-08	-7.77
24	Na+	1.0	7.68D-01	-.11	5.51D-01	-.26
29	SO4 2-	-2.0	1.73D-02	-1.76	2.03D-03	-2.69
30	H4SiO4	.0	2.40D-05	-4.62	3.04D-05	-4.52
31	Sr 2+	2.0	3.59D-05	-4.45	1.44D-05	-4.84
38	Au+	1.0	3.57D-19	-18.45	2.85D-19	-18.55
53	Fe 3+	3.0	1.73D-13	-12.76	1.17D-14	-13.93
54	Mn 3+	3.0	2.45D-25	-24.61	3.17D-26	-25.50
55	NH4 +	1.0	3.64D-05	-4.44	2.90D-05	-4.54
56	NO2 -	-1.0	1.47D-05	-4.83	1.17D-05	-4.93
65	OH-	-1.0	3.43D-08	-7.46	2.73D-08	-7.56
66	H3SiO4 -	-1.0	1.59D-08	-7.80	1.27D-08	-7.90
78	MgCO3 0	.0	2.14D-06	-5.67	2.71D-06	-5.57
79	MgHCO3 +	1.0	3.15D-04	-3.50	2.51D-04	-3.60

80	MgSO4 0	.0	9.28D-03	-2.03	1.18D-02	-1.93
85	CaHCO3 +	1.0	4.16D-05	-4.38	3.31D-05	-4.48
86	CaCO3 0	.0	4.72D-07	-6.33	5.99D-07	-6.22
87	CaSO4 0	.0	1.17D-03	-2.93	1.49D-03	-2.83
93	NaCO3 -	-1.0	1.48D-06	-5.83	1.18D-06	-5.93
94	NaHCO3 0	.0	2.12D-04	-3.67	2.69D-04	-3.57
95	NaSO4 -	-1.0	7.03D-03	-2.15	5.60D-03	-2.25
99	KSO4 -	-1.0	8.14D-06	-5.09	6.49D-06	-5.19
113	FeOH 2+	2.0	5.14D-10	-9.29	2.07D-10	-9.68
114	FeOH2 +	1.0	2.35D-07	-6.63	1.88D-07	-6.73
115	FeOH3 0	.0	5.20D-08	-7.28	6.60D-08	-7.18
116	FeOH4 -	-1.0	2.06D-10	-9.69	1.65D-10	-9.78
120	FeSO4 +	1.0	3.28D-13	-12.48	2.61D-13	-12.58
121	FeCl 2+	2.0	4.53D-13	-12.34	1.83D-13	-12.74
122	FeCl2 +	1.0	5.27D-13	-12.28	4.20D-13	-12.38
131	Fe(SO4)2	-1.0	1.46D-14	-13.84	1.16D-14	-13.94
135	SrHCO3 +	1.0	2.39D-07	-6.62	1.90D-07	-6.72
136	SrCO3	.0	8.43D-10	-9.07	1.07D-09	-8.97
137	SrSO4	.0	4.50D-06	-5.35	5.72D-06	-5.24
142	MnCl +	1.0	1.02D-06	-5.99	8.12D-07	-6.09
143	MnCl2 0	.0	1.44D-07	-6.84	1.82D-07	-6.74
146	Mn(OH)3	-1.0	1.57D-22	-21.80	1.25D-22	-21.90
148	MnSO4 0	.0	1.10D-07	-6.96	1.40D-07	-6.85
149	MnHCO3 +	1.0	3.77D-08	-7.42	3.00D-08	-7.52
150	MnCO3 0	.0	2.78D-09	-8.56	3.53D-09	-8.45
278	HCO3 -	-1.0	1.09D-03	-2.96	8.70D-04	-3.06
279	H2CO3 0	.0	5.43D-04	-3.26	6.90D-04	-3.16
387	AuCl 0	.0	5.78D-15	-14.24	7.34D-15	-14.13
388	AuCl2 -	-1.0	9.46D-11	-10.02	7.54D-11	-10.12
392	AuCl4 -	-1.0	5.57D-30	-29.25	4.44D-30	-29.35
397	AuOH 0	.0	4.89D-15	-14.31	6.21D-15	-14.21
398	Au(OH)2-	-1.0	2.14D-12	-11.67	1.70D-12	-11.77
410	AuI2 -	-1.0	8.33D-13	-12.08	6.63D-13	-12.18

---- LOOK MIN IAP ----

PHASE	LOG IAP	LOG KT	LOG IAP/KT
Calcite	-9.3751	-8.4749	-.90
Gypsum	-5.1548	-4.5800	-.57
Dolo-ord	-17.9211	-17.0900	-.83
Magnesit	-8.5460	-8.0300	-.52
Epsomite	-4.3928	-2.1400	-2.25
Strontia	-11.7801	-9.2700	-2.51
Celestit	-7.5329	-6.6300	-.90
Halite	-.5476	1.5800	-2.13
Quartz	-4.4897	-3.9800	-.51
SiO2(a)	-4.4897	-2.7148	-1.77
FeS PPT	-112.9587	-37.5800	-75.38
Siderite	-14.2732	-10.5500	-3.72
Fe3(OH)8	42.3390	46.2900	-3.95
Ferrihyl	18.3996	17.0000	1.40
Goethite	18.4130	12.0200	6.39
K-Jarosi	27.1618	24.3000	2.86
Rhod-cry	-13.3518	-11.1300	-2.22
Pyrocroi	6.4612	15.2000	-8.74
Hausmani	45.1570	61.0300	-15.87
Manganit	19.3345	25.3400	-6.01
Pyrolusi	32.2078	41.3800	-9.17
Au_Metal	-24.9691	-28.6000	3.63
CO2(gas)	-19.8264	-18.1500	-1.68
O2(gas)	51.4663	83.1200	-31.65
CH4(GAS)	-122.7859	-41.0800	-81.71

Appendix 3: Correlation Coefficient Tables

A: Entire Data Set

Mean Values and Standard Deviations

Element	Mean	Std.Dev.
Eh	0.49	0.17
pH	4.9	1.2
HCO3	49	61
Br	37	12
I	0.5	0.4
NO3	11	29
K	67	25
Ca	670	270
Sr	7	4
TDS	84000	27000
Au	0.3	0.6
Si	8	11
Al	8	14
Cr	0.05	0.09
Mn	3	4
Fe	0.7	2.2
Co	0.20	0.18
Ni	0.27	0.26
Cu	0.08	0.06
Zn	0.29	0.82
Ag	0.026	0.019
As	0.10	0.14
Bi	0.11	0.10
Sc	0.09	0.06

Number of observations: 50
Number of variables: 24

Significance Level	Coefficient
95%	0.235
99%	0.328
99.9%	0.451

KEY: See Overleaf
0.78 - Significant at the 99.9 % level
0.43 - Significant at the 99 – 99.9 % level
0.25 - Significant at the 95 – 99 % level
0.1 - Not significant

Correlation Matrix

	Eh	pH	HCO3	Br	I	NO3	K	Ca	Sr	TDS	Au	Si
Eh	1	**-0.60**	**-0.46**	-0.28	0.0	0.30	-0.31	**-0.47**	-0.27	**-0.49**	**0.50**	0.26
pH	**-0.60**	1	**0.78**	**0.54**	*-0.45*	-0.2	0.30	**0.61**	**0.46**	**0.67**	-0.25	**-0.45**
HCO3	**-0.46**	**0.78**	1	*0.39*	-0.2	-0.1	0.2	*0.39*	0.26	*0.43*	-0.2	-0.2
Br	-0.28	**0.54**	*0.39*	1	-0.1	-0.1	**0.66**	0.25	*0.38*	**0.82**	0.0	-0.29
I	0.0	*-0.45*	-0.2	-0.1	1	0.1	0.0	-0.30	-0.2	-0.2	0.1	0.26
NO3	0.30	-0.2	-0.1	-0.1	0.1	1	0.0	-0.30	-0.2	-0.26	*0.45*	0.29
K	-0.31	0.30	0.2	**0.66**	0.0	0.0	1	0.0	0.1	**0.78**	-0.1	-0.2
Ca	**-0.47**	**0.61**	*0.39*	0.25	-0.30	-0.30	0.0	1	**0.78**	*0.39*	-0.2	*-0.41*
Sr	-0.27	**0.46**	0.26	*0.38*	-0.2	-0.2	0.1	**0.78**	1	*0.42*	-0.1	-0.32
TDS	**-0.49**	**0.67**	*0.43*	**0.82**	-0.2	-0.26	**0.78**	*0.39*	*0.42*	1	-0.2	**-0.51**
Au	**0.50**	-0.25	-0.2	0.0	0.1	*0.45*	-0.1	-0.2	-0.1	-0.2	1	0.1
Si	0.26	**-0.45**	-0.2	-0.29	0.26	0.29	-0.2	*-0.41*	-0.32	**-0.51**	0.1	1
Al	**0.48**	**-0.73**	*-0.45*	*-0.40*	0.31	0.2	-0.1	**-0.61**	*-0.43*	**-0.53**	0.1	**0.66**
Cr	0.0	0.26	0.2	0.2	-0.32	-0.1	-0.2	0.2	0.2	0.1	0.0	0.2
Mn	-0.1	0.0	0.0	*0.38*	0.28	-0.1	0.1	0.1	0.2	0.2	-0.1	-0.2
Fe	*-0.41*	0.0	0.0	-0.1	0.2	-0.1	0.1	0.0	-0.1	0.0	-0.1	0.0
Co	0.0	-0.1	-0.1	*0.36*	0.2	0.1	0.2	0.0	0.2	0.1	0.0	0.0
Ni	0.1	-0.1	0.0	0.2	0.2	*0.34*	0.0	-0.2	0.0	-0.1	0.2	*0.38*
Cu	0.2	-0.1	-0.1	0.27	0.1	0.0	0.2	-0.2	-0.2	0.2	0.31	-0.1
Zn	-0.1	-0.2	-0.1	0.1	0.25	-0.1	0.1	-0.1	-0.1	0.0	-0.1	0.2
Ag	-0.1	*0.36*	0.27	*0.37*	-0.29	-0.2	0.0	0.31	0.29	*0.40*	0.0	-0.29
As	0.29	**-0.56**	*-0.36*	*-0.39*	0.2	0.2	-0.30	-0.32	-0.27	**-0.54**	0.0	**0.70**
Bi	-0.2	0.31	0.27	0.1	-0.2	-0.2	*-0.39*	*0.43*	*0.38*	0.0	-0.1	-0.1
Sc	0.1	0.1	0.1	0.1	-0.2	-0.1	-0.2	0.2	0.30	0.0	0.0	0.0

	Al	Cr	Mn	Fe	Co	Ni	Cu	Zn	Ag	As	Bi	Sc
Eh	**0.48**	0.0	-0.1	*-0.41*	0.0	0.1	0.2	-0.1	-0.1	0.29	-0.2	0.1
pH	**-0.73**	0.26	0.0	0.0	-0.1	-0.1	-0.1	-0.2	*0.36*	**-0.56**	0.31	0.1
HCO3	*-0.45*	0.2	0.0	0.0	-0.1	0.0	-0.1	-0.1	0.27	*-0.36*	0.27	0.1
Br	*-0.40*	0.2	*0.38*	-0.1	*0.36*	0.2	0.27	0.1	*0.37*	*-0.39*	0.1	0.1
I	0.31	-0.32	0.28	0.2	0.2	0.2	0.1	0.25	-0.29	0.2	-0.2	-0.2
NO3	0.2	-0.1	-0.1	-0.1	0.1	*0.34*	0.0	-0.1	-0.2	0.2	-0.2	-0.1
K	-0.1	-0.2	0.1	0.1	0.2	0.0	0.2	0.1	0.0	-0.30	*-0.39*	-0.2
Ca	**-0.61**	0.2	0.1	0.0	0.0	-0.2	-0.2	-0.1	0.31	-0.32	*0.43*	0.2
Sr	*-0.43*	0.2	0.2	-0.1	0.2	0.0	-0.2	-0.1	0.29	-0.27	*0.38*	0.30
TDS	**-0.53**	0.1	0.2	0.0	0.1	-0.1	0.2	0.0	*0.40*	**-0.54**	0.0	0.0
Au	0.1	0.0	-0.1	-0.1	0.0	0.2	0.31	-0.1	0.0	0.0	-0.1	0.0
Si	**0.66**	0.2	-0.2	0.0	0.0	*0.38*	-0.1	0.2	-0.29	**0.70**	-0.1	0.0
Al	1	-0.2	0.0	0.0	0.1	0.2	0.1	0.2	*-0.33*	**0.79**	*-0.34*	-0.1
Cr	-0.2	1	-0.25	-0.2	-0.2	0.2	0.0	-0.1	*0.40*	-0.1	**0.45**	*0.44*
Mn	0.0	-0.25	1	0.1	**0.64**	0.24	0.2	0.24	-0.1	0.1	0.1	0.0
Fe	0.0	-0.2	0.1	1	-0.1	-0.2	-0.1	-0.1	-0.2	-0.1	-0.1	-0.1
Co	0.1	-0.2	**0.64**	-0.1	1	**0.65**	0.31	**0.61**	0.0	0.0	-0.1	0.0
Ni	0.2	0.2	0.24	-0.2	**0.65**	1	0.2	**0.65**	0.1	0.24	0.1	0.2
Cu	0.1	0.0	0.2	-0.1	0.31	0.2	1	0.2	0.31	0.0	0.0	0.2
Zn	0.2	-0.1	0.24	-0.1	**0.61**	**0.65**	0.2	1	0.0	0.27	0.1	0.0
Ag	*-0.33*	*0.40*	-0.1	-0.2	0.0	0.1	0.31	0.0	1	-0.29	**0.57**	**0.73**
As	**0.79**	-0.1	0.1	-0.1	0.0	0.24	0.0	0.27	-0.29	1	0.1	0.0
Bi	*-0.34*	**0.45**	0.1	-0.1	-0.1	0.1	0.0	0.1	**0.57**	0.1	1	**0.71**
Sc	-0.1	*0.44*	0.0	-0.1	0.0	0.2	0.2	0.0	**0.73**	0.0	**0.71**	1

B: Shale Waters

Mean Values and Standard Deviations

Element	Mean	Std.Dev.
Eh	0.51	0.08
pH	4.4	1.3
HCO3	26	41
Br	22	3
I	0.26	0.17
NO3	3.5	1.1
K	54	18
Ca	560	220
Sr	4.2	2.2
TDS	59000	15000
Au	0.10	0.05
Si	16	19
Al	18	21
Cr	0.020	0.019
Mn	0.15	0.08
Fe	0.4	0.7
Co	0.036	0.021
Ni	0.11	0.10
Cu	0.020	0.009
Zn	Below Detection	
Ag	0.004	0.008
As	0.23	0.20
Bi	0.04	0.06
Sc	0.026	0.012

Number of observations: 5
Number of variables: 23

Significance Level	Coefficient
95%	0.805
99%	0.934
99.9%	0.991

KEY: See Overleaf	
0.99	- Significant at the 99.9 % level
0.97	- Significant at the 99 - 99.9 % level
0.83	- Significant at the 95 - 99 % level
0.3	- Not significant

Correlation Matrix

	Eh	pH	HCO3	Br	I	NO3	K	Ca	Sr	TDS	Au	Si
Eh	1	-0.91	-0.87	-0.3	0.6	0.1	0.84	-0.5	-0.4	-0.4	0.6	0.8
pH	-0.91	1	0.88	-0.1	-0.91	0.3	-0.7	0.6	0.3	0.3	-0.6	-0.81
HCO3	-0.87	0.88	1	0.1	-0.7	0.1	-0.6	0.2	0.0	0.0	-0.8	-0.5
Br	-0.3	-0.1	0.1	1	0.5	*-0.98*	-0.2	0.0	0.4	0.6	0.1	-0.2
I	0.6	-0.91	-0.7	0.5	1	-0.7	0.4	-0.5	-0.1	-0.1	0.5	0.7
NO3	0.1	0.3	0.1	*-0.98*	-0.7	1	0.1	0.1	-0.3	-0.4	-0.2	0.0
K	0.84	-0.7	-0.6	-0.2	0.4	0.1	1	-0.5	-0.4	-0.3	0.6	0.6
Ca	-0.5	0.6	0.2	0.0	-0.5	0.1	-0.5	1	0.90	0.82	0.2	-0.91
Sr	-0.4	0.3	0.0	0.4	-0.1	-0.3	-0.4	0.90	1	*0.97*	0.4	-0.8
TDS	-0.4	0.3	0.0	0.6	-0.1	-0.4	-0.3	0.82	*0.97*	1	0.4	-0.8
Au	0.6	-0.6	-0.8	0.1	0.5	-0.2	0.6	0.2	0.4	0.4	1	0.0
Si	0.8	-0.81	-0.5	-0.2	0.7	0.0	0.6	-0.91	-0.8	-0.8	0.0	1
Al	0.83	-0.83	-0.5	-0.2	0.7	-0.1	0.7	-0.91	-0.8	-0.8	0.1	**0.99**
Cr	0.8	-0.5	-0.5	-0.6	0.1	0.5	0.90	-0.4	-0.6	-0.6	0.4	0.6
Mn	-0.3	0.0	-0.2	0.7	0.3	-0.7	-0.3	0.6	0.88	0.92	0.4	-0.5
Fe	-0.1	-0.2	-0.3	0.8	0.4	-0.7	-0.1	0.5	0.81	0.88	0.6	-0.4
Co	0.83	-0.7	-0.83	-0.5	0.4	0.4	0.5	-0.2	-0.2	-0.3	0.4	0.6
Ni	0.83	-0.86	-0.6	-0.1	0.7	-0.1	0.6	-0.87	-0.7	-0.7	0.1	**0.99**
Cu	-0.6	0.3	0.5	0.85	0.0	-0.7	-0.3	0.2	0.4	0.6	0	-0.5
Ag	-0.1	-0.1	-0.3	0.7	0.4	-0.7	-0.2	0.5	0.83	0.89	0.6	-0.4
As	0.84	-0.7	-0.5	-0.5	0.5	0.3	0.6	-0.8	-0.8	-0.84	0.0	*0.94*
Bi	-0.2	0.5	0.1	-0.7	-0.8	0.83	-0.2	0.7	0.3	0.1	0.0	-0.5
Sc	0.6	-0.5	-0.3	-0.1	0.3	0.0	0.92	-0.5	-0.5	-0.4	0.5	0.5

	Al	Cr	Mn	Fe	Co	Ni	Cu	Zn	Ag	As	Bi	Sc
Eh	0.83	0.8	-0.3	-0.1	0.83	0.83	-0.6		-0.1	0.84	-0.2	0.6
pH	-0.83	-0.5	0.0	-0.2	-0.7	-0.86	0.3		-0.1	-0.7	0.5	-0.5
HCO3	-0.5	-0.5	-0.2	-0.3	-0.83	-0.6	0.5		-0.3	-0.5	0.1	-0.3
Br	-0.2	-0.6	0.7	0.8	-0.5	-0.1	0.85		0.7	-0.5	-0.7	-0.1
I	0.7	0.1	0.3	0.4	0.4	0.7	0.0		0.4	0.5	-0.8	0.3
NO3	-0.1	0.5	-0.7	-0.7	0.4	-0.1	-0.7		-0.7	0.3	0.83	0.0
K	0.7	0.90	-0.3	-0.1	0.5	0.6	-0.3		-0.2	0.6	-0.2	0.92
Ca	-0.91	-0.4	0.6	0.5	-0.2	-0.87	0.2		0.5	-0.8	0.7	-0.5
Sr	-0.8	-0.6	0.88	0.81	-0.2	-0.7	0.4		0.83	-0.8	0.3	-0.5
TDS	-0.8	-0.6	0.92	0.88	-0.3	-0.7	0.6		0.89	-0.84	0.1	-0.4
Au	0.1	0.4	0.4	0.6	0.4	0.1	0		0.6	0.0	0.0	0.5
Si	**0.99**	0.6	-0.5	-0.4	0.6	**0.99**	-0.5		-0.4	*0.94*	-0.5	0.5
Al	1	0.6	-0.5	-0.4	0.6	*0.99*	-0.5		-0.4	0.92	-0.5	0.6
Cr	0.6	1	-0.6	-0.5	0.6	0.5	-0.6		-0.5	0.7	0.1	0.8
Mn	-0.5	-0.6	1	*0.98*	-0.2	-0.4	0.6		*0.99*	-0.7	-0.2	-0.4
Fe	-0.4	-0.5	*0.98*	1	-0.2	-0.3	0.6		**1.00**	-0.6	-0.3	-0.2
Co	0.6	0.6	-0.2	-0.2	1	0.6	-0.87		-0.1	0.8	0.2	0.1
Ni	*0.99*	0.5	-0.4	-0.3	0.6	1	-0.5		-0.3	0.92	-0.5	0.5
Cu	-0.5	-0.6	0.6	0.6	-0.87	-0.5	1		0.6	-0.8	-0.4	0
Ag	-0.4	-0.5	*0.99*	**1.00**	-0.1	-0.3	0.6		1	-0.6	-0.2	-0.3
As	0.92	0.7	-0.7	-0.6	0.8	0.92	-0.8		-0.6	1	-0.2	0.4
Bi	-0.5	0.1	-0.2	-0.3	0.2	-0.5	-0.4		-0.2	-0.2	1	-0.3
Sc	0.6	0.8	-0.4	-0.2	0.1	0.5	0		-0.3	0.4	-0.3	1

C: Mafic Waters

Mean Values and Standard Deviations

Element	Mean	Std.Dev.
Eh	0.56	0.21
pH	4.3	0.8
HCO3	14	27
Br	32	6
I	0.6	0.5
NO3	6	8
K	57	9
Ca	580	180
Sr	6.4	2.4
TDS	74000	9000
Au	0.5	0.8
Si	5	9
Al	11	15
Cr	0.028	0.019
Mn	3	4
Fe	1	3
Co	0.20	0.10
Ni	0.18	0.10
Cu	0.09	0.05
Zn	0.11	0.11
Ag	0.027	0.016
As	0.10	0.13
Bi	0.10	0.08
Sc	0.09	0.03

Number of observations: 20
Number of variables: 24

Significance Level	Coefficient
95%	0.378
99%	0.516
99.9%	0.679

KEY: See Overleaf	
0.75	- Significant at the 99.9 % level
0.68	- Significant at the 99 - 99.9 % level
0.49	- Significant at the 95 - 99 % level
0.3	- Not significant

Correlation Matrix

	Eh	pH	HCO3	Br	I	NO3	K	Ca	Sr	TDS	Au	Si
Eh	1	*-0.64*	-0.51	0.2	0.0	-0.1	0.0	-0.49	-0.2	-0.3	0.38	0.1
pH	*-0.64*	1	**0.75**	0.0	*-0.56*	-0.1	-0.2	**0.78**	0.49	*0.68*	-0.2	*-0.58*
HCO3	-0.51	**0.75**	1	-0.3	-0.3	0.0	-0.3	0.47	0.3	0.3	0.0	-0.3
Br	0.2	0.0	-0.3	1	0.0	-0.2	0.1	-0.2	-0.1	0.1	0.1	-0.3
I	0.0	*-0.56*	-0.3	0.0	1	0.0	0.1	-0.45	-0.4	-0.49	0.1	0.50
NO3	-0.1	-0.1	0.0	-0.2	0.0	1	0.3	-0.2	-0.2	-0.1	0.0	0.3
K	0.0	-0.2	-0.3	0.1	0.1	0.3	1	-0.3	-0.1	0.2	0.1	0.1
Ca	-0.49	**0.78**	0.47	-0.2	-0.45	-0.2	-0.3	1	**0.79**	**0.76**	-0.2	-0.49
Sr	-0.2	0.49	0.3	-0.1	-0.4	-0.2	-0.1	**0.79**	1	**0.68**	0.0	*-0.62*
TDS	-0.3	*0.68*	0.3	0.1	-0.49	-0.1	0.2	**0.76**	**0.68**	1	0.0	**-0.68**
Au	0.38	-0.2	0.0	0.1	0.1	0.0	0.1	-0.2	0.0	0.0	1	-0.1
Si	0.1	*-0.58*	-0.3	-0.3	0.50	0.3	0.1	-0.49	*-0.62*	**-0.68**	-0.1	1
Al	0.45	**-0.71**	-0.4	-0.3	0.3	0.2	0.1	**-0.76**	*-0.55*	*-0.65*	0.0	*0.57*
Cr	-0.1	0.47	0.2	0.0	*-0.57*	-0.4	-0.1	0.44	0.3	*0.64*	-0.2	-0.51
Mn	0.0	-0.2	-0.2	0.42	0.2	-0.3	*-0.63*	-0.2	-0.2	-0.40	-0.1	0.0
Fe	*-0.54*	0.3	0.4	-0.4	0.2	-0.2	-0.2	0.1	-0.1	-0.3	-0.2	0.2
Co	0.3	0.0	-0.3	**0.77**	-0.2	-0.4	-0.3	-0.1	-0.1	0.0	0.2	-0.4
Ni	0.42	-0.2	-0.4	**0.80**	0.0	-0.45	-0.3	-0.2	-0.1	-0.1	0.4	-0.3
Cu	*0.59*	-0.42	-0.3	0.3	0.0	-0.2	0.0	-0.41	-0.2	-0.1	*0.55*	-0.2
Zn	0.47	-0.2	-0.2	0.1	-0.3	-0.3	0.1	-0.1	0.2	0.2	0.4	-0.4
Ag	-0.1	0.41	0.3	0.0	-0.4	-0.3	0.0	0.38	0.49	**0.69**	-0.1	**-0.71**
As	0.3	*-0.53*	-0.3	-0.3	0.2	0.2	-0.3	-0.41	-0.44	*-0.59*	-0.2	*0.59*
Bi	-0.50	*0.54*	0.3	-0.1	-0.3	-0.3	-0.49	*0.58*	0.3	0.49	-0.3	-0.43
Sc	-0.2	0.2	0.2	-0.3	-0.3	-0.1	-0.1	0.2	0.1	0.3	-0.46	-0.2

	Al	Cr	Mn	Fe	Co	Ni	Cu	Zn	Ag	As	Bi	Sc
Eh	0.45	-0.1	0.0	*-0.54*	0.3	0.42	*0.59*	0.47	-0.1	0.3	-0.50	-0.2
pH	**-0.71**	0.47	-0.2	0.3	0.0	-0.2	-0.42	-0.2	0.41	*-0.53*	*0.54*	0.2
HCO3	-0.4	0.2	-0.2	0.4	-0.3	-0.4	-0.3	-0.2	0.3	-0.3	0.3	0.2
Br	-0.3	0.0	0.42	-0.4	**0.77**	**0.80**	0.3	0.1	0.0	-0.3	-0.1	-0.3
I	0.3	*-0.57*	0.2	0.2	-0.2	0.0	0.0	-0.3	-0.4	0.2	-0.3	-0.3
NO3	0.2	-0.4	-0.3	-0.2	-0.4	-0.45	-0.2	-0.3	-0.3	0.2	-0.3	-0.1
K	0.1	-0.1	*-0.63*	-0.2	-0.3	-0.3	0.0	0.1	0.0	-0.3	-0.49	-0.1
Ca	**-0.76**	0.44	-0.2	0.1	-0.1	-0.2	-0.41	-0.1	0.38	-0.41	*0.58*	0.2
Sr	*-0.55*	0.3	-0.2	-0.1	-0.1	-0.1	-0.2	0.2	0.49	-0.44	0.3	0.1
TDS	*-0.65*	*0.64*	-0.40	-0.3	0.0	-0.1	-0.1	0.2	**0.69**	*-0.59*	0.49	0.3
Au	0.0	-0.2	-0.1	-0.2	0.2	0.4	*0.55*	0.4	-0.1	-0.2	-0.3	-0.46
Si	*0.57*	-0.51	0.0	0.2	-0.4	-0.3	-0.2	-0.4	**-0.71**	*0.59*	-0.43	-0.2
Al	1	-0.3	0.0	-0.1	-0.3	-0.2	0.3	0.0	-0.2	**0.76**	-0.48	0.2
Cr	-0.3	1	-0.2	-0.3	0.1	0.0	0.1	0.3	**0.76**	-0.3	*0.60*	*0.60*
Mn	0.0	-0.2	1	0.1	*0.67*	*0.66*	0.2	-0.1	-0.2	0.3	0.3	0.0
Fe	-0.1	-0.3	0.1	1	-0.3	-0.3	-0.40	-0.3	-0.3	-0.1	0.0	-0.1
Co	-0.3	0.1	*0.67*	-0.3	1	**0.93**	0.3	0.3	0.0	-0.1	0.3	-0.1
Ni	-0.2	0.0	*0.66*	-0.3	**0.93**	1	0.51	0.3	0.0	-0.1	0.1	-0.3
Cu	0.3	0.1	0.2	-0.40	0.3	0.51	1	*0.62*	0.3	0.1	-0.1	0.1
Zn	0.0	0.3	-0.1	-0.3	0.3	0.3	*0.62*	1	0.3	-0.2	0.0	0.0
Ag	-0.2	**0.76**	-0.2	-0.3	0.0	0.0	0.3	0.3	1	-0.4	0.49	*0.66*
As	**0.76**	-0.3	0.3	-0.1	-0.1	-0.1	0.1	-0.2	-0.4	1	-0.1	0.2
Bi	-0.48	*0.60*	0.3	0.0	0.3	0.1	-0.1	0.0	0.49	-0.1	1	*0.61*
Sc	0.2	*0.60*	0.0	-0.1	-0.1	-0.3	0.1	0.0	*0.66*	0.2	*0.61*	1

D: Ultramafic Waters

Mean Values and Standard Deviations

Element	Mean	Std.Dev.
Eh	0.52	0.13
pH	5.5	0.9
HCO3	90	60
Br	43	7
I	0.38	0.27
NO3	30	60
K	63	21
Ca	710	250
Sr	9.0	2.9
TDS	89000	20000
Au	0.5	0.6
Si	15	9
Al	4	9
Cr	0.17	0.14
Mn	0.8	0.8
Fe	0.004	0.012
Co	0.14	0.07
Ni	0.49	0.20
Cu	0.07	0.04
Zn	0.09	0.12
Ag	0.040	0.023
As	0.10	0.11
Bi	0.18	0.13
Sc	0.14	0.07

Number of observations: 10
Number of variables: 24

Significance Level	Coefficient
95%	0.549
99%	0.715
99.9%	0.872

KEY: See Overleaf	
0.91	- Significant at the 99.9 % level
0.80	- Significant at the 99 - 99.9 % level
0.61	- Significant at the 95 - 99 % level
0.3	- Not significant

Correlation Matrix

	Eh	pH	HCO3	Br	I	NO3	K	Ca	Sr	TDS	Au	Si
Eh	1	-0.77	-0.72	-0.83	0.4	**0.91**	-0.1	-0.61	-0.81	-0.85	0.87	0.4
pH	-0.77	1	**0.90**	0.61	-0.4	-0.84	-0.1	0.60	0.62	0.64	-0.81	-0.1
HCO3	-0.72	**0.90**	1	0.4	-0.4	-0.67	0.0	0.4	0.4	0.5	-0.63	0.0
Br	-0.83	0.61	0.4	1	-0.4	-0.86	0.4	0.5	0.80	**0.96**	-0.85	-0.78
I	0.4	-0.4	-0.4	-0.4	1	0.5	0.2	-0.4	-0.3	-0.2	0.3	0.0
NO3	**0.91**	-0.84	-0.67	-0.86	0.5	1	0.1	-0.78	**-0.90**	-0.83	**0.95**	0.5
K	-0.1	-0.1	0.0	0.4	0.2	0.1	1	-0.62	-0.2	0.4	0.0	-0.55
Ca	-0.61	0.60	0.4	0.5	-0.4	-0.78	-0.62	1	0.85	0.4	-0.75	-0.2
Sr	-0.81	0.62	0.4	0.80	-0.3	**-0.90**	-0.2	0.85	1	0.73	-0.86	-0.5
TDS	-0.85	0.64	0.5	**0.96**	-0.2	-0.83	0.4	0.4	0.73	1	-0.86	-0.80
Au	0.87	-0.81	-0.63	-0.85	0.3	**0.95**	0.0	-0.75	-0.86	-0.86	1	0.60
Si	0.4	-0.1	0.0	-0.78	0.0	0.5	-0.55	-0.2	-0.5	-0.80	0.60	1
Al	0.77	-0.80	-0.5	**-0.89**	0.3	**0.93**	0.0	-0.69	-0.85	-0.85	**0.95**	0.63
Cr	-0.3	0.4	0.2	0.3	-0.70	-0.5	-0.4	0.4	0.4	0.1	-0.2	0.2
Mn	-0.3	0.2	0.4	0.3	0.0	-0.1	0.74	-0.3	-0.1	0.5	-0.2	-0.4
Fe	-0.1	0.3	0.4	0.1	0.0	-0.2	-0.1	0.0	0.0	0.1	0.0	0.1
Co	0.4	-0.61	-0.3	-0.5	0.67	0.70	0.4	-0.65	-0.61	-0.4	0.58	0.2
Ni	0.5	-0.2	0.0	-0.65	0.5	0.62	0.0	-0.58	-0.75	-0.5	0.5	0.5
Cu	0.3	-0.2	0.1	-0.5	-0.2	0.2	-0.3	-0.1	-0.3	-0.3	0.3	0.3
Zn	-0.3	0.0	-0.1	0.2	0.0	-0.4	-0.4	0.73	0.61	0.2	-0.4	-0.3
Ag	-0.5	0.59	0.68	0.4	-0.5	-0.61	-0.2	0.5	0.4	0.5	-0.58	-0.2
As	0.4	-0.5	-0.4	-0.65	0.3	0.4	-0.60	0.1	-0.2	-0.64	0.4	0.4
Bi	-0.4	0.5	0.4	0.3	-0.5	-0.61	-0.61	0.78	0.55	0.2	-0.5	-0.1
Sc	-0.4	0.4	0.5	0.3	-0.4	-0.5	-0.3	0.57	0.4	0.4	-0.5	-0.2

	Al	Cr	Mn	Fe	Co	Ni	Cu	Zn	Ag	As	Bi	Sc
Eh	0.77	-0.3	-0.3	-0.1	0.4	0.5	0.3	-0.3	-0.5	0.4	-0.4	-0.4
pH	-0.80	0.4	0.2	0.3	-0.61	-0.2	-0.2	0.0	0.59	-0.5	0.5	0.4
HCO3	-0.5	0.2	0.4	0.4	-0.3	0.0	0.1	-0.1	0.68	-0.4	0.4	0.5
Br	**-0.89**	0.3	0.3	0.1	-0.5	-0.65	-0.5	0.2	0.4	-0.65	0.3	0.3
I	0.3	-0.70	0.0	0.0	0.67	0.5	-0.2	0.0	-0.5	0.3	-0.5	-0.4
NO3	**0.93**	-0.5	-0.1	-0.2	0.70	0.62	0.2	-0.4	-0.61	0.4	-0.61	-0.5
K	0.0	-0.4	0.74	-0.1	0.4	0.0	-0.3	-0.4	-0.2	-0.60	-0.61	-0.3
Ca	-0.69	0.4	-0.3	0.0	-0.65	-0.58	-0.1	0.73	0.5	0.1	0.78	0.57
Sr	-0.85	0.4	-0.1	0.0	-0.61	-0.75	-0.3	0.61	0.4	-0.2	0.55	0.4
TDS	-0.85	0.1	0.5	0.1	-0.4	-0.5	-0.3	0.2	0.5	-0.64	0.2	0.4
Au	**0.95**	-0.2	-0.2	0.0	0.58	0.5	0.3	-0.4	-0.58	0.4	-0.5	-0.5
Si	0.63	0.2	-0.4	0.1	0.2	0.5	0.3	-0.3	-0.2	0.4	-0.1	-0.2
Al	1	-0.4	-0.1	-0.1	0.72	0.5	0.4	-0.3	-0.5	0.58	-0.5	-0.4
Cr	-0.4	1	-0.4	0.2	-0.81	-0.5	-0.1	-0.1	0.1	-0.2	0.4	0.1
Mn	-0.1	-0.4	1	0.0	0.3	0.0	0.2	-0.1	0.4	-0.4	-0.1	0.3
Fe	-0.1	0.2	0.0	1	-0.3	0.0	0.3	-0.3	0.3	-0.3	0.2	0.3
Co	0.72	-0.81	0.3	-0.3	1	0.5	0.2	-0.1	-0.4	0.4	-0.58	-0.3
Ni	0.5	-0.5	0.0	0.0	0.5	1	0.1	-0.56	-0.3	0.1	-0.5	-0.4
Cu	0.4	-0.1	0.2	0.3	0.2	0.1	1	0.2	0.57	0.5	0.5	0.66
Zn	-0.3	-0.1	-0.1	-0.3	-0.1	-0.56	0.2	1	0.4	0.5	0.60	0.56
Ag	-0.5	0.1	0.4	0.3	-0.4	-0.3	0.57	0.4	1	-0.1	0.83	**0.95**
As	0.58	-0.2	-0.4	-0.3	0.4	0.1	0.5	0.5	-0.1	1	0.2	0.1
Bi	-0.5	0.4	-0.1	0.2	-0.58	-0.5	0.5	0.60	0.83	0.2	1	**0.91**
Sc	-0.4	0.1	0.3	0.3	-0.3	-0.4	0.66	0.56	**0.95**	0.1	**0.91**	1

E: Deep Waters

Mean Values and Standard Deviations

Element	Mean	Std.Dev.
Eh	0.34	0.09
pH	6.3	0.3
HCO3	98	28
Br	54	3
I	0.42	0.17
NO3	3.8	0.9
K	103	26
Ca	870	330
Sr	10	8
TDS	12600	21000
	0	
Au	0.12	0.11
Si	0.2	0.5
Al	Below Detection	
Cr	0.016	0.012
Mn	5.5	2.6
Fe	0.9	1.4
Co	0.30	0.10
Ni	0.19	0.05
Cu	0.09	0.08
Zn	0.36	0.28
Ag	0.027	0.008
As	0.01	0.03
Bi	0.07	0.09
Sc	0.05	0.04

Number of observations: 9
Number of variables: 23

Significance Level	Coefficient
95%	0.582
99%	0.75
99.9%	0.898

KEY: See Overleaf	
0.99	- Significant at the 99.9 % level
0.82	- Significant at the 99 - 99.9 % level
0.64	- Significant at the 95 - 99 % level
0.3	- Not significant

Correlation Matrix

	Eh	pH	HCO3	Br	I	NO3	K	Ca	Sr	TDS	Au	Si
Eh	1	*0.82*	0.5	-0.4	*-0.76*	-0.65	-0.4	-0.1	0.0	-0.4	0.6	-0.2
pH	*0.82*	1	0.1	-0.4	-0.5	-0.6	-0.4	0.1	0.2	-0.4	0.64	0.0
HCO3	0.5	0.1	1	-0.5	-0.2	-0.1	-0.5	0.3	0.0	-0.6	-0.1	0.1
Br	-0.4	-0.4	-0.5	1	0.1	-0.1	*0.82*	-0.4	0.0	*0.87*	-0.1	-0.1
I	*-0.76*	-0.5	-0.2	0.1	1	0.4	0.0	0.3	0.2	0.0	-0.60	0.5
NO3	-0.65	-0.6	-0.1	-0.1	0.4	1	0.3	-0.1	-0.5	0.2	-0.66	-0.3
K	-0.4	-0.4	-0.5	*0.82*	0.0	0.3	1	-0.64	-0.4	**0.99**	-0.3	-0.5
Ca	-0.1	0.1	0.3	-0.4	0.3	-0.1	-0.64	1	*0.83*	-0.6	0.1	*0.90*
Sr	0.0	0.2	0.0	0.0	0.2	-0.5	-0.4	*0.83*	1	-0.3	0.4	**0.94**
TDS	-0.4	-0.4	-0.6	*0.87*	0.0	0.2	**0.99**	-0.6	-0.3	1	-0.2	-0.4
Au	0.6	0.64	-0.1	-0.1	-0.60	-0.66	-0.3	0.1	0.4	-0.2	1	0.1
Si	-0.2	0.0	0.1	-0.1	0.5	-0.3	-0.5	*0.90*	**0.94**	-0.4	0.1	1
Cr	-0.1	-0.1	0.4	-0.67	0.2	0.60	-0.4	0.2	-0.3	-0.5	-0.2	-0.2
Mn	-0.1	-0.1	0.2	-0.1	0.1	-0.3	-0.4	*0.81*	*0.78*	-0.3	0.3	0.71
Fe	-0.73	-0.5	-0.6	*0.76*	0.5	0.5	0.74	-0.3	-0.2	0.75	-0.4	-0.1
Co	0.3	0.0	0.6	-0.5	-0.3	-0.3	-0.64	0.64	0.5	-0.59	0.4	0.4
Ni	0.3	0.1	0.61	-0.60	-0.3	0.0	-0.59	0.3	0.0	-0.61	0.4	0.0
Cu	-0.3	-0.5	0.0	0.3	0.4	0.2	0.2	-0.5	-0.4	0.2	-0.6	-0.3
Zn	-0.1	-0.3	0.0	-0.1	0.0	0.2	0.0	-0.4	-0.4	-0.1	0.0	-0.5
Ag	0.3	0.3	0.5	-0.1	-0.2	0.3	0.1	-0.1	-0.4	0.1	-0.1	-0.3
As	-0.2	0.0	0.1	-0.1	0.5	-0.3	-0.5	*0.90*	**0.94**	-0.4	0.1	**1.00**
Bi	0.4	0.5	0.2	-0.2	-0.1	-0.72	-0.60	0.60	*0.75*	-0.5	0.5	0.68
Sc	0.62	0.66	0.1	0.0	-0.5	*-0.88*	-0.3	0.2	0.59	-0.2	*0.89*	0.3

	Al	Cr	Mn	Fe	Co	Ni	Cu	Zn	Ag	As	Bi	Sc
Eh		-0.1	-0.1	-0.73	0.3	0.3	-0.3	-0.1	0.3	-0.2	0.4	0.62
pH		-0.1	-0.1	-0.5	0.0	0.1	-0.5	-0.3	0.3	0.0	0.5	0.66
HCO3		0.4	0.2	-0.6	0.6	0.61	0.0	0.0	0.5	0.1	0.2	0.1
Br		-0.67	-0.1	*0.76*	-0.5	-0.60	0.3	-0.1	-0.1	-0.1	-0.2	0.0
I		0.2	0.1	0.5	-0.3	-0.3	0.4	0.0	-0.2	0.5	-0.1	-0.5
NO3		0.60	-0.3	0.5	-0.3	0.0	0.2	0.2	0.3	-0.3	-0.72	*-0.88*
K		-0.4	-0.4	0.74	-0.64	-0.59	0.2	0.0	0.1	-0.5	-0.60	-0.3
Ca		0.2	*0.81*	-0.3	0.64	0.3	-0.5	-0.4	-0.1	*0.90*	0.60	0.2
Sr		-0.3	*0.78*	-0.2	0.5	0.0	-0.4	-0.4	-0.4	**0.94**	*0.75*	0.59
TDS		-0.5	-0.3	0.75	-0.59	-0.61	0.2	-0.1	0.1	-0.4	-0.5	-0.2
Au		-0.2	0.3	-0.4	0.4	0.4	-0.6	0.0	-0.1	0.1	0.5	*0.89*
Si		-0.2	0.71	-0.1	0.4	0.0	-0.3	-0.5	-0.3	**1.00**	0.68	0.3
Cr		1	-0.1	-0.2	0.2	0.62	0.0	0.2	0.3	-0.2	-0.2	-0.5
Mn		-0.1	1	-0.3	*0.83*	0.5	-0.5	0.0	-0.3	0.71	0.4	0.4
Fe		-0.2	-0.3	1	-0.69	-0.5	0.4	-0.2	0.1	-0.1	-0.4	-0.3
Co		0.2	*0.83*	-0.69	1	*0.76*	-0.4	0.1	-0.2	0.4	0.4	0.4
Ni		0.62	0.5	-0.5	*0.76*	1	-0.2	0.4	0.2	0.0	0.1	0.2
Cu		0.0	-0.5	0.4	-0.4	-0.2	1	0.5	-0.1	-0.3	-0.4	-0.5
Zn		0.2	0.0	-0.2	0.1	0.4	0.5	1	-0.3	-0.5	-0.58	-0.3
Ag		0.3	-0.3	0.1	-0.2	0.2	-0.1	-0.3	1	-0.3	-0.1	-0.1
As		-0.2	0.71	-0.1	0.4	0.0	-0.3	-0.5	-0.3	1	0.68	0.3
Bi		-0.2	0.4	-0.4	0.4	0.1	-0.4	-0.58	-0.1	0.68	1	0.71
Sc		-0.5	0.4	-0.3	0.4	0.2	-0.5	-0.3	-0.1	0.3	0.71	1